MICROFLUIDIC MODEL OF VASCULARIZED TUMOR MICROENVIRONMENT: PDMS AND INJECTION-MOLDED PLASTIC 3D CULTURE PLATFORMS

A Dissertation
Presented to
The Academic Faculty

by

JUNGHO AHN

Doctor of Philosophy in Mechanical Engineering
Joint Ph. D. Program with Seoul National University
George W. Woodruff School of Mechanical Engineering

Georgia Institute of Technology
May 2020

MICROFLUIDIC MODEL OF VASCULARIZED TUMOR MICROENVIRONMENT: PDMS AND INJECTION-MOLDED PLASTIC 3D CULTURE PLATFORMS

Approved by:

Dr. YongTae Kim, Advisor (GT)
School of Mechanical Engineering
Georgia Institute of Technology

Dr. Noo Li Jeon, Advisor (SNU)
School of Mechanical Engineering
Seoul National University

Dr. J. Brandon Dixon (GT)
School of Mechanical Engineering
Georgia Institute of Technology

Dr. Yongdae Shin (SNU)
School of Mechanical Engineering
Seoul National University

Dr. Todd Sulchek (GT)
School of Mechanical Engineering
Georgia Institute of Technology

Dr. Jangho Kim (CNU)
Department of Biosystems Engineering
Chonnam National University

Date Approved: November 11, 2019

[To the students of the Georgia Institute of Technology]

ACKNOWLEDGEMENTS

I am greatly indebted to my principal supervisor in Seoul National University, Professor Noo Li Jeon for supervising me with his instructive criticism, valuable advice and support throughout the last total 6 years and for his careful feedback and comments on this thesis. His broad and enthusiastic knowledge of organ-on-a-chip field and his logical way of thinking have inspired me throughout the years I spent in his laboratory. I also owe my deepest gratitude to my co-supervisor in Georgia Institute of Technology, Professor YongTae Kim, for mentoring me to have confidence all the time, his bottomless support, precious advice and critical review of this thesis. His confidence in science and optimistic attitude in general encouraged me to believe in myself.

Besides my advisors, I would like to thank the rest of my thesis committee: Professor J. Brandon Dixon, Professor Todd Sulchek, Professor Yongdae Shin, and Professor Jangho Kim, for their insightful comments and encouragement, but also the critical question which incented me to widen my research from various perspectives.

I am also grateful to Dr. Sudong Kim, Dr. Minhwan Chung, Dr. Hyunjae Lee and Dr. Yositaka J. Sei who provided me an opportunity to join their team. An equal amount of gratitude is owed to Prof. Tae-eun Park in UNIST and my colleagues Ms. Somin Lee, Mr. Jihoon Ko, Mr. Suryong Kim, Ms. Jungeun Lim, Mr. Jungseub Lee in Seoul National University and Dr. SongIh Ahn in Georgia Institute of Technology. I also thank my fellow labmates in for the simulating discussions, for the sleepless nights we were working together and for all the fun we have had in the last 6 years.

Last but the most, I would like to take this opportunity to express my profound gratitude to my beloved parents and older sister back home for their endless love and everlasting support, and for always being proud of me.

TABLE OF CONTENTS

ACKNOWLEDGEMENTS **iv**

LIST OF TABLES **viii**

LIST OF FIGURES **ix**

LIST OF SYMBOLS AND ABBREVIATIONS **xviii**

SUMMARY **xx**

CHAPTER 1. Introduction **1**
1.1 Tumor-Stromal Interactions on a Chip **3**
1.2 Tumor-Vasculature Interactions on a Chip **5**
1.3 Cancer Cells Transmigration through Vasculature: Metastasis on a Chip **7**
1.4 Tumor-Extracellular Matrix Interaction **9**
1.5 Microfluidic Platforms for Cancer Drug Delivery and Screening **10**
1.6 PDMS and Injection-molded Microfluidic System **12**
1.7 Aims and Approaches **14**

CHAPTER 2. PDMS 3D Culture Platform: Vascularized Tumor Spheroid Culture **16**
2.1 3D Microengineered Vascularized Tumor Spheroid Model for Drug Delivery and Efficacy Testing **16**
2.2 Materials and Methods **19**
2.2.1 Cell culture 19
2.2.2 Cell seeding in the microfluidic platform 20
2.2.3 Fabrication of the microfluidic device 20
2.2.4 CUBIC tissue clearing 21
2.2.5 Quantitative RT-PCR 21
2.2.6 Imaging 23
2.2.7 Permeability coefficient measurement 23
2.2.8 Statistical methods 24
2.3 Results **24**
2.3.1 Self-assembled 3D vascularized tumor spheroid model 24
2.3.2 Morphological and relative gene expression characterization of cancer only vs. cancer– EC hybrid spheroids 27
2.3.3 Angiogenic potential of cancer cell only vs. cancer– EC hybrid spheroid in the VTS model 29
2.3.4 Evaluation of vascularized tumor spheroid permeability 30
2.3.5 Axitinib performance in the vascularized spheroid tumor model 33
2.3.6 Reconstituting lymphatic endothelial cell-blood vascular endothelial cell incorporated vascularized tumor spheroid in vitro 37

2.4 Discussion 38
2.5 Conclusion 42

CHAPTER 3. Injection-molded 3D Culture Platform: Vascularized Tumor Spheroid Culture 44
3.1 Tumor Spheroid-on-a-chip: a Standardized Microfluidic Culture Platform for Investigating Tumor Angiogenesis 44
3.2 Materials and Methods 46
3.2.1 3D printing for prototypes 46
3.2.2 Fabrication of Sphero-IMPACT 47
3.2.3 Cell Culture 47
3.2.4 Retrovirus production and transfection 48
3.2.5 Spheroid preparation 48
3.2.6 Immunostaining 48
3.2.7 Migration, invasion and tumor spheroid-induced angiogenesis assay 49
3.2.8 Drug testing 49
3.2.9 Imaging and data quantification 50
3.2.10 Statistical analysis 50
3.3 Results and Discussion 50
3.3.1 Sphero-IMPACT design optimization and considerations 50
3.3.2 Gel patterning principle 55
3.3.3 Angiogenesis assay 59
3.3.4 Tumor migration and invasion 65
3.3.5 Tumor angiogenesis and drug screening 67
3.4 Conclusion 69

CHAPTER 4. General Discussion and Future Perspectives 73
4.1 EPR Effect 73
4.2 Solid Tumor Stress 73
4.3 Normalization of Tumor Blood Vessels 74
4.4 Future Microfluidic Platforms 75

CHAPTER 5. Conclusion 77

REFERENCES 79

LIST OF TABLES

Table 1. Primers used for qRT-PCR and RT-PCR.22

LIST OF FIGURES

Figure 1.1 The tumor microenvironment (TME) heterogeneously consists of cellular and non-cellular components including the surrounding blood vessels, immune cells, fibroblasts, cancer stem cells and extracellular matrix (ECM).3

Figure 1.2 Tumor-stromal interactions on a chip. (A) 3D Microfluidic model to investigate the carcinoma associated fibroblast promoted tumor spheroid invasion. (i, ii) microfluidic chip design (iii) cell loading step. Salivary gland adenoid cystic carcinoma cell line (ACC-M) were co cultured with carcinoma associated fibroblasts (CAFs). ACC-M invaded CAF-embedded matrix in a spheroid fashion. However, ACC-M cells did not invade the adjacent matrix when co-cultured with the fibroblast cell line (HFL1). (B) 3D culture of tumor spheroids and fibroblasts in a compartmentalized microfluidic chip. (i, ii) Fluorescence images of HT-29 tumor spheroids and CCD-18Co human normal fibroblast cell line. HT-29 spheroids and CCD-18Co cells proliferated within the space of the corresponding channels over 5 days, during which their growth and interaction were monitored and characterized.4

Figure 1.3 Tumor angiogenesis on a chip. (A) Human glioblastoma multiforme cells, (U87MG) were used to induce angiogenic sprouting. Fluorescence image shows angiogenic sprouts grown for 2 and 4 days under co-culture with U87MG cancer cells and human umbilical vein endothelial cells (HUVEC) (i, ii). Scale bar: 50 μm; (B) Pre-vascularized tumor (PVT) spheroid model. PVT spheroid model were introduced breast cancer (MCF10A, MDA-MB-231), Lung cancer (A549) and colon cancer (SW620). Representative fluorescence images of PVT spheroid model shows robust angiogenic

sprouting. Various PVT spheroid showed different angiogneic sprouting behavior. Intravasation events were only observed for SW620 cancer cells. Scale bar: 100 μm.7

Figure 1.4 Metastasis on a chip. (A) A human 3D vascularized organotypic microfluidic system to study cancer cell extravasation (i) Cancer cell extravasation was monitored in real time within a vascular network (ii) magnified image. Scale bar: 100 μm; (B) Human umbilical vein pericytes were cocultured with human umbilical vein endothelial cells to form pericyte-covered lumens. The extravasation rate from HUVEC-only cultures was significantly higher when compared to HUVEC-pericyte coculture. Scale bar: 20 μm; (C) Design of biomimetic multi-organ chip (i, ii) multi-organ chip included an upstream "lung organ" and three downstream "distant organ" such as bone, brain, liver; (iii, iv) The microfluidic chip was compartmentalized using human epithelial and stromal cells cultured on separated side of a porous membrane in order to mimic (v–vii) physiological respiration in the microfluidic system; which was followed by the introduction of (viii–x) lung fibroblast cells to investigate lung cancer metastasis to distant organ.8

Figure 1.5 Probing the efficacy of drug delivery using TME on a chip. (A) Droplet-based microfluidic system for multicellular tumor spheroid formation and anticancer drug testing. (i) Schematic of the droplet formation and cell culture microfluidic chips. Each chamber contains 14 sieves for alginate droplet trapping; (ii) Breast tumor cells proliferating and forming multicellular spheroids while encapsulated in alginate beads. Tumor cells were perfused with doxorubicin and live/dead assay was assessed. Scale bar: 100 μm; (B) Tumor on a chip provides an optical window into nanoparticle tissue transport. (i) Schematic of the microfluidic device; (ii) MDA-MB-435 breast cancer cell embedded within microfluidic device (iii) Effect of nanoparticle size on tissue accumulation. 40 nm

fluorescent PEG-nanoparticles entered the tumor spheroid and accumulated in the interstitial spaces but 110 nm nanoparticles were excluded from the spheroid. Scale bar: 100 μm.12

Figure 2.1 In vitro three-dimensional vascularized tumor model. Schematic representation of microfluidic design for in vivo like 3D vascularized tumor formation by tumor spheroid and ECs mixture in the center channel under paracrine interactions with stromal fibroblasts in the outermost side channels.25

Figure 2.2 Bright field images of the development of vascularized tumor spheroid, composed of tumor spheroid enveloped by endothelial cells. White and yellow lines indicate tumor spheroid area. Scale bars, 200 μm. 26

Figure 2.3 (A) Representative confocal images compare before (left line)/after (right line) clearing in the same sample. CUBIC tissue clearing does not lead to volume changes. Scale bars, 150 μm. (A, below) 3D reconstruction image of vascularized tumor. Tumor spheroid is enveloped by blood vessels. (B) Before/after clearing comparison of z axis imaging depth. (C) Before/after clearing comparison of xy plane relative intensity according to distance. (D) Before tissue cleared confocal image of vascularized tumor spheroid (left, top). After tissue cleared vascularized tumor spheroid (left, bottom) and 3D reconstruction image of vascularized tumor spheroid (right).26

Figure 2.4 Multicellular tumor spheroid characterization. (A) Representative confocal images of HepG2 – ECs spheroid with different cell ratio and spheroid sphericity of different cancer: EC ratios. All spheroid were fixed at day 5. (Scale bars, 100 μm. n=4-6). (B) RT-PCR results of cancer cell monoculture and cancer cell co-cultured with ECs. Gene

analysis considered markers 1) PTEN, 2) p53, 3) E-cadherin, 4) α-SMA, 5) CXCL12 and CXCR4.The internal standard housekeeping gene was GAPDH. (n=3-4).28

Figure 2.5 RT-PCR results of ECs monoculture and ECs co-cultured with tumor (HepG2) at day 2.29

Figure 2.6 Representative confocal images compared total blood vessel volume induced by vascularized tumor model of cancer cell only (HepG2) spheroid and cancer cells HepG2 – ECs spheroid. (Scale bars, 400 μm. n=4-6).30

Figure 2.7 Evaluation of vascularized tumor spheroid: permeability measurement and nanoparticle delivery. (A) Time series fluorescence micrographs were taken and analyzed for intensity changes in the perivascular region to measure permeability. After cell culture medium was removed, FITC-dextran (10kDa, 70kDa) solution was introduced and image were captured every 10 s. Red circles in bottom images represent focal intercellular openings (FIOs) (Scale bars, 100 μm) (B) The graphs shows permeability coefficient for 4 different conditions (10 kDa) (n=5-6). (C) The graphs shows permeability coefficient for two conditions (70 kDa). (D) qRT-PCR result of ICAM-1 mRNA expression (n=3-4) (E) Number of focal intercellular openings. [ROI] 1; < 200 μm of the tumor spheroid boundary and [ROI] 2; > 200 μm of the tumor spheroid boundary (70 kDa).32

Figure 2.8 Silica nanoparticle (NP) delivery through vasculature of vascularized tumor model at 3 time-points (top). Scale bars, 400 μm. Silica nanoparticle distribution at different z sections (bottom).34

Figure 2.9 Antiangiogenesis and antitumor activities of Axitinib in VTS model. (A) Timeline of cancer drug treatment experiment. In the early stage of vascularized tumor model, Axitinib were introduced into the reservoirs a day after spheroid – ECs gel suspension injected to the central channel. (B) Representative confocal images show Axitinib dosage dependent response of spheroid and vasculature in the early stage of VTS model. Scale bars, 300 μm. Relative spheroid area (C), blood vessel area (D), number of disconnected blood vessel (E) in response to two different dosage of Axitinib (1 nM, 10 nM) at the early stage of VTS model. (F) Timeline of cancer drug treatment experiment. In the late stage of vascularized tumor model, Axitinib were introduced into the reservoirs 4 days after spheroid – ECs gel suspension injected to the central channel, which vasculature fully enveloped HepG2 – ECs hybrid spheroid. (G) Representative confocal images show Axitinib dosage dependent response of spheroid and vasculature in the late stage of VTS model. Scale bars, 300 μm. Relative spheroid area (H), blood vessel area per device (I), number of disconnected blood vessel per device (J) in response to two different dosage of Axitinib (1 nM, 10 nM) at the late stage of VTS model.36

Figure 2.10 Monitoring reliable and reproducible response of axitinib treatment. (A) Representative confocal images show 1 nM axitinib treated vascularized tumor spheroid conditions. (B) Spheroid area per device. Scale bar: 300 μm.36

Figure 2.11 Confocal image of HepG2 – EC spheroid with lymphatic endothelial cells (LECs, green; podoplanin) and vascular endothelial cells (ECs, red). Scale bar: 150 μm.37

Figure 3.1 Design of the standardized microfluidics platform for tumor spheroid-on-a-chip. (A) A conceptual image of Sphero-IMPACT based on a standard 96-well plate format. (B)

Sphero-IMPACT has a media reservoir on each side, centered on a fluid rail guide for cell culture. The rail guide contains a tapered hole functioned as a culture space for a cell spheroid. (C) Spontaneous fluid patterning by capillary action. Fluid can be transferred simply and robustly along the rail guide under hydrophilic condition. (D) The patterned fluid configures a concave meniscus at the edges of the structure. A fluorescence image showing GFP-expressing HUVECs patterned with fibrin gel which forming the meniscus, and RFP-expressing HUVECs seeded on the reservoir. (E) The cross-sections of the devices filled with a solution of Rodamin B under noted volume were converted to grayscale images for analysis. White dash lines indicate the fluid rail guide, and yellow dash lines are traces for curvature studies.53

Figure 3.2 Overall schematics of the structural components of tumor spheroid-on-a-chip. (A)Illustration of 96-well plate SBS format-based microplate. (B) A single array of tumorspheroidon-a-chip as a prototype model. (C-D) Schematic view detailing the dimensions of the device. (E) Photograph of the dye being patterned into the rail of the device.54

Figure 3.3 Process schematic of Sphero-IMPACT design optimization with 3D printing for mass production through injection molding. (A) 3D printing prototypes allow for rapid dimensional testing and optimization prior to high investment but high yield injection molded production. (B) During the process, we performed the platform validation through fluid patterning and cell culture testing. This process was approached through the trial and error method. (C) Once a design has been configured for injection molding, the design can be mass produced for easy accessibility for the end user.55

Figure 3.4 Fluid patterning under the hydrophilic and hydrophobic environment. (A)Investigation of the contact angle of the material used in the device under hydrophilic conditions to establish the fluid patterning technique. (B) The fluid interface showed surface imbalance under hydrophobic environment. After the plasma treatment, the fluid was well patterned under hydrophilic environment.58

Figure 3.5 Various in vitro model approaches of Sphero-IMPACT. (A) Vasculogenesis; the platform can perform co-culture modeling to develop a 3D perfusable blood vessel networks. (B) Angiogenesis; induction of directional angiogenesis by attaching HUVECs to patterned fibrin gel-meniscus in a rail guide structure. (C) Tumor migration assay; ease of experimentation and observation through the space for a spheroid inside the platform. (D) Tumor spheroid-induced angiogenesis; construct tumor model which is vascularized through co-culture of tumor spheroid and blood vessel.59

Figure 3.6 A diagram comparing the time required for production of the device between soft lithography and injection molding process.62

Figure 3.7 Engineered 3D perfusable blood vessel networks in Sphero-IMPACT. (A) An illustration of angiogenesis model configuration in Sphero-IMPACT. (B) A cell culture approach to construct angiogenesis model. (C) Investigating an optimal patterned volume for inducing effective angiogenic sprouts. Every sample was cultured for 5 days and stained with lectins (green) as markers of endothelial cells. Scale bar = 1000 μm. (D) The total vascular network area and the number of vessel sprouts were quantitatively evaluated to determine appropriate conditions for angiogenesis depending on the patterning volume. (E) Experimental Study on the transport of microbeads with the lapse of time through

perfusable blood vessel developed under 6.0 μl patterning volume condition. Scale bar = 500 μm. (F) Confocal images exhibiting vasculogenesis formed from GFP-expressing HUVECs reflecting the effect of LFs spheroids. Observation of cytoskeleton through F-actin (red) antibody staining. Scale bar = 1000 μm.64

Figure 3.8 Tumor invasion assay using a spheroid model. (A) Schematic depiction of tumor migration and invasion. (B) Configuration of the microfluidic device for modeling tumor spheroid migration and invasion into 3D ECM. (C) The optical microscope image showing the U87MG tumor spheroid in the spheroid region. Scale bar = 400 μm. (D) Representative confocal images of tumor migration and invasion under three different conditions. Scale bar = 600 μm. (E and F) Quantitative analysis of tumor cell migration area and migration distance. Bars indicate mean ± SEM from at least 4 devices per condition. *$p < 0.1$ and **$p < 0.01$ in the unpaired two-tailed Student's t-test.67

Figure 3.9 Tumor spheroid-induced angiogenesis and drug screening validation (A) Schematic depiction of angiogenic sprouts toward tumor spheroid positioned in the center hole. (B) Configuration of the microfluidic platform for modeling tumor angiogenesis. The tumor spheroid collected and mixed with fibrin gel is injected into the hole, and HUVECs are seeded on around the fibrin gel surface. (C) Maximum projection images of the tumor angiogenesis cultured for 4 days in Sphero-IMPACT. Tumor spheroid formed from GFP-expressing U87MG, and blood vessels assembled from RFP-expressing HUVECs. Under the same culture conditions, the types of target drugs were treated with medium every two days. Scale bar = 500 μm. (D–F) Quantitative analysis of the total vascular network area, number of sprouts and sprouting length depending on each drug condition. Bars represent

mean ± SEM from at least 8 devices per condition. ****$p < 0.0001$ in the unpaired two-tailed Student's t-test.71

Figure 3.10 Comparison of angiogenic sprouts under different conditions. Under co-culture with U87MG cancer cells, angiogenic sprouts are characterized by the sprouts with branching tip cells (red arrow) and convoluted and aberrantly converged blood vessels (yellow arrow).72

LIST OF SYMBOLS AND ABBREVIATIONS

TME	Tumor microenvironment
PDMS	Polydimethylsiloxane
VTS	Vascularized tumor spheroid
EMT	Epithelial-mesenchymal transition
EC	Endothelial cells
LF	Lung fibroblasts
LEC	Lymphatic endothelial cell
FIOs	Focal intercellular openings
2D	2-Dimensional
3D	3-Dimensional
IMPACT	Injection-molded plastic array 3D spheroid culture platform
PS	Polystyrene
NPs	Nanoparticles
ECM	Extra cellular matrix
CAF	Carcinoma associated fibroblast
HUVEC	Human umbilical vein endothelial cells
EGM-2	Endothelial growth medium
RFP	Red fluorescent proteins
GFP	Green fluorescent proteins
FGM	Fibroblast growth medium
μVN	Microvascular network
ROI	Region of interest

TGF-β1	Transforming growth factor beta 1
TNF-α	Tumor necrosis factor alpha
BSA	Bovine serum albumin
CAD	Computer aided design
HCS	High-content screening
HTS	High-throughput screening
VEGF	Vascular endothelial growth factor

SUMMARY

The “Tumor microenvironment” (TME) has been increasingly recognized as an underlying factor in drug resistance and the recurrence of cancer, both of which are major obstacles to a cure. The TME is a complex, interacting system including the tumor itself, other noncancerous cell types such as immune, stromal and endothelial cells, and the extracellular matrix surrounding these cells. This complexity has largely prevented a comprehensive understanding of TME in conventional in vitro models, which have been too simple to recapitulate the intricate interactions. Therefore, developing in vitro assays that closely replicate the pathophysiology of 3D vascularized TME is critical to understand the formation and development of tumors and unravel the mechanisms by which tumor cells grow, metastasize, and resist against drugs.

To this end, this thesis first describes the method to create in vivo like vascularize tumor spheroid Polydimethylsiloxane (PDMS)-based model. We developed vascularized tumor spheroid (VTS) model that reproduces the pathological and morphological characteristics of in vivo vascularized solid TME. We used human hepatocellular carcinoma (HepG2) spheroid to reconstitute VTS. The VTS structure closely recapitulates a vascularized tumor microenvironment where cancer cells can interface with self-assembled vascular endothelial cells within 3D hydrogel. We introduced on-chip tissue clearing technology that enables 3D intact visualization of the tumor-endothelium interaction. We also conducted comparative studies of spheroid morphology, relative tumor suppressor (PTEN and p53) and epithelial-mesenchymal transition (EMT) gene expressions, and microvascular network formation induced by the spheroid. Notably, we observed that

cancer-EC hybrid spheroids enhance uniformity of spheroid, tumor aggressiveness, and tumor angiogenesis compared to those with cancer cells only. Moreover, the microvasculature co-cultured with the tumor spheroid showed a higher permeability coefficient compared to control and increased focal intercellular openings (FIOs) of microvascular network located in adjacent to tumor spheroid, demonstrating hallmarks of tumor vasculature; a leaky and fenestrated structure of endothelium. We further visualized and quantitatively demonstrated the effects of the FDA approved cancer drug; Axitinib by monitoring blood vessel area and spheroid tumor size, highlighting the significance of tumor vascularization and revealing the importance of the dose and treatment timing. The 3D VTS model will be a useful platform to better understand how tumor develops and metastasizes in vasculature, screen drugs and their compositions (fine drug cocktails) for heterogeneous cancer treatment, and explore new therapeutic strategies with 3D vascularized models of patient-derived multicellular tumor spheroids.

Secondly, this thesis introduces Injection-molded based vascularized tumor microenvironment platform considering standardized application for industrialization. The field of microfluidics-based three-dimensional (3D) cell culture system is rapidly progressing from academic proof-of-concept studies to valid solutions to real-world problems. PDMS-based platform has been widely adopted as in vitro platforms for mimicking tumor microenvironment. However, PDMS has not been welcomed as a standardized commercial application for preclinical screening due to inherent material limitations that make it difficult to scale-up production. Here, we present an injection-molded plastic array 3D spheroid culture platform (Sphero-IMPACT). The platform is made of polystyrene (PS) in a standardized 96-well plate format with a user-friendly

interface. This interface describes a simpler design that incorporates a tapered hole in the center of the rail to pattern a large spheroid with 3D extracellular matrix and various cell types. This hole is designed to accommodate standard pipette tip for automated system. The platform that mediate open microfluidics allows implement spontaneous fluid patterning with high repeatability from the end user. To demonstrate versatile use of the platform, we developed 3D perfusable blood vessel network and tumor spheroid assays. In addition, we established a tumor spheroid induced angiogenesis model that can be applicable for drug screening. Sphero-IMPACT has the potential to provide a robust and reproducible in vitro assay related to vascularized cancer research. This easy-to-use, ready-to-use platform can be translated into an enhanced preclinical model that faithfully reflects the complex tumor microenvironment.

CHAPTER 1. INTRODUCTION

The cost of drug development has dramatically increased during the last several decades due to the inefficiency of current pre-clinical drug screening models. Major disadvantages of conventional drug screening models are (i) the dissimilarity between two-dimensional (2D) in vitro cell culture systems and in vivo models; and (ii) the phylogenetic difference between human and animal models. Advanced 3D cell culture model systems have demonstrated advantages in providing more physiologically relevant conditions and more predictive ability [1, 2]. The integration of microfluidic technology and cell biology research has recently reached a significant milestone with the development of "organ-on-a-chip" technologies that reconstitute organ-level in vivo characteristics [3]. Developing improved in vitro models through these innovative technologies will promote fundamental cancer research and accelerate drug discovery and clinical translation.

A tumor microenvironment (TME) consists of a heterogeneous mix of cellular and non-cellular components including surrounding blood vessels, immune cells, fibroblasts, cancer stem cells and extracellular matrix (ECM) (Figure 1) [4]. The elucidation of the complex cellular interactions within the TME remains one of the main challenges in the treatment of cancer [5]. It has become increasingly recognized that the study of human cancer cannot be simplified to homogeneous collections of neoplastic cells, but must instead be studied as complex multicellular systems to properly reflect interactions between malignant and non-malignant cells [1, 6, 7]. This interplay between the tumor and the stroma has been recognized as a characteristic property of the TME, and this paradigm is now considered to be a hallmark of cancer biology [8]. Animal models are conventionally

the gold standard for screening cancer therapeutics because of their capabilities to sustain the complex TME [9]. However, accurate mimicry of human tumorigenesis is extremely difficult, questioning the usefulness of existing in vivo models for therapeutic efficacy translation. Meanwhile, recent advancements in the microengineering of TME using organ-on-a-chip technologies have enabled the development of pathophysiologically relevant human tumorigenesis models.

In this thesis, we proposed a novel, physiologically relevant in vitro vascularized tumor microenvironment models. Using the advanced 3D microengineered technology, we developed two microfluidic platforms: PDMS and injection-molded microfluidic platforms. We designed geometrically defined vascularized tumor spheroid model and investigated hallmarks of tumor vasculatures using PDMS platform. We also highlighted significance of tumor vascularization and revealing the importance of treatment timing. Based on the model, we further developed injection-molded plastic array 3D spheroid culture platform, which made of polystyrene (PS) in a standardized 96-well plate format with user-friendly interface. We propose vascularized tumor spheroid model as the next generation of 3D microfluidic system for robust high-throughput and high-content assays with drug candidate evaluation and investigation of specific pathogenesis.

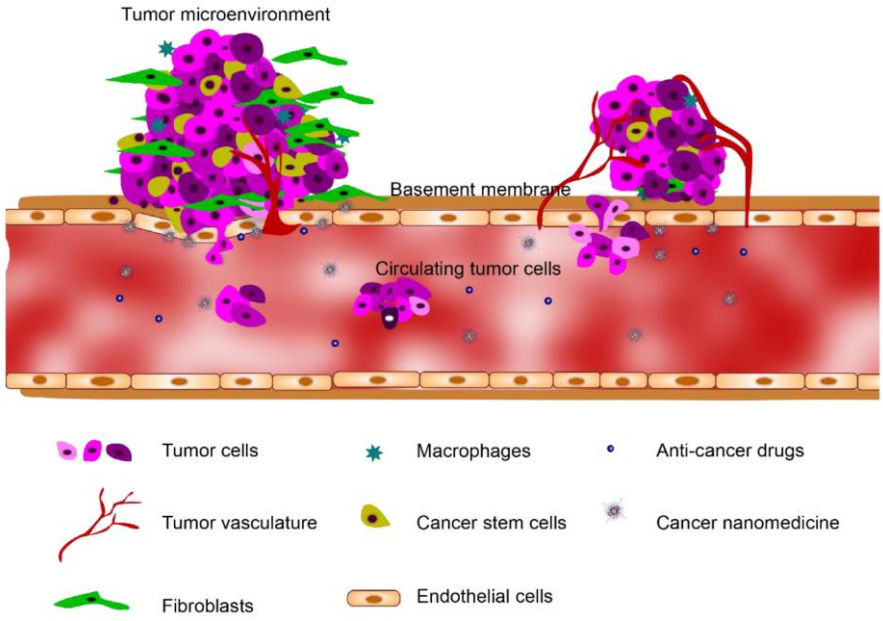

Figure 1.1 The tumor microenvironment (TME) heterogeneously consists of cellular and non-cellular components including the surrounding blood vessels, immune cells, fibroblasts, cancer stem cells and extracellular matrix (ECM).

1.1 Tumor-Stromal Interactions on a Chip

Tumors interact with the surrounding microenvironments incessantly. Tumors typically consist of cancer cells and stromal cells (i.e., fibroblast and immune cells) that are nourished through vascular networking. Understanding the interactions between the tumor, stroma, and vasculature is key to the development of cancer treatments. Especially, the stromal cells and tumor microenvironment modulate tumor sensitivity, which affects tumor cell signaling, proliferation, and drug resistance [10]. Emerging microfabrication techniques enable the reconstitution of complex in vitro co-culture models for studying tumor-stromal interactions. Microfluidic systems provide greater spatial organization through controlled compartmentalization and higher sensitivity and control over the diffusion of soluble factors than traditional Transwell inserts [11]. Several key microfluidic tumor-stromal co-culture models have been developed to investigate the interactions. A

microfluidic device designed to study salivary gland adenoid cystic carcinoma (ACC) cells and CAFs interactions when seeded in a 3D ECM has shown the potential of these platforms as a high-throughput parallel co-culture assay. This approach revealed that CAFs promoted ACC cell invasion into the 3D matrix, identifying a potential target for anti-cancer chemotherapies (Figure 1.2A) [12]. In addition to compartmentalized microfluidics, several other approaches have been developed to study cancer-stromal interactions. Continuous media supplementation allowed for 3D culture of a mixture of lung cancer cells and stromal cells for studies of the cancer-stromal cellular interactions [13]. Recently, microfluidic systems offered a physiologically relevant in vitro tumor spheroid model to study the TME. Integrating 3D tumor spheroids with CAFs in proximity within a hydrogel scaffold exhibited mutual interactions (e.g., growth rate, ECM expression, morphological changes and increased migration in fibroblast) between the spheroids and fibroblasts (Figure 1.2B) [14].

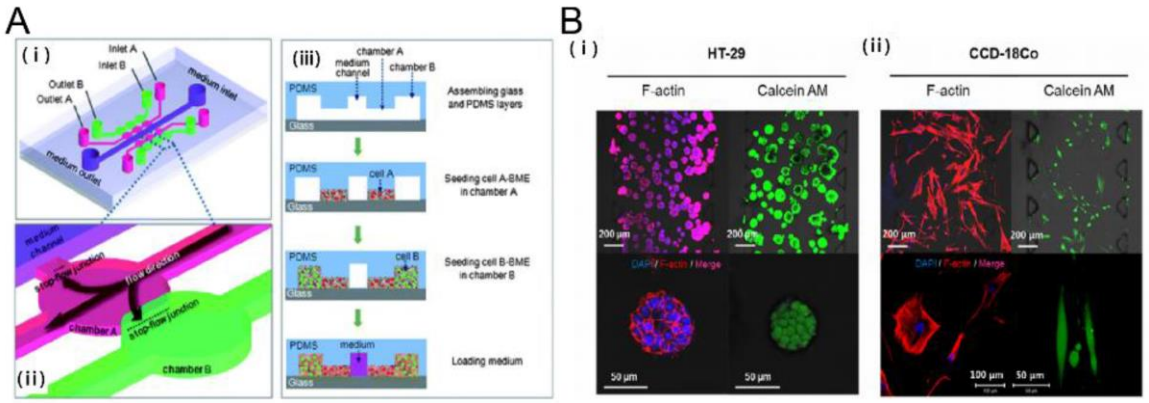

Figure 1.2 Tumor-stromal interactions on a chip. (A) 3D Microfluidic model to investigate the carcinoma associated fibroblast promoted tumor spheroid invasion. (i, ii) microfluidic chip design (iii) cell loading step. Salivary gland adenoid cystic carcinoma cell line (ACC-M) were co cultured with carcinoma associated fibroblasts (CAFs). ACC-M invaded CAF-embedded matrix in a spheroid fashion. However, ACC-M cells did not invade the adjacent matrix when co-cultured with the fibroblast cell line (HFL1). (B) 3D culture of tumor spheroids and fibroblasts in a compartmentalized microfluidic chip. (i,

ii) Fluorescence images of HT-29 tumor spheroids and CCD-18Co human normal fibroblast cell line. HT-29 spheroids and CCD-18Co cells proliferated within the space of the corresponding channels over 5 days, during which their growth and interaction were monitored and characterized.

In addition to fibroblasts, cancer cells actively recruit macrophages to remodel the TME and produce growth factors that increase the invasiveness of cancer cells [15]. MDA-MB-231 metastatic breast cancer cells and tumor-associated macrophages were embedded in collagen I and patterned within a microfluidic channel. It was found in this study that the tumor-associated macrophages invade the neighboring gels containing MDA-MB-231 cells, rather than migrating [16].

As Stephen Paget suggested in the "Seed & Soil" hypothesis in 1889, tumor cells are like seeds being carried in all directions only if they settle into an appropriate soil. Stromal cells and ECM (soil) play a mutual supportive role in the initiation and progression of carcinogenesis (seeds). It remains extremely difficult to fully replicate the complex tumor-stromal interactions, although many microfluidic systems have created successful TMEs to study tumor-stromal interactions within microfluidic chips. Therefore, the critical elements to be mimicked or possibly ignored in a specific TME model should be carefully defined in a study to clarify the domain over which the study is relevant.

1.2 Tumor-Vasculature Interactions on a Chip

Tumor growth and metastasis depend on angiogenic vascular networks, the growth of which are largely guided by chemical signals from tumor cells. Without the formation of new blood vessels, carcinomas neither grow well nor metastasize to colonial distant organs [17]. This rapidly growing angiogenic vasculature around the tumor is highly leaky, forming an aberrant vascular architecture [18]. Several 3D microfluidic systems have been

developed to mimic these characteristics of cancer angiogenesis. Many of these microsystems allowed 2D endothelial monolayers to be vertically established in the side walls, which is designed to better image angiogenic sprouting into a 3D hydrogel. For example, a fibrin gel was either patterned into a microfluidic channel as a provisional matrix for endothelial sprouts or into a side channel for highly malignant human glioblastoma (U87MG). Endothelial cells (ECs) that were attached to the fibrin gel formed a pre-existing wall, 3D sprouting was promoted by the U87MG secretion factors. When compared to lung fibroblast-induced sprouts, U87MG-induced sprouts exhibited aberrant morphology, which is a general characteristic of cancer vasculature (Figure 1.3A) [19]. In addition, leukemic-cell-induced bone marrow angiogenesis has been demonstrated using a microfluidic chip, in which a collagen gel was filled into the middle channel, and U937, HL-60 and K562 cell lines were seeded into an upper channel to study their angiogenic induction. Upon forming the microenvironment of a bone marrow stromal cell line HS5, a unique morphogenic signature of angiogenesis was induced by different types of leukemic cells with or without co-culture with bone marrow stromal cells [20]. In order to study the complex multicellular interactions in a completely three-dimensional setting, a pre-vascularized tumor (PVT) spheroid model was introduced to investigate early events of solid tumor progression. PVT spheroids were formed through direct co-culture of EC and tumor cells and embedded in a fibrin gel mixed with human fibroblasts. After 7 days of culture, PVT spheroids exhibited robust sprouting angiogenesis (Figure 1.3B) [21]. Despite major advances in the development of tumor-angiogenesis-on-a-chip devices, the mechanisms by which tumor cells interact with the TME remain to be further studied.

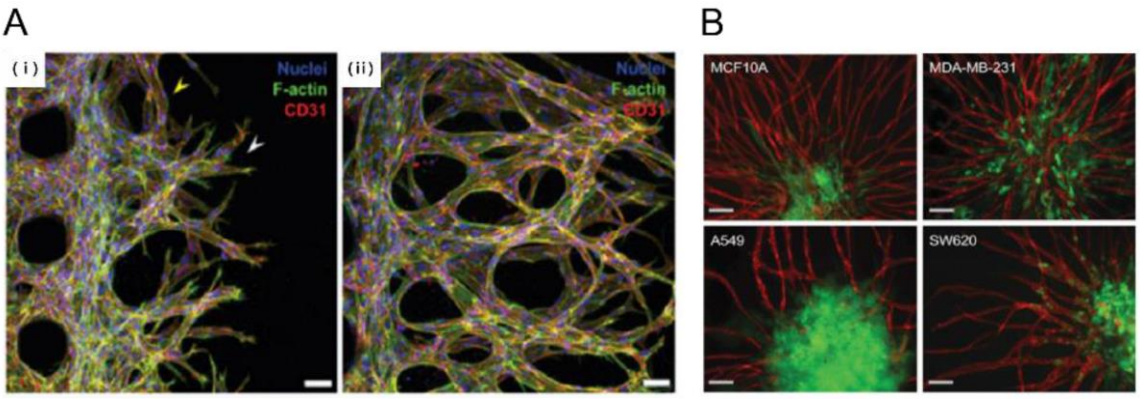

Figure 1.3 Tumor angiogenesis on a chip. (A) Human glioblastoma multiforme cells, (U87MG) were used to induce angiogenic sprouting. Fluorescence image shows angiogenic sprouts grown for 2 and 4 days under co-culture with U87MG cancer cells and human umbilical vein endothelial cells (HUVEC) (i, ii). Scale bar: 50 μm; (B) Pre-vascularized tumor (PVT) spheroid model. PVT spheroid model were introduced breast cancer (MCF10A, MDA-MB-231), Lung cancer (A549) and colon cancer (SW620). Representative fluorescence images of PVT spheroid model shows robust angiogenic sprouting. Various PVT spheroid showed different angiogneic sprouting behavior. Intravasation events were only observed for SW620 cancer cells. Scale bar: 100 μm.

1.3 Cancer Cells Transmigration through Vasculature: Metastasis on a Chip

In metastasis, cancer cells spread locally or distally by traveling through the blood or the lymphatic system to form a new tumor in other regions of the body [22]. This metastatic process involves a broad spectrum of invasion and migration mechanisms that include both single and collective cell migration strategies [23]. During metastasis, cancer cells disseminate to other parts of the body by entering the blood stream (intravasation) and getting out of the blood (extravasation) at proper metastatic sites [24]. Several microfluidic systems have been developed to mimic cancer cell transmigration through an endothelial cell lining. A 3D tumor vasculature interface was recreated in a microfluidic assay to characterize their interactions through tumor cell migration efficacy and endothelial permeability [25]. A microfluidic system was developed to mimic the specificity of human breast cancer metastasis into bone tissue by recreating a vascularized osteo-cell conditioned

microenvironment with BM-hMSC that secreted a bone-like matrix [26]. This was further developed to study human metastatic breast cancer cell extravasation within a perfusable human microvascularized bone-mimicking microenvironment (Figure 1.4A) [27]. The method of implementing an in vitro model of metastasis in human microcirculation was given through multiple steps: early metastatic seeding, arresting, and transendothelial migration (Figure 1.4B) [28]. Recently, a multi-organ microfluidic platform was developed to reconstitute an in vivo microenvironment of lung cancer metastasis. This study successfully reproduced lung cancer growth, invasion, and metastasis to target distant organs including bone, brain and liver (Figure 1.4C) [29].

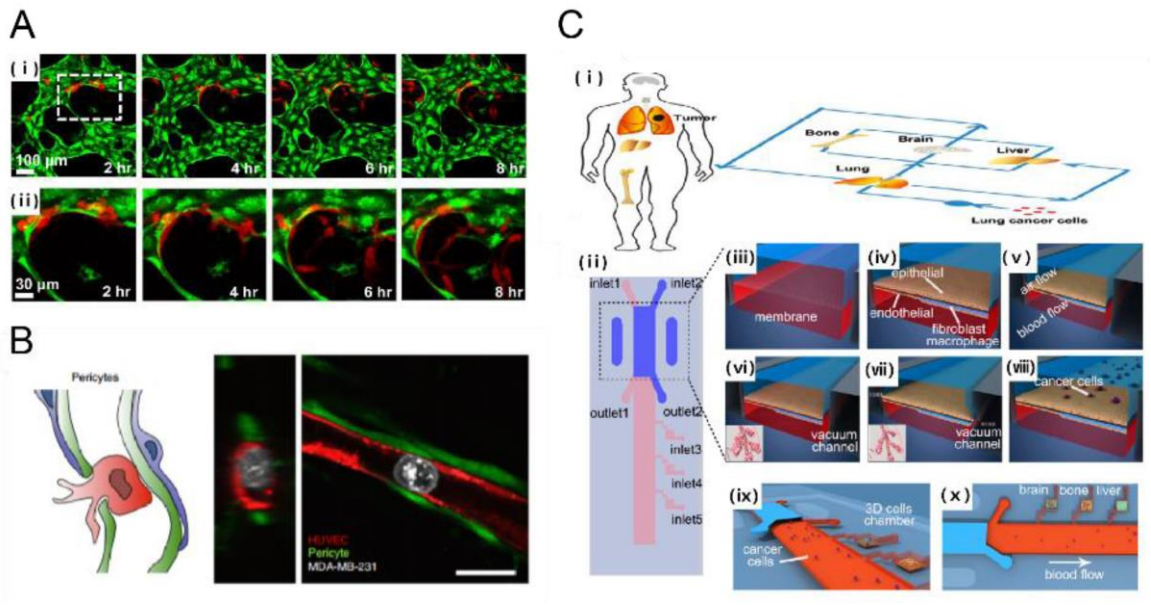

Figure 1.4 Metastasis on a chip. (A) A human 3D vascularized organotypic microfluidic system to study cancer cell extravasation (i) Cancer cell extravasation was monitored in real time within a vascular network (ii) magnified image. Scale bar: 100 μm; (B) Human umbilical vein pericytes were cocultured with human umbilical vein endothelial cells to form pericyte-covered lumens. The extravasation rate from HUVEC-only cultures was significantly higher when compared to HUVEC-pericyte coculture. Scale bar: 20 μm; (C) Design of biomimetic multi-organ chip (i, ii) multi-organ chip included an upstream "lung organ" and three downstream "distant organ" such as bone, brain, liver; (iii, iv) The microfluidic chip was compartmentalized using human epithelial and stromal cells

cultured on separated side of a porous membrane in order to mimic (v–vii) physiological respiration in the microfluidic system; which was followed by the introduction of (viii–x) lung fibroblast cells to investigate lung cancer metastasis to distant organ.

1.4 Tumor-Extracellular Matrix Interaction

The extracellular matrix (ECM), the key non-cellular component of the TME, consists of several distinct components including proteins and glycoproteins [30]. Tumor growth is associated with mechanical alteration in the microenvironment, including increased matrix stiffness and aberrant interstitial fluid flow [31]. Various microfluidic models have incorporated 3D ECM matrix components and hydrogels into compartmentalized channels [32]. Fibrin gels [19], collagen gels [33], and matrigels have been commonly used to reconstitute 3D microenvironments. These gels have the capacity to not only support tumor stroma such as fibroblasts and immune cells, but also to modify diffusion distance that allows for greater spatial control between different cell types. Furthermore, cancer cells in their intrinsic environment interact with a 3D ECM, characterized by physical parameters (e.g., porosity and stiffness) and by chemical parameters (e.g., adhesion site density and bound ligand concentration) [34]. Increased physical parameters of ECM alter the cellular force balance, leading to abnormal cell proliferation [35], , and especially, increase in the rigidity of the matrix activates integrins and promotes Rho/ROCK pathway [36]. The crosstalk between the integrin/Rho pathway and Erk signaling cascade may induce self-sustaining process, leading to neoplastic disorganization of cancer tissue architecture [34]. In addition, it is crucial to note that our understanding of cell migration in 3D ECM is based largely on fibrous matrices, such as collagenous matrix found in the breast and other connective tissues [37]. However, other tissues are composed of non-collagenous, less structured materials [38]. For example, brain ECM is composed of hyaluronic acid and

proteoglycans which form a more amorphous matrix [39]. Therefore, it is important to understand how their unique architecture contributes to tumor growth, and that the systematic consideration of 3D ECM properties should serve as an informative set of design criteria in the TME on a chip.

1.5 Microfluidic Platforms for Cancer Drug Delivery and Screening

3D microfluidic culture models are increasingly being used as prescreening tools for drug discovery including drug delivery and translation in oncology [40]. These models present more pathophysiologically relevant microenvironments of solid tumors in which the direct cell-cell interactions and metabolic mechanisms are better recapitulated in 3D multicellular spheroids than in conventional 2D cell culture models. Conventional routes to screening compounds are a time-consuming and complex procedure [41]. Microfluidic systems have the potential to enable high-throughput drug screening in a controllable and scalable manner [42]. A droplet-based microfluidic system was used to form alginate beads with entrapped breast tumor cells. After gelation, the alginate beads were trapped in a microsieve structure for cell culture in a continuous perfusion system. This microfluidic system maintained a constant location for each bead to allow tumor cells to proliferate and form spheroids. The dose-dependent response of the tumor spheroids to doxorubicin, a common anthracycline, showed a higher survival rate in the multicellular spheroid culture compared to the conventional monolayer culture (Figure 1.5A) [43]. Tumor spheroids have several structural, functional, and physiological similarities to tumors in vivo. 3D tumor spheroids enable them to communicate with each other as well as with their surroundings and provide an optimal environment for the cells to respond like they would in a tumor [44]. Furthermore, the inclusion of stromal cells to tumor cell culture showed a

significantly higher drug resistance compared to when tumor cells were cultured alone [13]. Furthermore, pH and oxygen sensor integrated microfluidic systems allowed the monitoring of the long-term response of T98G human brain cancer cells to several drugs [45]. Recent studies consider the importance of the TME properties when evaluating nanoparticles targeting tumor cells. A tumor-microenvironment on a chip (T-MOC) was used to investigate nanoparticle transport and the resulting variation to delivery efficacy due to changes in the TME properties including cut-off pore size, interstitial fluidic pressure, and tumor tissue microstructure [46]. To recapitulate the complex transport process around a tumor, the T-MOC employed a 3D structure formed by stacking microchannels with a porous membrane inserted. The capillary endothelium was cultured on the top layer, and the tumor interstitium and lymphatics were created in the bottom layer. Furthermore, incorporation of tumor-like spheroids into a microfluidic channel allowed for the real-time analysis of nanoparticle accumulation in pathophysiological flow conditions, showing that the penetration of nanoparticles into the tissue is limited by their diameter and that the retention could be improved by receptor targeting (Figure 1.5B) [47]. To gain a better understanding of cancer drug screening, more physiologically relevant models need to be developed to reconstitute the complex interactions within the TME that is known to increase drug resistance. The majority of the microfluidic systems employed in drug delivery rely on diffusive drug release over an extended time period, as the drug administration period lasts from several hours to weeks. To better mimic a physiological drug release profile, various flow patterns need to be incorporated with multiple cell types that exist in the TME, as pulsatile flow patterns are prevalent in vivo.

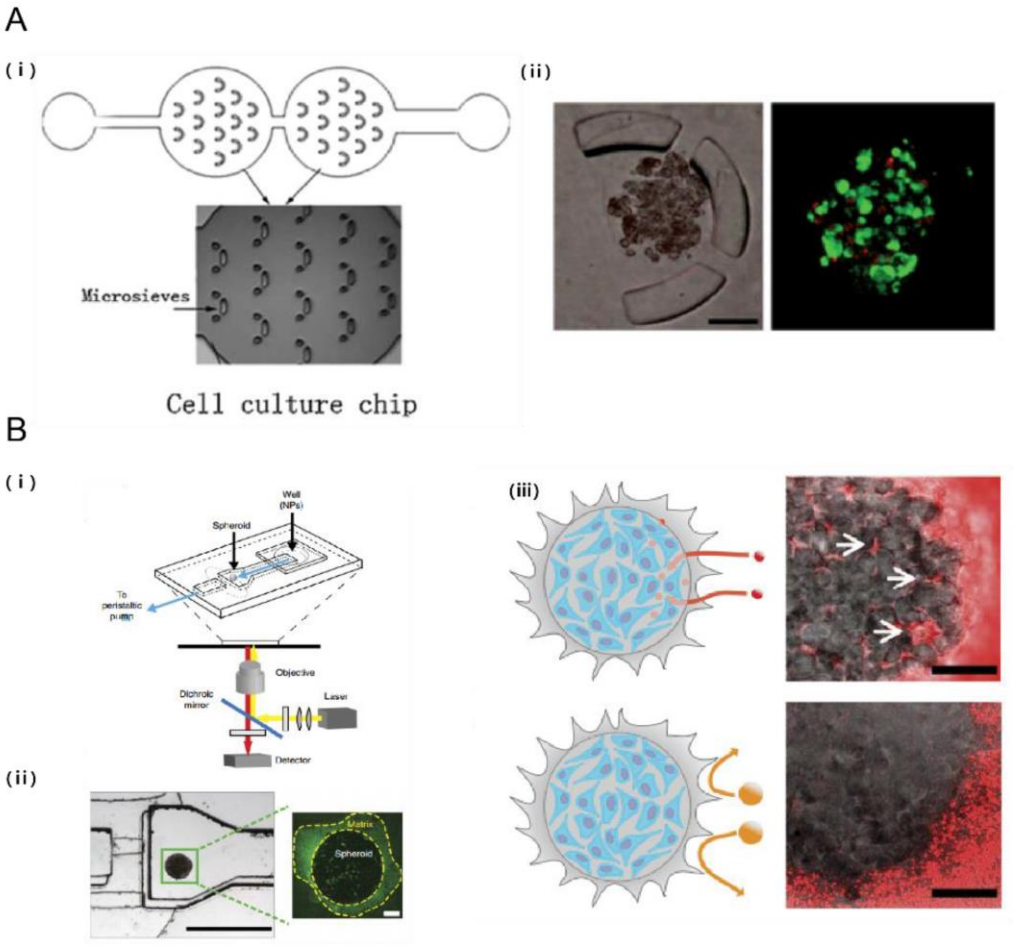

Figure 1.5 Probing the efficacy of drug delivery using TME on a chip. (A) Droplet-based microfluidic system for multicellular tumor spheroid formation and anticancer drug testing. (i) Schematic of the droplet formation and cell culture microfluidic chips. Each chamber contains 14 sieves for alginate droplet trapping; (ii) Breast tumor cells proliferating and forming multicellular spheroids while encapsulated in alginate beads. Tumor cells were perfused with doxorubicin and live/dead assay was assessed. Scale bar: 100 μm; (B) Tumor on a chip provides an optical window into nanoparticle tissue transport. (i) Schematic of the microfluidic device; (ii) MDA-MB-435 breast cancer cell embedded within microfluidic device (iii) Effect of nanoparticle size on tissue accumulation. 40 nm fluorescent PEG-nanoparticles entered the tumor spheroid and accumulated in the interstitial spaces but 110 nm nanoparticles were excluded from the spheroid. Scale bar: 100 μm.

1.6 PDMS and Injection-molded Microfluidic System

Conventional microfluidic platforms have historically utilized soft lithographic fabrication methods with replica-molded polydimethylsiloxane (PDMS) [48]. The advent of PDMS microfluidic systems allowed for unprecedented control over cell patterning and microphysiological conditions with a reduction in the cell and media requirements. Recent advances in microfluidic vascularized tumor co-culturing have exploited soft lithography to fabricate microchannels and compartments to simulate the incorporation of cancerous masses into established vessel networks, the formation of new vessel networks in tumor tissues, and the observation of metastatic intra/extravasation [49]. Unfortunately, soft lithographic fabrication methods have several material and logistical limitations related to their scalability and the accessibility of microfluidic platforms for industrial-scale integration [50]. Although soft lithographic replica molding is one of the most commonly used techniques for pilot-scale production, the expensive and rate-limited fabrication processes that are used render soft lithography unsuitable for industrial-scale mass production [51]. In addition, the lack of an industry standard form factor and the incorporation of many hand-processed fabrication practices introduce challenges for advancing to automated loading, handling, and imaging procedures. Limited attempts at standardizing PDMS microfluidic inputs have not yet seen wide scale implementation. Small molecule adsorption into PDMS also poses a problem for the establishment of controlled dosages for drug development applications. The application of microfluidic organ-on-chip designs to injection molded thermopolymer substrates such as polystyrene (PS) has been a large trend in microfluidics as a means for the production of highly scalable devices that do not exhibit the same adsorptive material limitations of PDMS [51, 52]. Mass-producible injection-molded microfluidic platforms provide a higher degree of

uniformity between devices due to the minimization of human-manipulated production steps that are prevalent in pilot-scale PDMS replica molding. Such methods also allow for the implementation of higher-throughput experimentation and require less time and effort, which could potentially improve the efficiency of drug development.

1.7 Aims and Approaches

This study focused upon five predominant aims in order to address unmet needs in mimicking vascularized tumor microenvironment. The major aims of this study were:

1. To establish an in vitro model of direct interaction between the tumor spheroid and vascular endothelial cells in 3-dimensional and find optimal condition for tumor spheroid formation, tumor spheroid vascularization and tumor vasculature perfusion with natural endothelial morphogenesis in making the lumenized structure.
2. To investigate the characteristic features and response of in vivo TME vasculature; leaky and aberrant tumor vasculature.
3. To evaluate the developed vascularized tumor model for demonstrating a proof-of-concept application of the model for drug screening with varied dose and treatment timing by monitoring tumor spheroid and vasculature simultaneously.
4. To establish an injection-molded plastic array 3D spheroid culture platform, which made of polystyrene (PS) in a standardized 96-well plate format with a user-friendly interface.
5. To demonstrate versatile use of the injection-molded plastic array 3D spheroid culture platform, we developed 3D perfusable blood vessel network and tumor

spheroid assays. In addition, we established a tumor spheroid induced angiogenesis model that can be applicable for drug screening.

Although many in vitro tumor-on-a-chip model have been developed, the three-dimensional vascularized tumor spheroid model that closely recapitulate in vivo tumor microenvironment is still absent. Therefore, we presented a micropathological system of a 3D in vitro perfusable vascularized tumor model that recapitulates the close interactions of tumor spheroids, endothelial cells, and stromal fibroblasts. Also, for tumor-on-a-chip industrial application, by utilizing a standardized injection-molded PS platform and capillary force-based fluid patterning, we introduced a novel injection-molded plastic array 3D spheroid culture (IMPACT) platform, which may serve as a mass-producible platform for wider applications. We propose our platforms as the next generation of tumor-on-a-chip for biological, clinical, and pharmaceutical investigations requiring robust high-throughput and high-content assay.

CHAPTER 2. PDMS 3D CULTURE PLATFORM: VASCULARIZED TUMOR SPHEROID CULTURE

2.1 3D Microengineered Vascularized Tumor Spheroid Model for Drug Delivery and Efficacy Testing

The tumor microenvironment (TME) plays an active role in tumor initiation and development. Tumor cells efficiently recruit endothelial cells (ECs) and other stromal cells (e.g., fibroblasts) through intricate pathways, in turn providing tumor cell growth signals, intermediate metabolites, and favorable environments for tumor progression and metastasis [53]. Tumor growth depends on angiogenesis that occurs with growth factors (e.g., VEGF) secreted by tumor cells [7]. Tumor angiogenesis is one valid therapeutic target of many solid tumors, and particularly of their metastasis [54]. The TME is comprised of cellular and non-cellular components, including surrounding blood vessels, fibroblasts, immune cells, cancer stem cells, and extracellular matrix (ECM) [55]. The elucidation of these complex cellular interactions within the TME remains a key challenge in the treatment of cancer. It is increasingly recognized that cancer should be studied as complex multicellular systems to properly reflect the interactions between malignant and non-malignant cells, not as simplified as conventional models leveraging homogenous collections of neoplastic cells [56]. This interplay between the tumor and stroma has been recognized as a critical characteristic of the TME, and this paradigm is now in turn considered to be a hallmark of cancer research [57].

Nevertheless, most in vitro studies exploit two-dimensional (2D) tumor cell cultures with no consideration of the TME, which is not suitable to study the effects of the complex spatial organization and interaction of tumor-associated cells [58]. While xenograft animal models of cancer can provide essential in vivo characteristics on tumor growth and responses to drug molecules, it remains extremely difficult to accurately mimic the process of human tumorigenesis due to species discrepancies and limited mechanistic approaches of animal models [9]. This challenge highlights the importance of more realistic TME modeling in vitro. Recent advances in engineered TME using multicellular organ-on-a-chip technology have enabled the development of pathologically and physiologically relevant human tumorigenesis models of processes, such as tumor metastasis [27, 59], tumor angiogenesis [60, 61], and tumor-stroma interactions [14, 62].

The multicellular tumor spheroid model is the most advanced, widely used method to mimic the solid TME [63, 64]. Tumor spheroids are compact heterogeneous cellular aggregates that consist of multiple single cells (e.g., epithelial, mesenchymal, endothelial). Distinct from those of 2D cultures and biopsy samples, multicellular spheroids can provide proliferative gradients, reduced drug and gas exchange, and cell–cell and cell–ECM interactions [65]. Therefore, tumor spheroid models are considered the gold standard for avascular in vitro tumor research [66]. To better understand the interaction between cancer cell and endothelial cells within the spheroid, cancer cells – endothelial cell multicellular spheroids have been investigated of their morphology and spatial invasiveness [67]. Indeed, several microfluidic approaches have made important progress toward the recapitulating in vivo TME [68, 69]. Nonetheless, these microfluidic approaches failed to provide sufficiently large enough (as large as 500 μm) tumor spheroid for mimicking a necrotic

core and gradient distributions of critical metabolites and growth factors that can be obtained from solid tumor mass [70]. Multicellular (cancer cells – fibroblasts) spheroid connected with vessel-like tubular structure model evaluated the drug response of paclitaxel and gemcitabine [71]. Unfortunately, as this vascularized TME models did not follow natural endothelial morphogenesis in making the lumenized structure, they were still limited in their ability to reconstitute the characteristic features and response of in vivo TME endothelium; leaky and aberrant tumor vasculature. In addition, there is no in vitro TME models have been reported the direct interactions between tumor spheroids (> 500 μm in diameter) and ECs within a 3D ECM, integrating with 3D perfusable blood vessel network.

Here we present a micropathological system in a 3D in vitro perfusable vascularized tumor model that recapitulates the close interactions of tumor spheroids, ECs, and stromal fibroblasts. We incorporated multicellular tumor spheroids (> 500 μm in diameter) into a microfluidic chip that allows the co-culture of 3D perfusable microvessels exhibiting paracrine interactions with stromal fibroblasts. Subsequently, the tumor spheroid was enveloped by perivascular ECs, which was validated using CUBIC tissue-clearing method that reduces light scattering in biological tissues by lipid removal and refractive index (RI) matching. By this method, we were able to visualize 3D tumor spheroid–vasculature structures. We first cultured and compared cancer cell only and cancer–EC hybrid spheroids, and analyzed their morphological characteristics and relative gene expression. Notably, we found that the cancer–EC hybrid spheroids showed greater pro-angiogenic behavior than the cancer cell only spheroid. We next investigated permeability coefficient of the tumor spheroid associated vasculature and monitored tumor spheroid size and

vasculature area in response to the FDA approved cancer drug; Axitinib using the vascularized tumor model with highlighting the importance of tumor vascularization and revealing the significance of the dose and treatment timing. Such 3D vascularized tumor model could closely recapitulate morphological characteristic of in vivo solid tumor, representing a promising platform for in vitro pre-clinical experimentation.

2.2 Materials and Methods

2.2.1 Cell culture

Human umbilical vein endothelial cells (HUVECs, Lonza) were cultured in Endothelial Growth Medium (EGM-2) and passage 4 was used for the experiments. Red fluorescent protein (RFP) expressing HUVECs were obtained from Anigio-Proteomie (Boston, MA). Normal human lung fibroblasts (LFs, Lonza) were cultured in Fibroblast Growth Medium (FGM-2, Lonza) and passage 6 was used for the experiments. Human hepatocyte carcinoma cells (HepG2, Korean Cell Line Bank) were cultured in DMEM supplemented with 10 % FBS, penicillin (100 U/ml) and streptomycin (100 U/ml). All cells were maintained in a humidified incubator at 37 ℃ and 5% CO_2. In this study, we prepared four kinds of spheroids: a HepG2 monoculture spheroid HepG2 and HUVEC co-culture spheroid with different ratio (1:4, 1:1, and 4:1) They were grown in a 96-well plate with U-shaped bottom wells (Sumitomo Bakelite, Tokyo, Japan). For suspension culture, EGM-2 medium was used for the cancer monoculture spheroid and the co-culture spheroid. All cell suspensions were prepared for total 5000 cells and mixed with 1% volume ratio of Matrigel in 200 μL of medium. After pre-culturing in a 96-well plate, a spheroid was introduced into the VTS device. We used 4 to 6 days cultured spheroid for the experiments.

2.2.2 Cell seeding in the microfluidic platform

A tumor spheroid was collected from a 96-well plate using a 200 μL pipette tip and mixed with HUVECs suspension in the fibrinogen solution, at a concentration of 5×10^6 cell/mL. The cell and spheroid solution were mixed with thrombin (0.5 U/ml, Sigma) and then immediately introduced into a central channel and settled at the bottom of the channel (Figure 2.1). Because the diameter of the spheroid (> 500 μm) was greater than the channel height (150 μm), the spheroid was set to be stationary at the bottom of the channel. When the spheroid-ECs gel suspension was injected, an excess amount of the HUVEC and gel flowed out through the other two outlet of center channel and did not leak to media channel. The spheroid-ECs suspended gel was allowed to clot for 5 min at room temperature. Next, LFs were suspended in the fibrinogen solution, mixed with thrombin (0.5 U/mL, Sigma) and then immediately injected into left and right stromal cell culture channel. The inlet reservoirs of the cell culture medium channels were loaded with EGM-2 media, and then the culture medium was aspirated at the other reservoir to fill media channels. Following loading all four reservoirs, the microfluidic platforms were incubated at 37 ℃ and 5% CO_2.

2.2.3 Fabrication of the microfluidic device

The microfluidic device was fabricated with PDMS (poly dimethysiloxane, Sylgard 184, Dow Corning) using soft lithography and replica molding. The microfluidic device was modified from a previously reported device from our group. The channels were separated by micro-posts with 150 μm heights and 100 μm intervals. Slide cover glass (50 mm x 70 mm, Matsunami) and PDMS were covalently bonded to each other by air plasma treatment (Fetmo Science). 120 μm thick structure was patterned on the silicon wafer by

photolithography with SU-8 150 photoresist (MicroChem). The PDMS base mixed with a curing agent at a ratio of 10:1 (w/w) was poured on the silicon wafer and cured for 3 hour on a 90℃ hotplate. PDMS was detached from the wafer when fully solidified. Using biopsy punch 1 mm and 6 mm, cell injection ports and reservoirs for culture media were punched out. Gel injection port also punched out by biopsy punch 1mm; used for loading cancer spheroid and medium. After bonded, the device was stored in a 80 ℃ dry oven for 3 days to be completely cured and to make its surface hydrophobic.

2.2.4 CUBIC tissue clearing

ScaleCUBIC-1 (reagent 1) was prepared as a mixture of 25 wt% urea (Nacalai Tesque Inc., 35904-45, Japan), 25 wt% N,N,N',N'-tetrakis(2-hydroxypropyl) ethylenediamine (Tokyo Chemical Industry CO., LTD., T0781, Japan), and 15 wt% polyethylene glycol mono-p-isooctylphenyl ether/Triton X-100 (Nacalai Tesque Inc., 25987-85, Japan). ScaleCUBIC-2 (reagent 2) was prepared as a mixture of 50 wt% sucrose (Nacalai Tesque Inc., 30403-55, Japan), 25 wt% urea, 10 wt% 2,20,20'-nitrilotriethanol (Wako Pure Chemical Industries Ltd., 145-05605, Japan), and 0.1% (v/v) Triton X-100. To prevent loss of 3D blood vessels and spheroid information, we used CUBIC tissue-clearing protocols based on hydrophilic reagents that preserve fluorescence. After sample fixation, we introduced the CUBIC 1 solution into the medium channel for 1 week and conducted immunohistochemistry analysis. CUBIC 2 (RI-matching) solution was introduced 1 day before confocal imaging.

2.2.5 Quantitative RT-PCR

RT-PCR quantitative analysis of HepG2, and HUVEC was conducted using an indirect transwell co-culture system. Total RNA was extracted from cells using TRIzol (Invitrogen) according to the manufacturer's instructions. Complementary DNA was then synthesized from the extracted RNA using Superscript Ⅲ First-Strand Synthesis System (Invitrogen). Quantitative Real-time RT-PCR was performed with SYBR Green PCR Master Mix (Applied Biosystems, USA) using ABI 7300 Real time PCR system (Applied Biosystems, USA). Relative quantification of target mRNA expression levels was determined by 2(ΔΔ threshold cycle) (2−ΔΔCT) method. The expression level of each gene was normalized to GAPDH. At least three independent experiments were performed. The sequences of primers used are included in Table.

Table 1. Primers used for qRT-PCR and RT-PCR.

Genes	Forward sequence	Reverse sequence
GAPDH	TGATGACATCAAGAAGGTGGTG	ACCCTGTTGCTGTAGCCAAAT
PTEN	CAGCCATCATCAAAGAGATCG	TTGTTCCTGTATACGCCTTCAA
P53	GGGTTGCAGGAGGTGCTTACGC	TGCTGAGGAGGGGCCAGACC
E-cadherin	GCTGGACCGAGAGAGTTTCC	CGACGTTAGCCTCGTTCTCA
α-SMA	CAAGTGATCACCATCGGAAATG	GACTCCATCCCGATGAAGGA
CXCR4	GGTGGTCTATGTTGGCGTCT	ACACAACCACCCACAAGTCA
CXCR7	GAGGCTCCTTTCTGCAGTGTAT	TTCTGAGGCGGGCAATCAA
CXCL12	AGATGCCCATGCCGATTCTT	AAGGGCACAGTTTGGAGTGT
VEGFR2	CGGTCAACAAAGTCGGGAGA	CAGTGCACCACAAAGACACG

PECAM1	GTGCTGCAATGTGCTGTGAA	GCTTGGTCCAAAATGCCTGG
VE-cadherin	CTTCACCCAGACCAAGTACACA	AATGGTGAAAGCGTCCTGGT
vWF	CGTGGTCCTGAAGCAGACATA	TTGCTGCTGGTGAGGTCATT
VEGF-A	ACGAAAGCGCAAGAAATCCC	CTCCAGGGCATTAGACAGCA
MCP-1	AGTCTCTGCCGCCCTTCT	GTGACTGGGGCATTGATT
ICAM1	GGGAGCTTCGTGTCCTGTAT	ACAGAGGTAGGTGCCCTCAA

2.2.6 Imaging

The 3D reconstruction and cross section of the vessels were imaged using a confocal microscope (Olympus FV1000). The microscope and charge-coupled device (CCD) camera were controlled by MetaMorph (MolecularDevice, USA) software for time-lapse imaging.

2.2.7 Permeability coefficient measurement

To calculate the permeability coefficient, fluorescence images of FITC-dextran (10 kDa and 70 kDa) solutions were introduced into one of the two remaining media reservoirs. An open, perfusable microvessel allowed solution perfusion into the lumen. 10 x magnification pictures were obtained at 10 second interval over 10 min using time-lapse mode in FV1000.

The derivation process for this equation was detailed in a previous paper from our group [72]. The permeability coefficient P was derived using the equation below:

$$P=1/I_W \times (dI/dt)/I_j$$

where I_W is the length of vessel wall from the micropost that separates the microvessel from the perivascular region, I_j is the mean intensity in the microvessel region and I is the total intensity in the perivascular region.

2.2.8 Statistical methods

Prism (GraphPad, USA) was used for one-way ANOVA analysis with Tukey's post-test. *** denotes $p<0.001$, ** denotes $0.001<p<.01$, * denotes $0.01<p<0.05$. For significant testing between two conditions non-paired student's t-test as used. All data were expressed as the mean ± standard deviation (SD).

2.3 Results

2.3.1 Self-assembled 3D vascularized tumor spheroid model

Tumor development occurs in two stages. When the tumor is relatively small, there is no development of neovessels yet to provide nutrients and oxygen to tumor cells; however, as the tumor grows, tumor cells stimulate ECs to initiate angiogenesis for tumor vascularization. The interaction between the tumor and blood vessels ultimately leads to the systemic spread of malignant tumor cells through the whole body (i.e., metastasis). To engineer a vascularized tumor spheroid (VTS) model at a chip level, we loaded a tumor spheroid and HUVEC suspension mixed with fibrin gel into the center channel of our VTS chip (Figure 2.1). We first demonstrated that the growth of the tumor spheroid within fibrin

matrix. Assessment of the spheroid growth in the device 5 days after implantation demonstrated significant growth of the spheroid (> 115%). Following HUVEC elongation at day 1, the formation of the vascular network and lumen structures were observed after 3–4 days (Figure 2.2). Further development of the microvascular network (μVN) resulted in a densely interconnected microvascular system by day 5. To clearly present the 3D blood vessels and spheroid in our VTS chip, we applied CUBIC tissue clearing method that uses hydrophilic reagents to preserve fluorescence, allowing accurate 3D signal visualization and quantification of the vascularized tumor spheroid. This approach significantly increased z-direction penetration imaging depth (132 ± 19 to 384 ± 10 μm) while maintaining evenly distributed DAPI signals in the transverse direction (Figure 2.3).

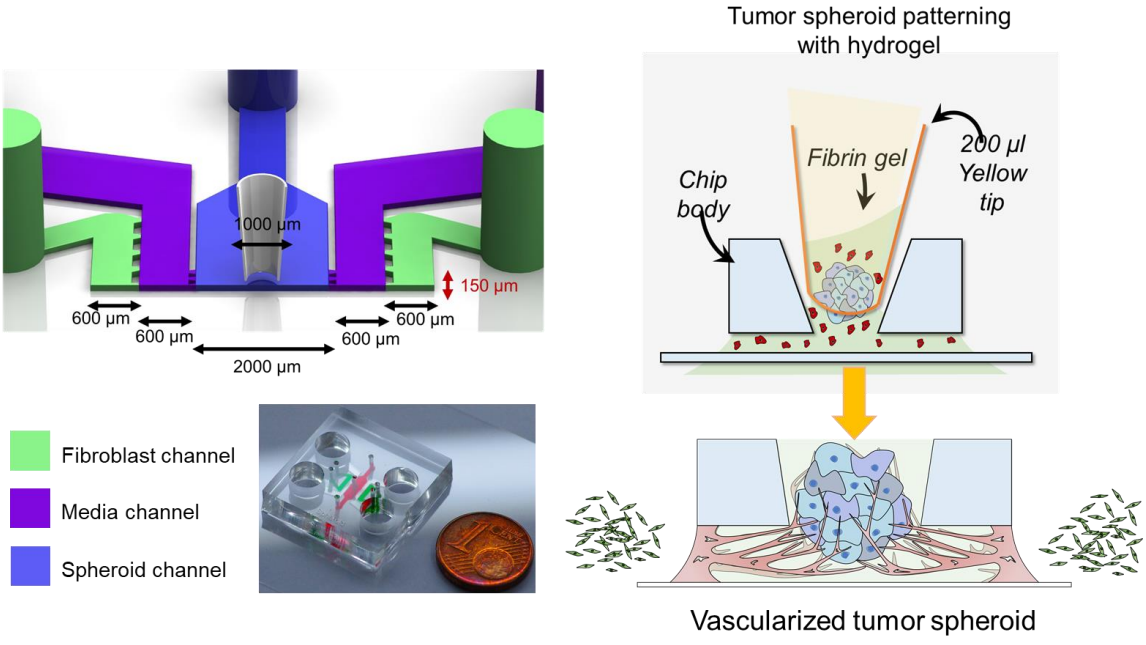

Figure 2.1 In vitro three-dimensional vascularized tumor model. Schematic representation of microfluidic design for in vivo like 3D vascularized tumor formation by

tumor spheroid and ECs mixture in the center channel under paracrine interactions with stromal fibroblasts in the outermost side channels.

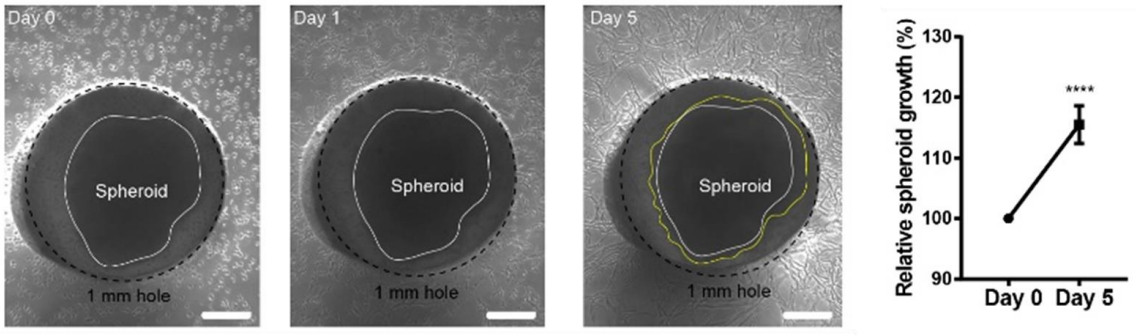

Figure 2.2 Bright field images of the development of vascularized tumor spheroid, composed of tumor spheroid enveloped by endothelial cells. White and yellow lines indicate tumor spheroid area. Scale bars, 200 μm.

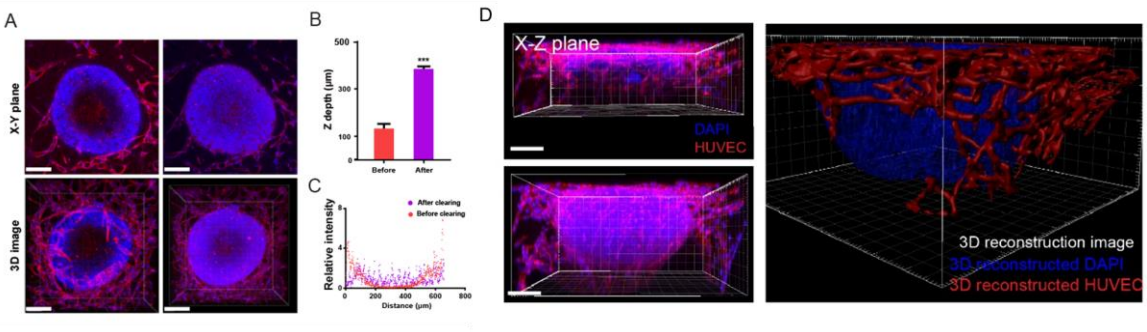

Figure 2.3 (A) Representative confocal images compare before (left line)/after (right line) clearing in the same sample. CUBIC tissue clearing does not lead to volume changes. Scale bars, 150 μm. (A, below) 3D reconstruction image of vascularized tumor. Tumor spheroid is enveloped by blood vessels. (B) Before/after clearing comparison of z axis imaging depth. (C) Before/after clearing comparison of xy plane relative intensity according to distance. (D) Before tissue cleared confocal image of vascularized tumor spheroid (left, top). After tissue cleared vascularized tumor spheroid (left, bottom) and 3D reconstruction image of vascularized tumor spheroid (right).

2.3.2 Morphological and relative gene expression characterization of cancer only vs. cancer– EC hybrid spheroids

We investigated the significance of cancer – EC co-culture in spheroid formation and relative gene expression change. We used HepG2 (human hepatocellular carcinoma) with human umbilical vein endothelial cell (HUVEC) cell lines to form the cancer specific hybrid spheroids. Spheroid formation and growth were investigated with varied cancer-to-EC seeding ratios (cancer cells only, 4:1, 1:1, and 1:4) for a total of 5,000 cells. Tissue-clearing by CUBIC allowed us to investigate spheroid volume, sphericity and HUVEC volume. In HepG2, the spheroid volume significantly decreased as the HUVEC ratio increased (1:1 and 1:4). The HepG2:EC 1:1 ratio spheroid exhibited the greatest sphericity, showing a significant morphological difference compared to the cancer-only spheroid (Figure 2.4A). The mixture of HepG2 EC spheroids showed that as the EC ratio increased, ECs tend to aggregate at the center of the spheroid. To further explore tumor–EC interaction, we examined the expression of tumor suppressor genes (PTEN and p53), epithelial-mesenchymal transition (EMT) markers (E-cadherin and alpha smooth muscle actin (α-SMA). When HepG2 cells were co-cultured with ECs by using Transwell, PTEN and p53 mRNA expression was significantly downregulated compared to the tumor monoculture, reflecting cancer aggressiveness, which plays a key role in the pathogenesis of human cancers in vivo. E-cadherin expression was significantly down-regulated, whereas SMA expression was significantly up-regulated in HepG2 compared to tumor monoculture controls (Figure 2.4B). This result indicates that HepG2 cells can increase their aggressiveness when co-cultured with ECs, causing a change in the signaling cascade. Furthermore, we investigated the expression of cytokine CXCL12 (stromal-derived factor

1α) and its receptor CXCR4, which are a crucial axis in cancer tumorigenesis and progression. HepG2 co-cultured with ECs showed higher CXCL12/CXCR4 expression compared to the cancer mono-culture condition.

To further investigate EC-cancer interaction, we checked EC angiogenic markers (vascular endothelial growth factor receptor 2 [VEGFR2], VE-cadherin, PECAM1, and VEGFA) using Transwell culture. When HUVECs were co-cultured with HepG2 cells, the relative mRNA expression of VEGFR2, VE-cadherin, and VEGFA were significantly upregulated compared to that of HUVEC monoculture. The mRNA expressions of CXCL12 was highly upregulated when co-cultured with HUVECs. In particular, von Wilebrand factor (vWF) expression was dramatically higher under both tumor co-culture conditions than in the HUVEC monoculture (Figure 2.5).

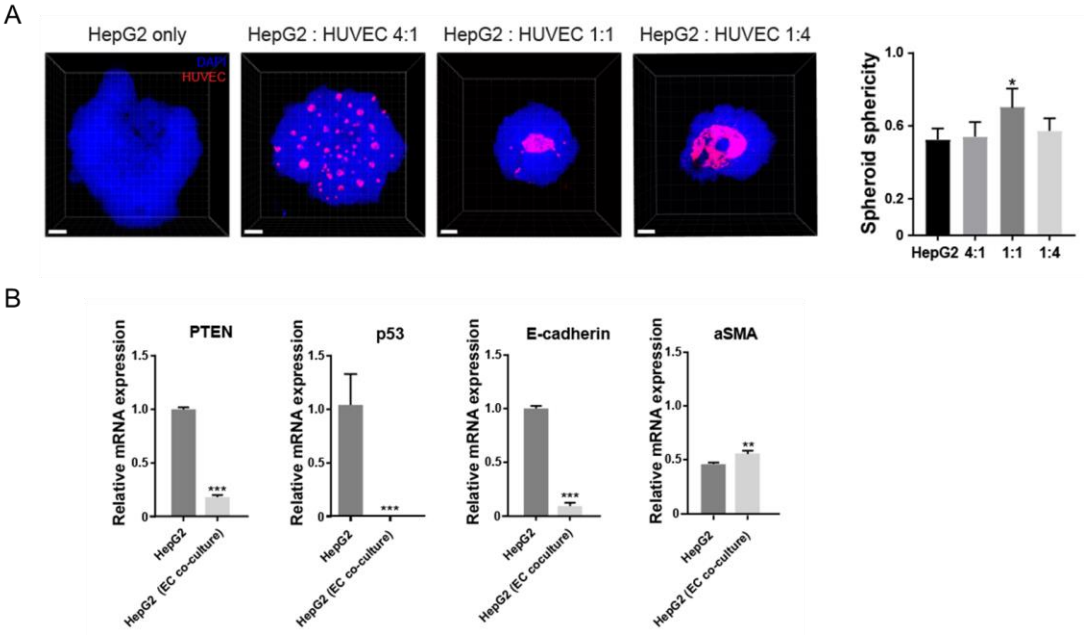

Figure 2.4 Multicellular tumor spheroid characterization. (A) Representative confocal images of HepG2 – ECs spheroid with different cell ratio and spheroid sphericity of different cancer: EC ratios. All spheroid were fixed at day 5. (Scale bars, 100 μm. n=4-6).

(B) RT-PCR results of cancer cell monoculture and cancer cell co-cultured with ECs. Gene analysis considered markers 1) PTEN, 2) p53, 3) E-cadherin, 4) α-SMA, 5) CXCL12 and CXCR4.The internal standard housekeeping gene was GAPDH. (n=3-4).

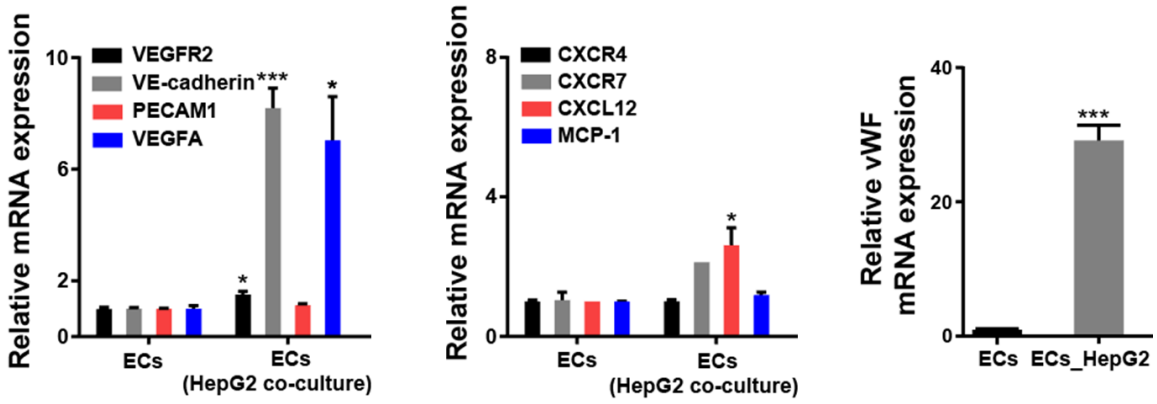

Figure 2.5 RT-PCR results of ECs monoculture and ECs co-cultured with tumor (HepG2) at day 2.

2.3.3 Angiogenic potential of cancer cell only vs. cancer– EC hybrid spheroid in the VTS model

We next evaluated whether the effects of the cancer-EC hybrid spheroid on angiogenesis acceleration. HepG2-EC (1:1 ratio) hybrid spheroids significantly increased blood vessel volume compared to cancer-only spheroids, indicating that the cancer–EC hybrid spheroids accelerate angiogenesis and that this model may be useful for better modeling of the initial primary or micrometastatic stages of solid tumor progression (Figure 2.6).

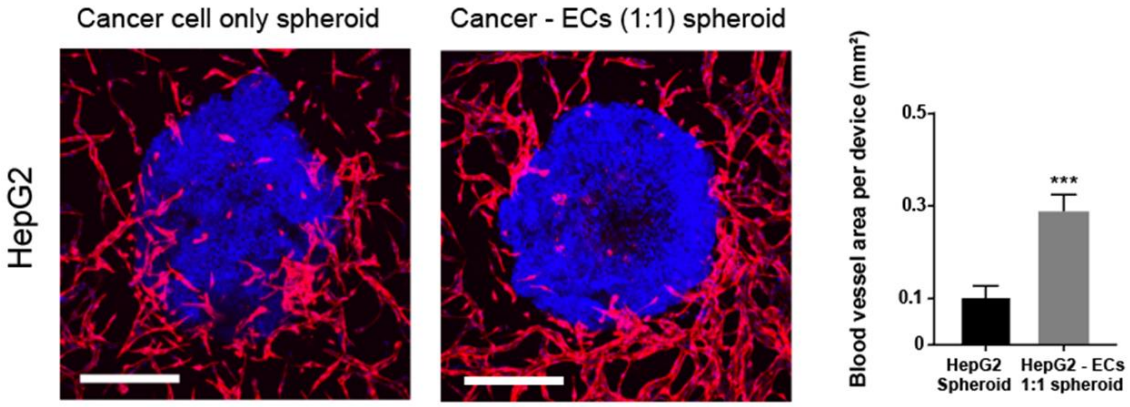

Figure 2.6 Representative confocal images compared total blood vessel volume induced by vascularized tumor model of cancer cell only (HepG2) spheroid and cancer cells HepG2 – ECs spheroid. (Scale bars, 400 μm. n=4-6).

2.3.4 Evaluation of vascularized tumor spheroid permeability

Tumor vasculature is generally abnormal with aberrant branching and leaky vessel walls. Based on our previous findings (spheroid sphericity and volume and tumor marker expression), we decided to use a cancer-EC hybrid spheroid with 1:1 ratio in our next experiments. Especially, HepG2–EC hybrid spheroids exhibited highly interconnected microvessel networks and interactions between blood vessels and the tumor spheroid. Therefore, we used the HepG2–EC hybrid spheroid for further permeability and drug delivery experiments. Permeability coefficients were determined by introducing solutions containing fluorescein isothiocyanate (FITC)–dextran tracers into the vasculature (10 and 70 kDa), and confocal imaging at 10-s intervals (Figure 2.7A). We then calculated apparent permeability, as described in the Methods. As shown in Figure 2.7B, the mean apparent permeability value of the vasculature only (with no tumor spheroid) was 1.80×10^{-5} cm/s, significantly lower than that of the HepG2-EC hybrid spheroid (5.93×10^{-5} cm/s). Interestingly, the addition of 50 and 100 ng/mL extrinsic tumor necrosis factor-alpha (TNF-

α) produced no significant difference (5.65×10^{-5} and 8.48×10^{-5} cm/s, respectively) when compared to HepG2-EC hybrid spheroid co-cultured condition (5.93×10^{-5} cm/s), but there was a significant difference when compared to the vasculature only; this suggests that TNF-α serves as a key factor in increased vascular permeability. In addition, when ECs were co-cultured with HepG2 cancer cells, ICAM-1 mRNA expression was significantly upregulated compared to monoculture HUVEC, indicating that increased vascular permeability was closely related to ICAM-1 expression (Figure 2.7C). We then introduced 70 kDa FITC–dextran tracers, a greater molecular weight than 10 kDa, into the vascular network. Permeability coefficient values decreased as the molecular weight of FITC–dextran increased; this result was consistent with those of previous studies. The addition of 70 kDa FITC–dextran yielded no significant difference in the permeability coefficient between vasculature only and HepG2-EC hybrid co-culture model (Figure 2.7D). However, we observed focal intercellular openings in the vasculature, especially adjacent to the tumor spheroid (region of interest [ROI] 1; < 200 μm of the tumor spheroid boundary) (Figure 2.7E). The number of intercellular openings significantly decreased when farther from the tumor spheroid boundary (ROI 2; > 200 μm from the tumor spheroid boundary). Thus, ECs located near tumor tissue, may have had loose interconnections, demonstrating the abnormality of tumor-associated vessels. Furthermore, we used 45 nm fluorescently-labeled silica NPs to show NP transport and distribution throughout the vasculature using a syringe pump at 450 μL/h. NPs gradually filled and distributed throughout the vasculature. NPs penetrated through the endothelial pores, corresponding to focal intercellular openings in the vasculature, which is a hallmark of tumor associated vasculature (Figure 2.8).

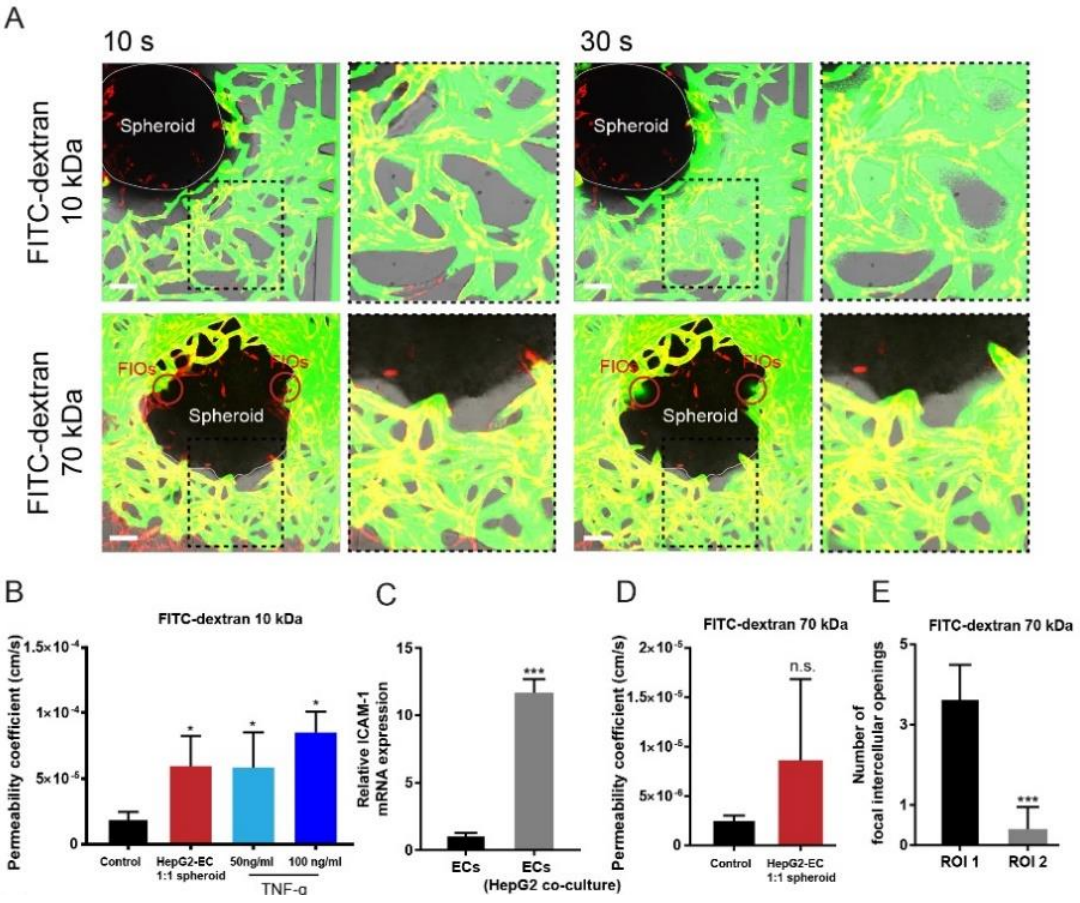

Figure 2.7 Evaluation of vascularized tumor spheroid: permeability measurement and nanoparticle delivery. (A) Time series fluorescence micrographs were taken and analyzed for intensity changes in the perivascular region to measure permeability. After cell culture medium was removed, FITC-dextran (10kDa, 70kDa) solution was introduced and image were captured every 10 s. Red circles in bottom images represent focal intercellular openings (FIOs) (Scale bars, 100 μm) (B) The graphs shows permeability coefficient for 4 different conditions (10 kDa) (n=5-6). (C) The graphs shows permeability coefficient for two conditions (70 kDa). (D) qRT-PCR result of ICAM-1 mRNA expression (n=3-4) (E) Number of focal intercellular openings. [ROI] 1; < 200 μm of the tumor spheroid boundary and [ROI] 2; > 200 μm of the tumor spheroid boundary (70 kDa).

2.3.5 Axitinib performance in the vascularized spheroid tumor model

Next, we determined the antitumor and anti-angiogenic activities of Axitinib, a Federal Drug Administration (FDA)-approved drug, in our VTS model. Axitinib is a potent inhibitor of two receptors involved in angiogenesis: VEGFRs 1, 2, and 3, and platelet-derived growth factor receptor (PDGFR). We administered Axitinib-containing media in the early and late stages of tumor vascularization and refreshed every 24 hours for 3 days. In the early stage, Axitinib was administered prior to formation of the 3D vascular network adjacent to the tumor spheroid (Figure 2.9A). We delivered 0, 1, and 10 nM Axitinib in the early stage of the tumor spheroid model (Figure 2.9B). The tumor spheroid area was not significantly different between vehicle controls with 1 and 10 nM Axitinib treatment (Figure 2.9C). However, Axitinib significantly reduced the blood vessel area and increased the number of disconnected blood vessels in a dose-dependent manner, indicating the anti-angiogenic effect of Axitinib is reproduced in our model (Figure 2.9D and E). In contrast, when Axitinib was administered in the late stage (day 4) (Figure 2.9F), following vascularization, the area of the tumor spheroid was significantly smaller than vehicle control following 10 nM Axitinib treatment, demonstrating the antitumor activities of Axitinib (Figure 2.9G and H). This result may be attributed to the direct interaction between perfused blood vessels and the tumor spheroid. The blood vessel area was significantly decreased and regressed in a dose dependent manner under our experimental conditions, whereas the number of disconnected blood vessel between the control and 1 nM Axitinib treatment group did not show a significant statistical difference. This result indicates drug resistance of tumor vasculature may serve as an irrigation system toward the tumor spheroid. In higher Axitinib dosage, blood vessels regressed and number of

disconnected blood vessel increased significantly compared to the vehicle control condition (Figure 2.9I and J). We note that the VTS chip could provide reliable and reproducible response of Axitinib treatment regarding spheroid size and blood vessel area monitoring, since the spheroid and EC gel mixture was gently loaded into center channel (Figure 2.10).

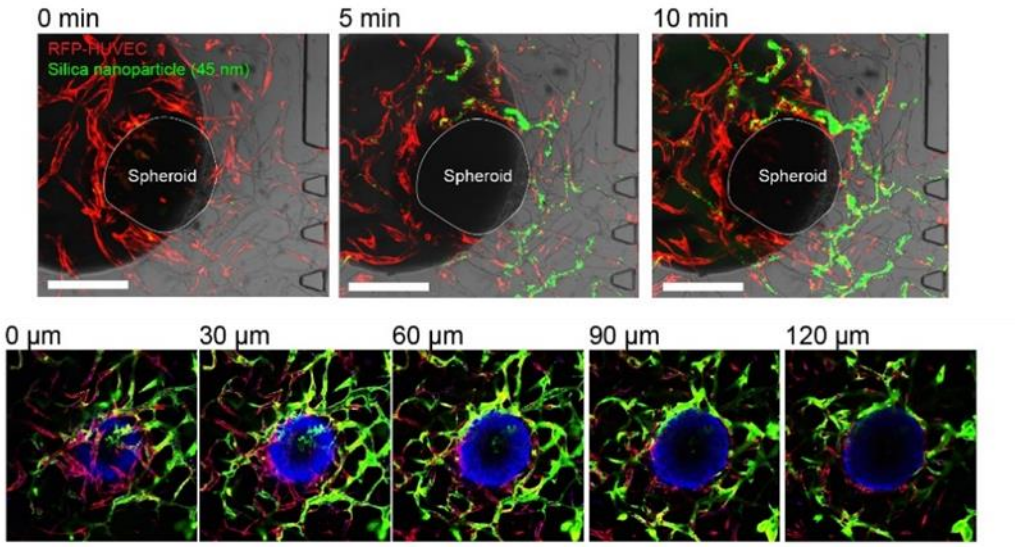

Figure 2.8 Silica nanoparticle (NP) delivery through vasculature of vascularized tumor model at 3 time-points (top). Scale bars, 400 μm. Silica nanoparticle distribution at different z sections (bottom).

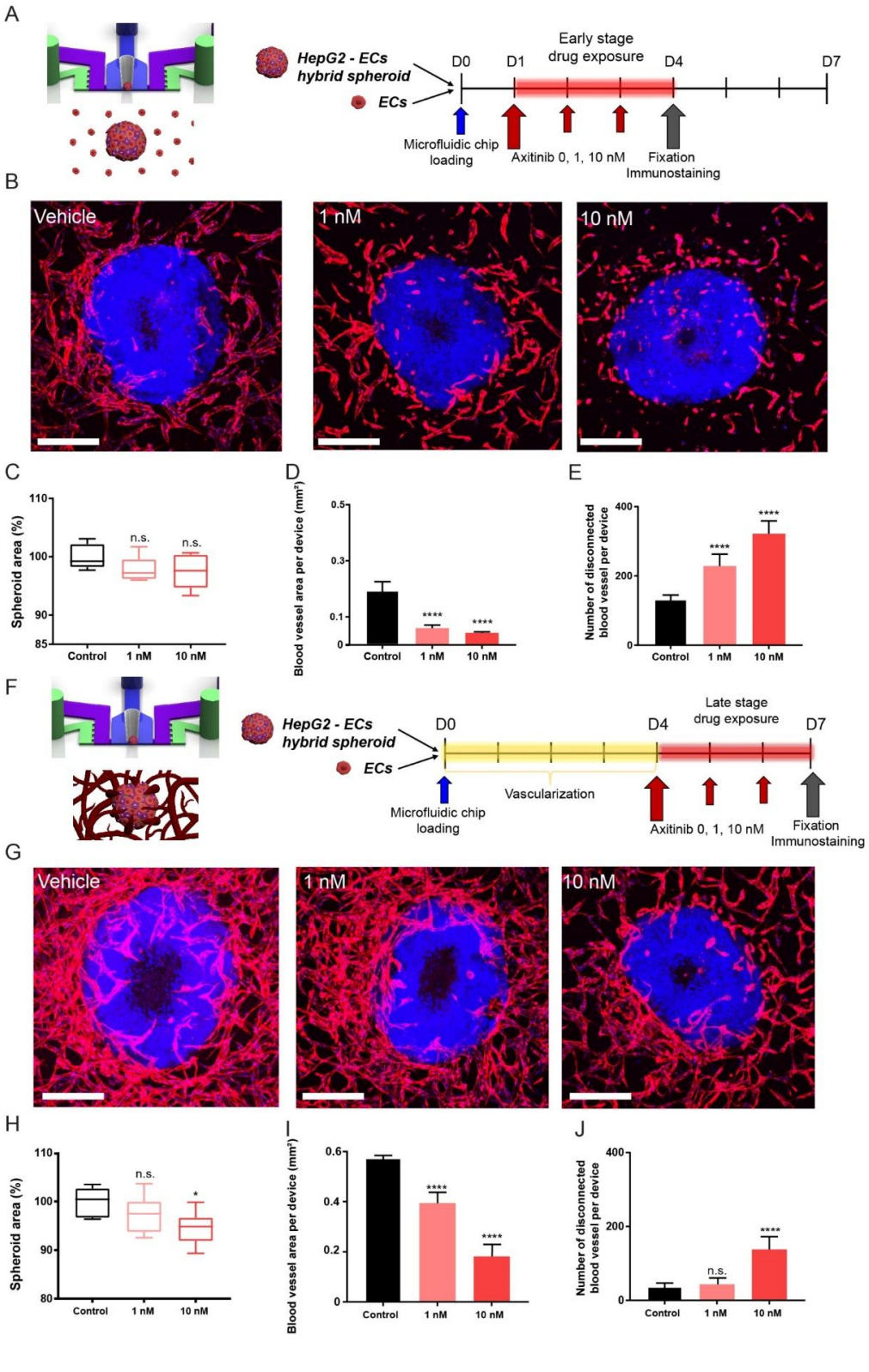
A
HepG2 - ECs hybrid spheroid
ECs
D0
D1
Early stage drug exposure
D4
D7
Microfluidic chip loading
Axitinib 0, 1, 10 nM
Fixation Immunostaining
B
Vehicle
1 nM
10 nM
C
Spheroid area (%)
n.s.
n.s.
Control
1 nM
10 nM
D
Blood vessel area per device (mm²)
****
****
E
Number of disconnected blood vessel per device
****
****
F
HepG2 - ECs hybrid spheroid
ECs
D0
D4
Late stage drug exposure
D7
Vascularization
Microfluidic chip loading
Axitinib 0, 1, 10 nM
Fixation Immunostaining
G
Vehicle
1 nM
10 nM
H
Spheroid area (%)
n.s.
*
I
Blood vessel area per device (mm²)
****
****
J
Number of disconnected blood vessel per device
n.s.
****

Figure 2.9 Antiangiogenesis and antitumor activities of Axitinib in VTS model. (A) Timeline of cancer drug treatment experiment. In the early stage of vascularized tumor model, Axitinib were introduced into the reservoirs a day after spheroid – ECs gel suspension injected to the central channel. (B) Representative confocal images show Axitinib dosage dependent response of spheroid and vasculature in the early stage of VTS model. Scale bars, 300 μm. Relative spheroid area (C), blood vessel area (D), number of disconnected blood vessel (E) in response to two different dosage of Axitinib (1 nM, 10 nM) at the early stage of VTS model. (F) Timeline of cancer drug treatment experiment. In the late stage of vascularized tumor model, Axitinib were introduced into the reservoirs 4 days after spheroid – ECs gel suspension injected to the central channel, which vasculature fully enveloped HepG2 – ECs hybrid spheroid. (G) Representative confocal images show Axitinib dosage dependent response of spheroid and vasculature in the late stage of VTS model. Scale bars, 300 μm. Relative spheroid area (H), blood vessel area per device (I), number of disconnected blood vessel per device (J) in response to two different dosage of Axitinib (1 nM, 10 nM) at the late stage of VTS model.

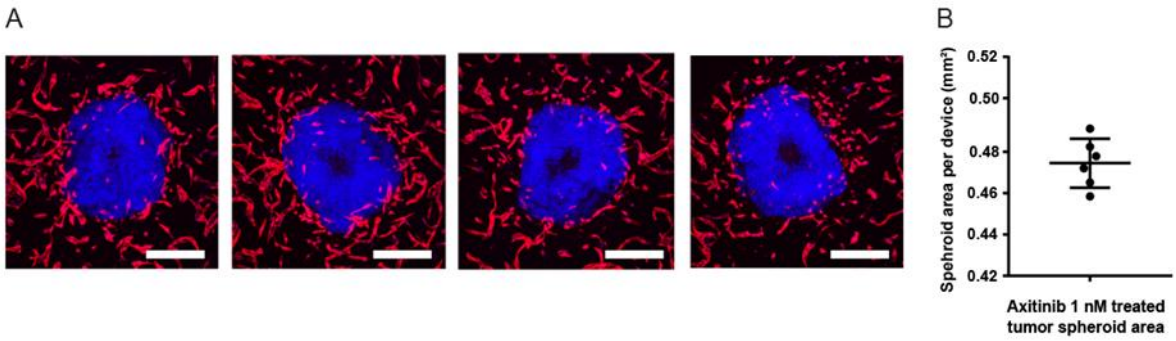

Figure 2.10 Monitoring reliable and reproducible response of axitinib treatment. (A) Representative confocal images show 1 nM axitinib treated vascularized tumor spheroid conditions. (B) Spheroid area per device. Scale bar: 300 μm.

2.3.6 Reconstituting lymphatic endothelial cell-blood vascular endothelial cell incorporated vascularized tumor spheroid in vitro

Lymphatic and blood vessels form an intricate system during tumorigenesis. The generation of new lymphatic vessels through lymphangiogenesis and the remodeling of pre-existing lymphatics are considered as important steps in cancer metastasis. To further demonstrate the feasibility of our system in mimicking pathological vascularized tumor processes, we patterned EC–lymphatic EC (LEC) suspension (5×10^6 cells/mL each) with HepG2–ECs spheroids into the center channel. We observed physical interactions between the tumor spheroid and lymphatic and blood vessels. Both networks exhibited physical contact with tumor spheroids, enfolding the spheroid boundary (Figure 2.11).

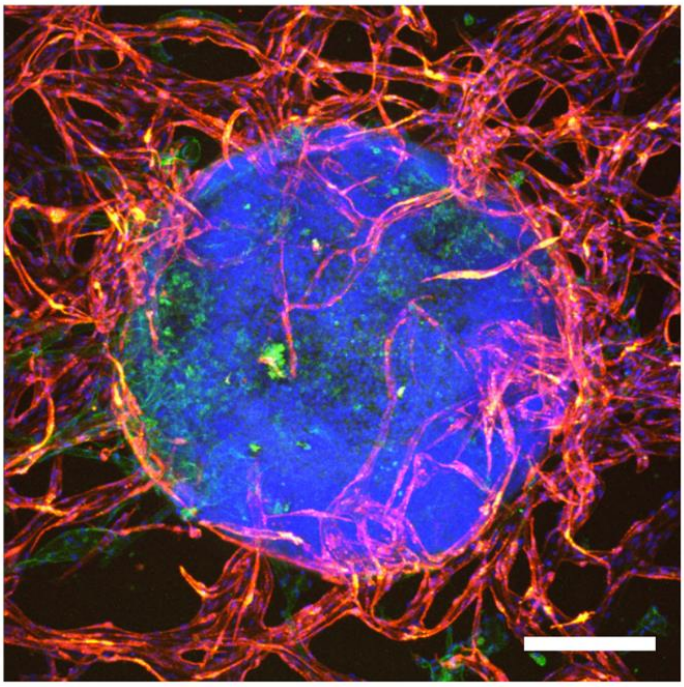

Figure 2.11 Confocal image of HepG2 – EC spheroid with lymphatic endothelial cells (LECs, green; podoplanin) and vascular endothelial cells (ECs, red). Scale bar: 150 μm.

2.4 Discussion

Current tumor-targeted drug-delivery systems are usually tested in xenograft mouse models. However, the data from these animal models often fail to reproduce the results in clinical studies. This translation issue is believed to be the phylogenetic difference between human and animal models. This absence of correlation has underscored the importance of developing alternative approaches ways to better predict the clinical efficacy. Recent advances in the microengineering of TME using organ-on-a-chip technologies have enabled the development of pathophysiologically relevant human tumorigenesis models.

Solid tumors are composed of tumor and stromal cells (vascular, fibroblast and immune cells) and ECM components in a highly interactive 3D microenvironment characterized by cell–cell and cell–ECM interactions, as well as local gradients of nutrients, growth factors, and oxygen [73]. The tumor stroma consists of non-tumor cells (e.g., fibroblasts, tumor-associated fibroblasts, endothelium, and immune cells) and a highly cross-linked fibril-like ECM structure with collagen and fibrin as its major constituents [74].

The tumor spheroid resembles a small tumor mass in its morphology, growth kinetics, cell–cell and cell–matrix interactions, and nutrient transport. Therefore, the tumor spheroid can serve as an excellent in vitro 3D tumor model.

Our results show that multicellular spheroids composed of tumor cells and ECs downregulated tumor suppressor gene and epithelial E-cadherin mRNA expressions. These results are consistent with those of several studies reporting such gene expression changes in association with tumor–EC interaction [75, 76]. Co-culture of tumor cells and ECs causes reprogramming of the signaling within and between the two cell types [77].

Furthermore, we demonstrated that the cancer HepG2–EC hybrid spheroid significantly enhanced angiogenesis compared to mono-cultured cancer spheroid. Our RT-PCR results suggest that the cancer–EC spheroid alters the molecular and cellular factors that drive angiogenesis. Thus, we demonstrated that the co-culture of cancers with ECs is required for accurate modeling of aggressive tumors in vitro. Multicellular hybrid spheroid will allow for more accurate modeling of the initial primary or metastatic stages of solid tumor progression than those with cancer cells only.

A main challenge of the conventional tumor spheroid models is the lack of vasculature adjacent to tumor spheroid. Through microengineering, we successfully incorporated tumor spheroid associated vasculature at the chip level. Our VTS on a chip model allowed us to investigate the interaction between ECs and the tumor spheroid. This model captured some of the complexity of in vivo tumors, including the 3D spheroid structure, EC vascularization, stromal fibroblasts, ECM, and nutrient and drug delivery via a 3D perfused vascular network. Our VTS model was able to simulate the vascular network in response to physiological cues from the tumor spheroid. To establish VTS, we loaded a tumor spheroid–EC suspension mixture within the fibrin matrix into a microfluidic channel. ECs self-assembled into the vascular network, forming complex structures interacting with the tumor spheroid.

To clearly obtain 3D in-depth confocal imaging of our model, we used the tissue-clearing CUBIC technique [78] to overcome the physical constraints imposed by light scattering and the subsequent challenge to mimic this complex biological system in a native 3D context. The CUBIC protocol uses basic aminoalcohol-based cocktails in addition to urea and Triton X-100 to enhance its clearing capability [79]. The benefits of this method

include the use of nontoxic reagents and ease of implementation. We introduced the clearing solution into the medium channel, allowing diffusion toward the spheroid. In the CUBIC-treated microfluidic chip, general VTS morphology was well-maintained at the cellular and subcellular levels, despite high lipid losses within the tissue.

One manifestation of tumor vessel abnormality is such defective and leaky endothelium that are disorganized and irregularly shaped with focal intercellular openings [80]. In addition, the vascular basement membrane has an abnormally loose association with ECs and pericytes. These physical characteristics together with cytokine (e.g., VEGF) production are responsible for elevated macromolecular permeability, leading to potential coupling between intravascular and interstitial flow [81]. Due to high pro-angiogenic signaling, the network of tumor-associated blood vessels is chaotic, with loose inter-endothelial cell junctions. The resulting leaky and collapsed/narrowed vessels lead to low perfusion and starve some tumor regions of nutrients. Our models with HepG2 showed distinct angiogenic behaviors; the HepG2–EC hybrid tumor spheroid produced a perfusable vascular network, whereas the U87MG–EC hybrid tumor spheroid showed poor vascular perfusion, demonstrating tumor-specific vascularization characteristics (Data not shown). When 70-kDa FITC–dextran was introduced into the HepG2–EC tumor spheroid model, we observed focal intercellular vascular openings especially adjacent to the tumor spheroid and the subsequent increase in the extravasation of NPs > 40 kDa due to the high tumor vessel permeability [82]. In the presence of vascular pores 200–1,200 nm in size, the fenestrated neovascular wall enhanced vascular permeability, resulting in increased drug accumulation in the tumor [83] indicating that these endothelial gaps or transcellular holes could explain the leakiness of tumor vessels [84]. Furthermore, we were able to

demonstrate real-time observation of NP delivery and transport through adjacent vasculature of the tumor spheroid in our model under pathophysiological flow conditions. This approach may provide a useful platform to test drug-loaded NP delivery to the tumor through vascular endothelial barriers.

As new cancer drugs are introduced for cancer treatment, and as an increasing number of candidates progress through preclinical and clinical development, it is important to improve our understanding of the effects of cancer drugs on tumor blood vessels and tissues [85]. Axitinib is a small-molecule oral tyrosine–kinase inhibitor (TKI) that is a more selective and potent inhibitor of VEGFR 1, 2, and 3 than many other clinical anti-angiogenic agents [86]. Inhibitory concentrations of Axitinib are 0.1 nM for VEGFR1, 0.2 nM for VEGFR2, and 0.1-0.3 nM for VEGFR3, whereas anti-PDGR activities and anti-Kit activities are nearly 10 times weaker (IC50: 5 nM for PDGFRα, 1.6 nM for PDGFRβ, and 1.7 nM for Kit) [87]. It was also confirmed that Axitinib had dose-dependent inhibitory effects on angiogenesis and tumor growth including xenograft model of human tumors: Axitinib induced regression of the tumor vasculature, with loss of endothelial sprouts and decreased vessel density. We successfully confirmed theses effects in our VTS model.

We demonstrated that Axitinib significantly decreased tumor spheroid growth at a high dose (10 nM) when administered via vascular network after vascularization. This finding implies that our VTS models promote cellular interaction with Axitinib, resulting in the suppression of tumor progression and growth, which corresponds to previous xenograft and clinical studies [88, 89]. More importantly, our model confirmed dose-dependent inhibition of angiogenesis by Axitinib before and after tumor vascularization. In particular, Axitinib caused tumor vasculature regression, with a loss of endothelial sprouts and

fenestration and a decrease in vessel density. Of note, after vascularization, even though we administered specific amount of Axitinib (1 nM), tumor spheroid associated blood vessels still served as a perfused tumor vasculature network, indicating necessity of higher dosage treatment of anti-angiogenesis drug to regress tumor vasculature. Overall, our VTS model may offer a promise approach to accelerate the clinical testing of large number of cancer drug candidates.

We though note that our vascularized tumor model could not recapitulate interconnection or penetration of the surrounding vasculature. Tumors can induce ECs to form new supply lines to a tumor during angiogenesis. Blood vessels grow into the tumor mass to supply nutrients and oxygen to rapidly dividing cancer cells. There is another way to feed a tumor, namely vasculogenic mimicry, in which cancer cells form blood-carrying channels; this process can supplement traditional angiogenesis [90, 91]. In this manner, tumor surrounding vessels hook up to channels within the tumor mass. Potential improvements to current models include the introduction of blood vessel growth into, or hook up to channels within, the tumor mass. However, challenges remain in reconstituting the fully functionality of vascularized tumor tissue.

2.5 Conclusion

We engineered a micropathological system of an in vitro 3D perfusable vascularized tumor spheroid model that exhibits the pathologically relevant structure with high reproducibility. We first analyzed the morphological characteristics of a cancer–EC spheroid mixture with varying cancer cell to EC ratios. When cancer cells were co-cultured with ECs, RT-PCR gene expression analysis showed that the cancer cells were highly aggressive. Microfluidic

experimental and RT-PCR results showed that cancer–EC spheroids had greater pro-angiogenic behavior than cancer cell-only spheroids. Our VTS model also exhibited leaky and fenestrated vasculature, which is a hallmark of tumor vasculature. Finally, we demonstrated a proof-of-concept application of the model for drug screening with varied dose and treatment timing, which is critical to screen drugs and fine their compositions for the treatment of heterogeneous tumors. With patient-derived multicellular tumor spheroids introduced to our VTS model, this approach may bridge highly specific human in vitro cultures and pathophysiological in vivo conditions to promote the study of tumor biology in the context of personalized precision medicine and immunotherapy.

CHAPTER 3. INJECTION-MOLDED 3D CULTURE PLATFORM: VASCULARIZED TUMOR SPHEROID CULTURE

3.1 Tumor Spheroid-on-a-chip: a Standardized Microfluidic Culture Platform for Investigating Tumor Angiogenesis

In vitro model systems drive biological studies by replicating human body processes and functions from the molecular to the whole organism level [92]. The human body is composed of both cellular and non-cellular components which are organized in a highly specialized manner [55]. However, it is difficult to mimic all the features of human biology with one in vitro model system. 3D cell culture systems have demonstrated many important advantages over 2D cell culture systems; 3D models more accurately mimic the complex in vivo microenvironment and produce cellular behavior which is closer to natural conditions [2].

In the area of cancer research, although tumors are complex 3D structures with their own distinct microenvironments, many conventional 2D culture studies ignore this complexity for convenience and simplicity [93, 94]. However, recent advances in engineered TMEs using microfluidics technology have enabled researchers to mimic physiologically relevant 3D TMEs [95], such as tumor angiogenesis [96], tumor metastasis [26], and tumor–stromal interaction [97]. Of note, 3D tumor spheroid models have been highlighted and have drawn attention for their potential applications in anti-cancer drug screening. Distinct from those of 2D cultures and biopsy samples, multicellular spheroids can provide proliferative gradients, reduced drug and gas exchange, and cell–cell and cell–ECM interactions which

are essential characteristics of a solid tumor microenvironment. However, without an appropriate in vitro model system, it has been impossible to observe tumor spheroid induced angiogenesis, which is an essential characteristic of the solid tumor microenvironment [63].

The Sphero-IMPACT is designed as a mass-producible injection-molded polystyrene (PS) device in a standardized 96-well plate SBS format. 3D printing and injection molding have enabled the rapid prototyping of platform designs to scale up production. Based on an understanding of open microfluidics, a platform utilizing geometrically modeled spontaneous capillary flow has been announced as having potential for a robust and reproducible liquid patterning tool [98]. Our previous publications debuting the IMPACT platform focused on the fabrication, fluid patterning mechanism and 3D vasculature formation assay with various patterning and culture conditions [52]. In this work, we propose a newly Sphero-IMPACT specialized in a 3D tumor spheroid culture assay with vasculature. The Sphero-IMPACT provides monitoring of vasculogenesis, angiogenesis, tumor cell migration and invasion from the spheroid and investigates the effect of anticancer drugs on angiogenesis induced by tumor spheroids.

This work describes a straightforward design that involves a hole in the middle of the rail to pattern a large spheroid (up to 800 μm) together with an extracellular matrix (ECM) as compared to previous publications. The tapered hole can accommodate pipette tips and allow one-step patterning of a spheroid in the region of interests with a highly reproducible manner. This standardized, plastic-based microfluidic platform is fully compatible with automated dispensing systems and automated microscopes. In addition, a mass-producible injection molded platform can provide a higher degree of uniformity per device due to the

lack of human manual labor steps. Such an approach also allows for the accessibility of higher throughput experimentation with less time and effort.

Our platform is designed to be easy-to-use by all experimenters and simple to use without complicated pre-treatment. By applying a lung fibroblast (LF) laden hydrogel in the center rail channel and attaching human umbilical vein endothelial cells (HUVECs) at the side of the center rail channel, we were able to observe robust angiogenic sprouting patterns with a different LF-hydrogel patterning volume. Also, we demonstrated that the tumor cell spheroid (brain glioblastoma, U87MG) invasion area increased by adding extrinsic transforming growth factor beta 1 (TGF-β1) and tumor necrosis factor alpha (TNF-α), demonstrating the ability to place the spheroid in the region of interests within our platform for direct observation. We further demonstrate the applicability of the platform to vascularization by introducing the tumor spheroids (sized 500–600 μm), providing physiologically relevant mimicry of 3D TMEs for anticancer drug efficacy testing. Our Sphero-IMPACT can potentially provide a cost-effective HTS platform with a physiologically relevant microenvironment for vascularized cancer biology and vascularized cancer drug screening.

3.2 Materials and Methods

3.2.1 3D printing for prototypes

Sphero-IMPACT was tested through 3D printing prior to injection molding. A prototype of Sphero-IMPACT was fabricated by a DLP type 3D printer (Perfactory mini 4, EnvisionTec) with the ERM (Enhanced Resolution Module) system. 3D printed models were rinsed with isopropyl alcohol for 20 min and post cured by 385 nm UV for 30 min.

For surface modification and biocompatibility, poly(c-xylene) was deposited with a thickness of 5 μm by plasma enhanced CVD (Lavida, Femtoscience). 3M™ 9795R advanced polyolefin diagnostic microfluidic medical tape (thickness: 50 μm) as the substrate for the chip is bonded to the 3D printed body part to complete the device. This tape is adhesive type coated with silicone acrylic, so it can be pressed and pasted.

3.2.2 Fabrication of Sphero-IMPACT

Polystyrene (PS) injection molding was performed at an R&D Factory (Korea). The aluminum alloy mold core was processed by machining and polishing. The clamping force at the time of injection was set at 130 tons with a maximum injection pressure of 55 bar, 15 seconds of cycle time, and a 220 ℃ nozzle temperature. The substrate was bonded to the injection-molded PS part to complete the device. The 3d printed spheroid chips and alloy mold core were designed by Solidworks, Dassault systems.

3.2.3 Cell Culture

Human umbilical vein endothelial cells (HUVECs, Lonza) were cultured in endothelial growth medium (EGM-2) and passage 4 was used for the experiments. Red or green fluorescent proteins (RFP and GFP) expressing HUVECs were obtained from Angio-Proteomie (Boston, MA). Normal human lung fibroblasts (LFs, Lonza) were cultured in fibroblast growth medium (FGM-2, Lonza) and passage 6 was used for the experiments. Human glioblastoma cells, U87MG (a gift from Dr Sun Ha Paek at Seoul National University) and human hepatocyte carcinoma cells (HepG2, Korean Cell Line Bank) were cultured in DMEM supplemented with 10% FBS, penicillin (100 U ml^{-1}) and streptomycin (100 U ml^{-1}). All cells were maintained in a humidified incubator at 37 ℃ and 5% CO_2.

3.2.4 Retrovirus production and transfection

The retroviral plasmid vector carrying GFP was purchased from Addgene. Retroviruses expressing GFP were obtained by transfecting a mixture of viral plasmid and retroviral packaging plasmids (gag/pol expressing vector, and VSV-G envelope vector) into HEK 293FT cells using Fugene 6 transfection reagent (Roche, Basel, Switzerland). 24 hours after transfection, the medium was replaced by fresh medium and viral supernatants were harvested at 48 and 72 hours. After filtration through a 0.45 μm filter with a PVDF membrane (Pall Life Sciences), HepG2 and U87MG were infected with retroviruses in the presence of polybrene (Sigma). 24 hours after infection, the cells were washed with PBS three times and expanded in growth medium.

3.2.5 Spheroid preparation

U87MG, the glioblastoma multiforme (GBM) spheroid was grown in a 96-wellplate with U-shaped bottom wells (Sumitomo Bakelite, Tokyo, Japan). The U87MG cell suspension was prepared for a total of 5000 cells per well and mixed with a 1% volume ratio of Matrigel. After pre-culturing in a U-shaped 96-wellplate for 4–5 days, a spheroid was introduced into the Sphero-IMPACT for tumor migration & invasion assay and tumor angiogenesis evaluation. For the LF spheroid, the LF cell suspension was prepared for a total of 10,000 cells per well and a mixed 1% volume ratio of Matrigel. FGM-2 was used to maintain the LF spheroid for 4–5 days.

3.2.6 Immunostaining

For immunofluorescence staining, cells in the device were fixed using paraformaldehyde (PFA, 4% w/v in PBS) for 15 min, permeabilized with Triton X-100 (0.1% v/v in PBS) for 30 min, and then blocked in bovine serum albumin (BSA, 3% w/v in PBS) for 1 h at room temperature. Endothelial cells were marked using Ulex europaeus agglutinin 1 (VECTOR, USA). Phalloidin (Alexa Fluor 594) and Hoechst 33342 were purchased from Molecular Probes.

3.2.7 Migration, invasion and tumor spheroid-induced angiogenesis assay

The 4–5 days cultured U87MG spheroid was collected from U-shaped 96-well plates. Using a 200 μL pipette tip, a tumor spheroid was mixed with a 2.5 mg mL^{-1} concentration of fibrinogen solution. The spheroid and fibrinogen solution were mixed with thrombin (0.5 U mL^{-1}, Sigma) and then immediately introduced into the central channel of the device. Since the spheroid (>500 μm) is greater than the channel height (100 μm), the spheroid was set to be stationary at the bottom of the channel. For tumor spheroid angiogenesis assay, the tumor spheroid and LF cell suspension at a concentration of 1×10^6 cell per mL were mixed with fibrinogen solution and mixed with thrombin. Next, the spheroid-cell-fibrinogen suspension was immediately introduced into the central channel of the device. We seeded additional HUVECs in both the media reservoirs and incubated them for 20 min to adapt to the surface of the fibrin gel. Next, we introduced EGM-2 media or cancer drug containing media for subsequent experiments.

3.2.8 Drug testing

For the monoclonal antibody drug, cetuximab (a gift from Dr. Jo) was diluted to 1 mg mL^{-1} with EGM-2 and bevacizumab (a gift from Dr. Jo) was used in 1 mg mL^{-1} concentration

in EGM-2. Each antibody drug was introduced to the media reservoir. For the inhibitors, sunitinib was dissolved in DMSO according to the manufacturers' instructions and added to cell culture media at a concentration of 1 μM.

3.2.9 Imaging and data quantification

The 3D reconstruction and cross section of the vessels were imaged using a confocal microscope (Olympus FV1000). The microscope and charge-coupled device (CCD) camera were controlled by MetaMorph (MolecularDevice, USA) software for time-lapse imaging. To quantify the vascular area coverage during angiogenesis blood vessel formation and tumor migration and invasion assay, z-projections of the 3D stacks images were obtained using ImageJ (NIH) and the proportion of the fluorescent pixels within the ROI of each image was calculated. The length of angiogenic sprouting and tumor cell migration & invasion were determined by manually measuring the distance from the original gel and spheroid interface.

3.2.10 Statistical analysis

Using Prism (GraphPad, USA), statistical comparisons of the values were obtained from an unpaired two-tailed Student's t-test analysis, with the threshold for statistical significance set at *$p < 0.1$. **$p < 0.01$; ***$p < 0.001$; ****$p < 0.0001$; and ns (not significant). The standard error of the mean (SEM) is presented in error bars.

3.3 Results and Discussion

3.3.1 Sphero-IMPACT design optimization and considerations

Sphero-IMPACT is a means to illuminate a more complex microphysiological system. This 3D cell culture array is designed to be able to introduce a cell spheroid, enabling more diverse assays for vascularized tumor models. The platform is designed to be highly compatible with most types of laboratory equipment (e.g., microscopes, automated dispensers) and has a 96-well plate specification to increase its value (Figure 3.1). The platform consists of a rail guide for cell patterning region and media reservoir each side. The cell patterning region contains a single hole in the center, designed to capture a large spheroid. As shown in Figure 3.1B, the tapered hole has a diameter of 0.83 mm and draft of 4.0 degrees, so that it fits a 200 μl pipette tip with a diameter of 0.9 mm. Then, the pipette tip completely seals the hole so that the tumor spheroid and hydrogel can be patterned in the channel in a single step without leaking. The medium reservoir is separated by a 5.0 mm wall in the center, which enables us to use different volumes of conditioning medium in each channel (Figure 3.2). Novel fabrication methods should be developed to increase the flexibility of microfluidics. 3D printing has recently emerged as an alternative microfluidics manufacturing method and has been demonstrated to be a potential solution to the problems associated with PDMS-based manufacturing methods [99]. This rapid prototyping requires just one step, in comparison to soft lithography, which requires several. The single step is to transfer a file prepared by computer aided design (CAD) software to the 3D printer and then wait for the output. Moreover, 3D printing has many advantages in terms of maximizing design flexibility, with convenience of optimization [99]. Concerning the design process, it enables users to change any component, for example ones that require modification for optimization purposes, using CAD software and is simple and easy to run [100]. We developed the Sphero-IMPACT using a following rapid prototyping process

involving fluid patterning and design optimization for 3D multiple cell culture (Figure 3.3). To deploy a 3D culture for cancer drug discovery and screening, we developed a standardized microfluidics platform Sphero-IMPACT with the following characteristics: (1) a 96-well plate SBS format-based design with fully automated imaging; (2) a single spheroid per well, centered for ease of imaging; (3) an HTS angiogenesis assay; and (4) uniform culture conditions for quantitative assessment of various cancer drugs. Although 3D printing has many advantages, it has throughput issues because its production rate is limited based on the specification of the equipment [101]. We achieved faster production by injection molding the final design. We adopted a PS quick delivery model (QDM) for injection molding to achieve greater conformity, transparency, and productivity [102]. Unlike other mass production techniques, as the mold core is made of aluminum alloy, QDM only provides about 3000 guaranteed shots. Hence, it can play an intermediate role between prototyping and mass production. As shown in Figure 3.1A, we designed a microchip array based on the SBS format which reflected a 9 mm pitch in the horizontal axis, and an 18 mm pitch in the vertical axis. Each unit configured reservoirs for media supply and a rail guide which includes a hole. In our actual cell culture experiment, we produced eight spheroid culture units in one chip, which fit onto a commonly used slide glass size (75 mm × 2 5 mm), as well as into the 96-well plate format. These properties are compatible with conventional automation cell culture systems and confocal microscopy systems, and thus raise the possibility of high-throughput drug screening.

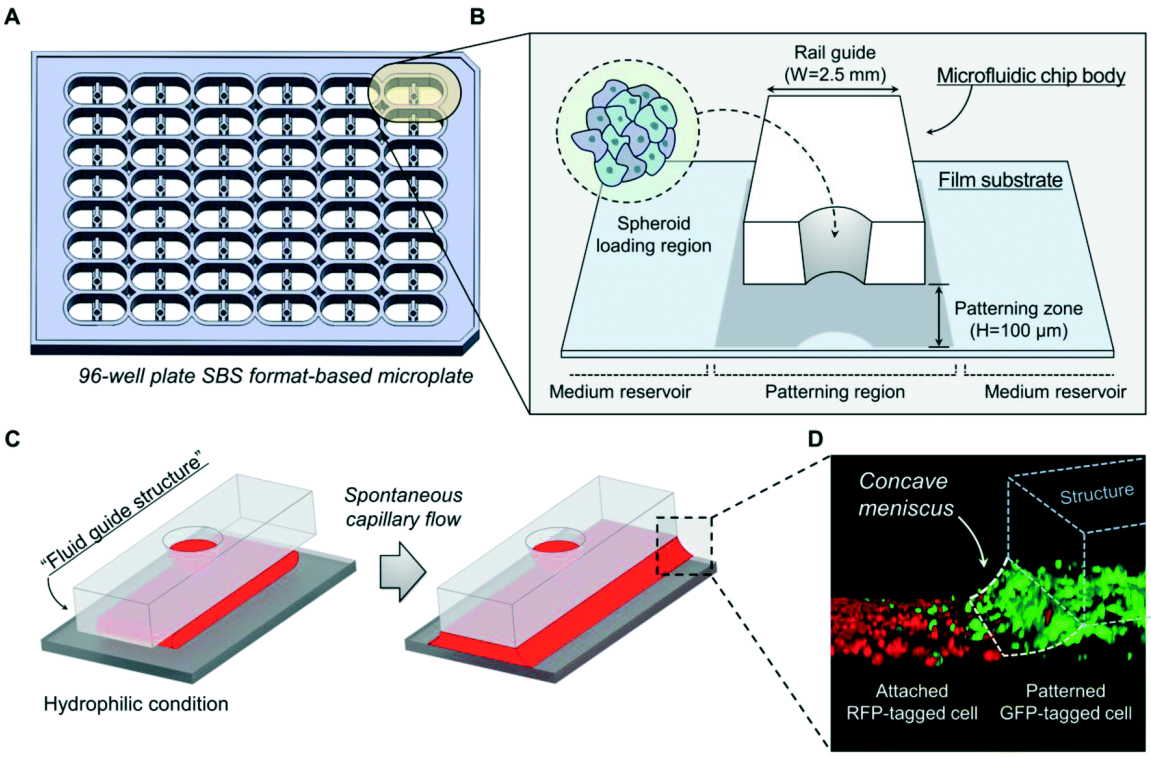

E

Volume	2.0 μl	4.0 μl	6.0 μl	8.0 μl
Grayscale image	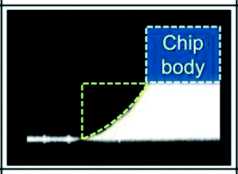	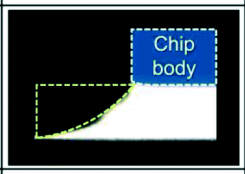	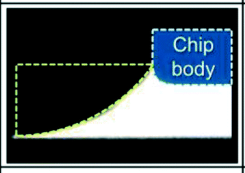	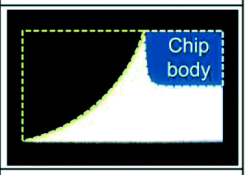
Radius of curvature	232 μm	257 μm	312 μm	280 μm

Figure 3.1 Design of the standardized microfluidics platform for tumor spheroid-on-a-chip. (A) A conceptual image of Sphero-IMPACT based on a standard 96-well plate format. (B) Sphero-IMPACT has a media reservoir on each side, centered on a fluid rail guide for cell culture. The rail guide contains a tapered hole functioned as a culture space for a cell spheroid. (C) Spontaneous fluid patterning by capillary action. Fluid can be transferred simply and robustly along the rail guide under hydrophilic condition. (D) The patterned fluid configures a concave meniscus at the edges of the structure. A fluorescence image showing GFP-expressing HUVECs patterned with fibrin gel which forming the meniscus, and RFP-expressing HUVECs seeded on the reservoir. (E) The cross-sections of the devices filled with a solution of Rodamin B under noted volume were converted to grayscale images for analysis. White dash lines indicate the fluid rail guide, and yellow dash lines are traces for curvature studies.

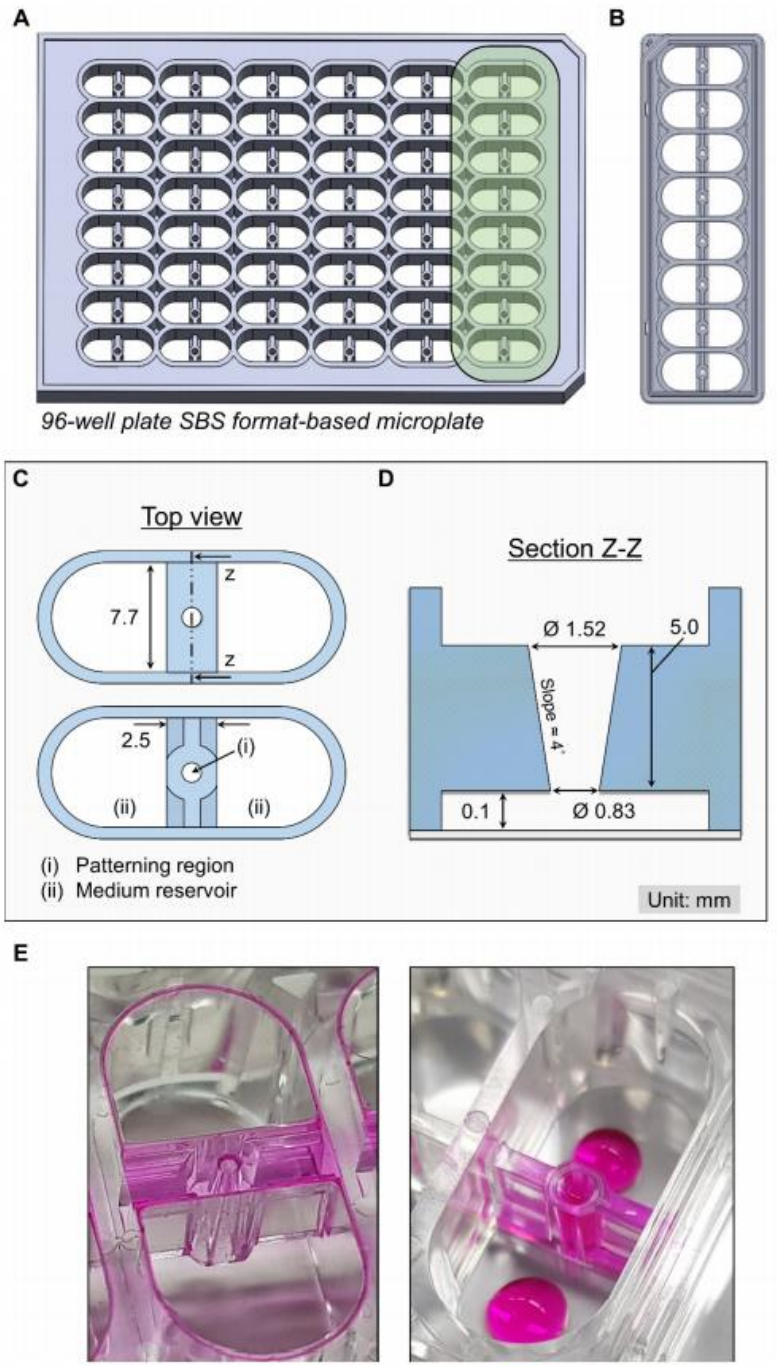

Figure 3.2 Overall schematics of the structural components of tumor spheroid-on-a-chip. (A)Illustration of 96-well plate SBS format-based microplate. (B) A single array of tumorspheroidon-a-chip as a prototype model. (C-D) Schematic view detailing the dimensions of the device. (E) Photograph of the dye being patterned into the rail of the device.

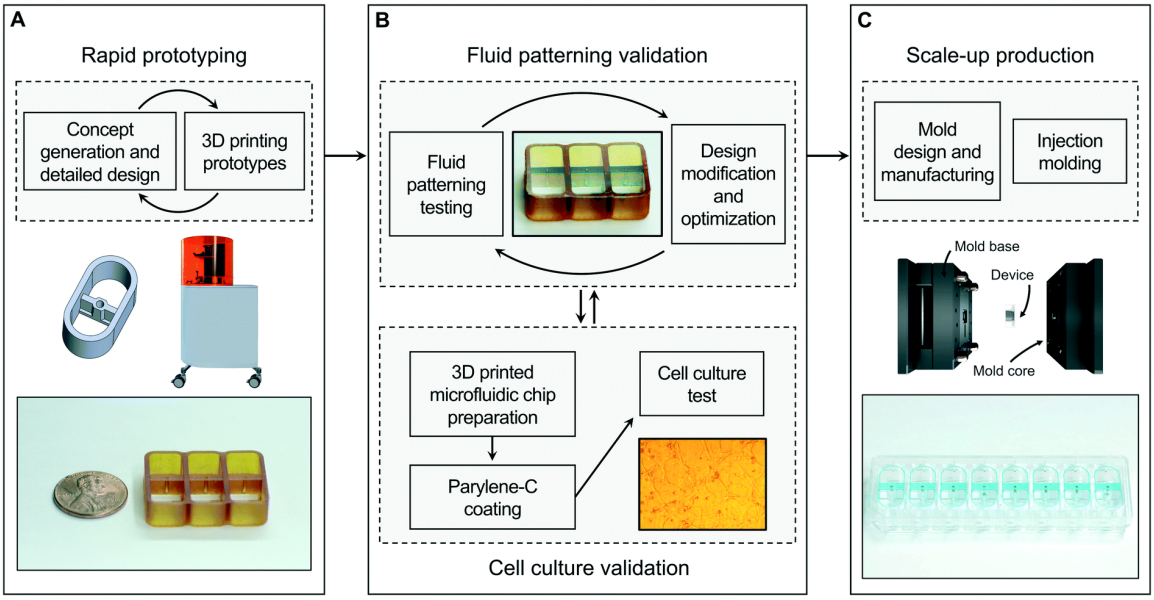

Figure 3.3 Process schematic of Sphero-IMPACT design optimization with 3D printing for mass production through injection molding. (A) 3D printing prototypes allow for rapid dimensional testing and optimization prior to high investment but high yield injection molded production. (B) During the process, we performed the platform validation through fluid patterning and cell culture testing. This process was approached through the trial and error method. (C) Once a design has been configured for injection molding, the design can be mass produced for easy accessibility for the end user.

3.3.2 Gel patterning principle

The proposed device is based on a different fluid patterning approach to that used in conventional PDMS chips. Fluid guide structures allow fluids to be easily transported spontaneously by capillary forces in a hydrophilic environment. Hence, structures can be designed to engineer capillary flow patterns [103, 104]. Important conditions for the patterning to work reliably is to have hydrophilic surfaces (contact angle <25°) and an adequate gap between the structure and substrate (<500 µm). The width of the structure is not critical [98]. We mainly considered the height from the substrate as the key factor influencing the patterning conditions. The channel depth from the substrate is 100 µm, so the device can transport fluid into the zone. The channel and substrate were hydrophilized

by plasma treatment to ensure that the contact angle was 0 degrees. Fluid exposed to this surface will trigger a capillary action when it encounters the rail guide structure. The fluid then formed concave meniscus between the edge of the structure and the substrate. Such an affinity environment for fluid patterning is significant in that it can acquire smooth fluid interfaces as well as spontaneous fluid transport (Figure 3.1C). We patterned the identical volume (4.0 μl) of fluid in both hydrophilic and hydrophobic conditions. In the hydrophobic environment, the interface of the fluid showed a surface imbalance due to the resistance of the rail guide structure. On the other hand, we visually confirmed that the fluid was well-patterned according to the guide structure in a hydrophilic environment (Figure 3.4). Based on this result, we applied this concaved meniscus surface as an additional cell culture region. First, we patterned GFP-expressing HUVECs with fibrin gel in the structure; then, we seeded suspension included RFP-expressing HUVECs onto the surface (Figure 3.1D). This approach has traditionally been considered as a way of resolving the issues presented by tilting the device to attach cells to the 3D gel surface. The RFP-expressing HUVECs were able to migrate towards the fibrin gel due to the growth factor surrounding the gel. The shape of this curved surface has been shown to vary with the volume of fluid injected. To assess the dependence of the geometry of the curved surface on the injection volume, Sphero-IMPACT was filled with rhodamine B solution volumes of 2.0, 4.0, 6.0 and 8.0 μl. The cross-section of the patterned area obtained from the imaging platform was converted into a grayscale image to distinguish the outlines of each surface. The converted images were analyzed by tracing the curvature with a yellow dashed line and the fluid guide structure with a white dashed line. We proceeded to explore the meniscus formed between the fluid guide structure and the substrate by the filled fluid

according to each volume (Figure 3.1E). Due to the larger curvature, the gentle interface of the gel makes cell seeding simpler than conventional methods. In previous studies, particularly with the PDMS-based chip, the meniscus caused by the hydrophobic environment was convex, which forced the cells to tilt more than 30 min at an angle of 90 degrees to be located on the gel interface.

The geometry of the interface between the hydrogel and the cell culture medium is important because the amount of additional endothelial cells that are injected into the medium reservoir in the cell suspension form depends on the radius of the curvature of the interface. In our tumor angiogenesis experiments, endothelial cells were only patterned in the medium reservoir. As shown in Figure 3.1E, the radius of the curvature increases with the injection volume, but decreases when the volume reaches 8.0 μl. This is due to the excess suspension flooding the wall of the central channel. Many other 3D vascularization platforms have been introduced, including additional procedures for placing endothelial cells on the hydrogel surface, such as surface coating [105] or gravity-driven attachment [106]. We attached endothelial cells to the patterned hydrogel using a fluid interface formed from a hydrophilic surface. Upon seeding, HUVECs form a monolayer as they reach confluency at the gel–media interface. Both the area of the vascular network and the number of sprouting volumes increases until the injected volume reaches 6.0 μl, then decreases when the volume reaches 8.0 μl. This shows that maximizing the radius of the curvature of the interface is key to enhancing the proliferation and efficiency of cell attachment, without requiring any additional treatment or procedures. This approach not only ensures the convenience of the experimenter but also reduces the variability of the results since there is no additional procedure. Sphero-IMPACT allows users to experience

a variety of assays based on intuitive design and usage. Here, we presented well-performed assays for vasculogenesis, angiogenesis, tumor migration and tumor spheroid-induced angiogenesis (Figure 3.5).

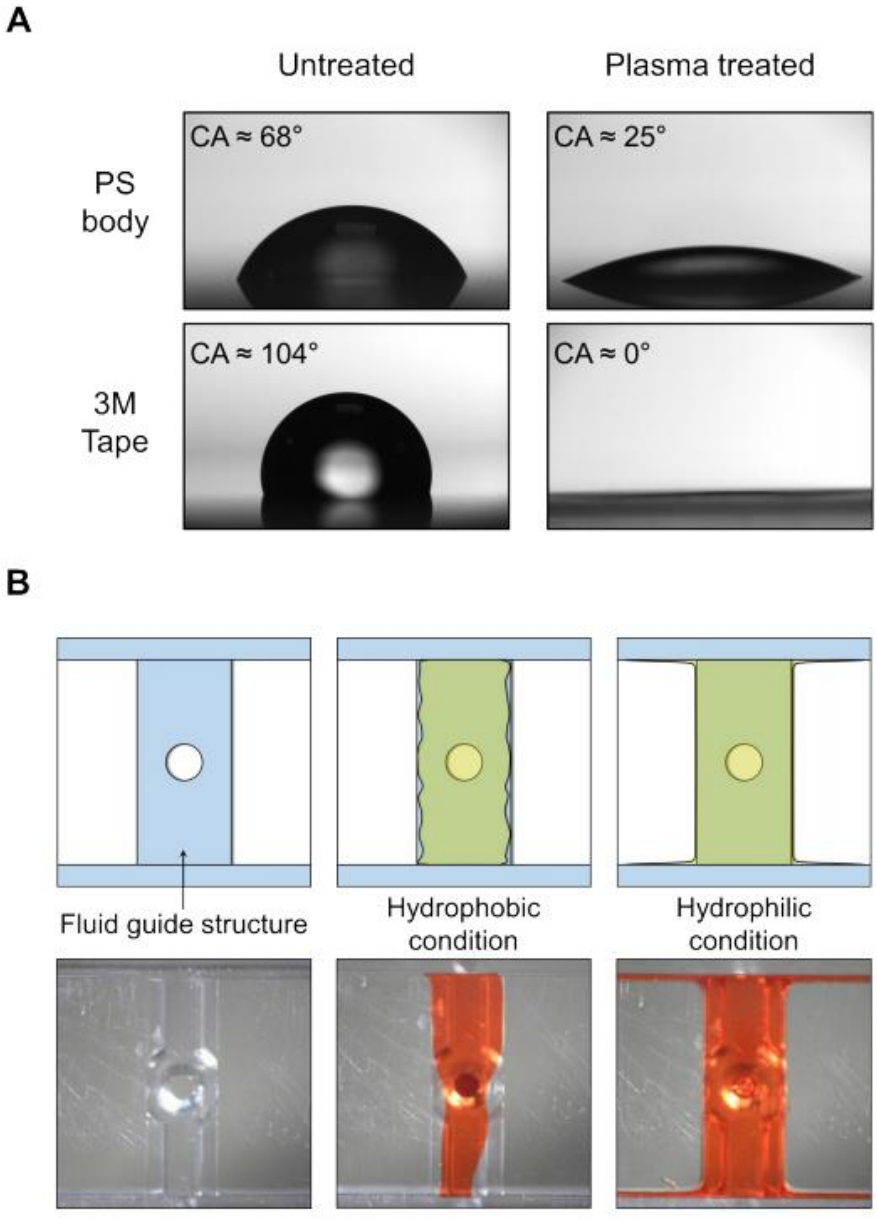

Figure 3.4 Fluid patterning under the hydrophilic and hydrophobic environment. (A)Investigation of the contact angle of the material used in the device under hydrophilic conditions to establish the fluid patterning technique. (B) The fluid interface showed surface imbalance under hydrophobic environment. After the plasma treatment, the fluid

was well patterned under hydrophilic environment.

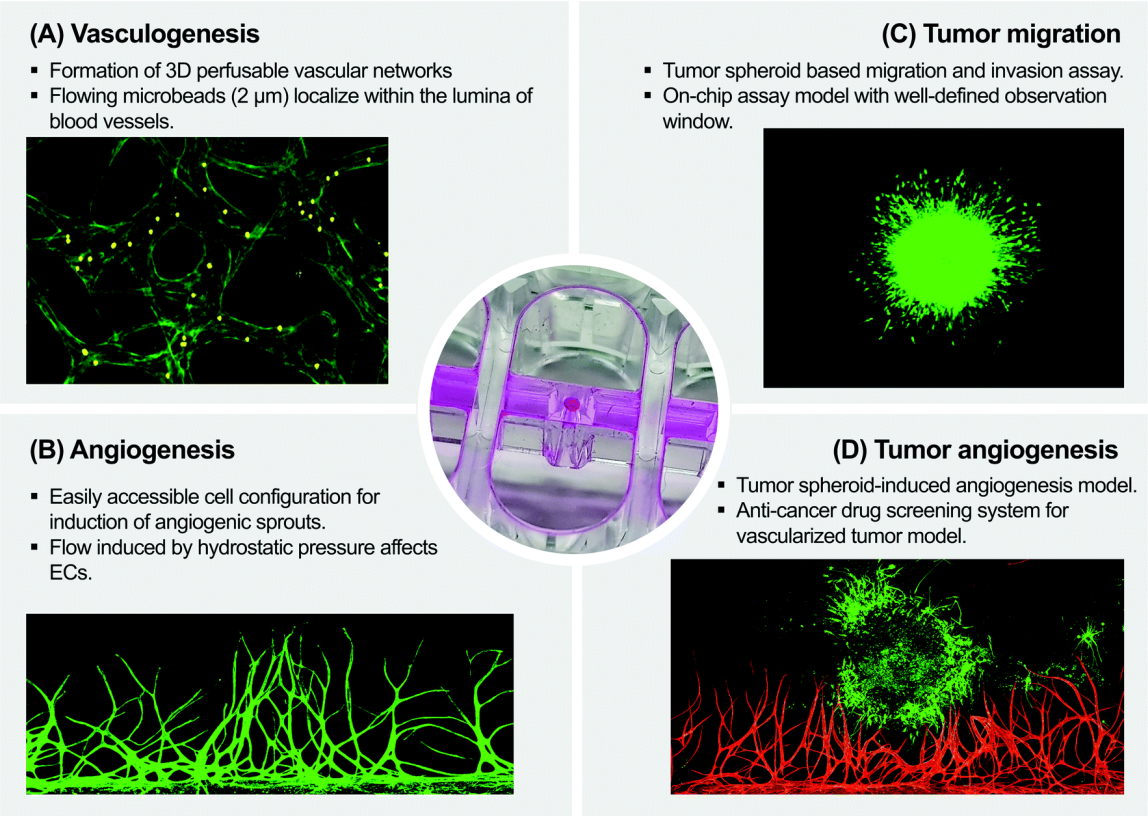

Figure 3.5 Various in vitro model approaches of Sphero-IMPACT. (A) Vasculogenesis; the platform can perform co-culture modeling to develop a 3D perfusable blood vessel networks. (B) Angiogenesis; induction of directional angiogenesis by attaching HUVECs to patterned fibrin gel-meniscus in a rail guide structure. (C) Tumor migration assay; ease of experimentation and observation through the space for a spheroid inside the platform. (D) Tumor spheroid-induced angiogenesis; construct tumor model which is vascularized through co-culture of tumor spheroid and blood vessel.

3.3.3 Angiogenesis assay

A wide and diverse variety of models have been actively developed for developmental and pathological angiogenesis[19, 107, 108]. Preexisting microfluidic platforms have adopted soft lithography with replica-molding using PDMS. The advent of the PDMS based microfluidic platform allowed for unprecedented control regarding cell patterning and

physiologically relevant 3D microenvironments with a reduction in the cell and media requirements. Moreover, several studies using this microfluidic platform have been reported recreating TME and angiogenesis in vitro. Although it has shown meaningful results, some of the disadvantages of the platform have lowered the possibility of being practically used.

Compared to the PDMS-based hydrophobic burst valve design, this work utilized the hydrophilic liquid guide to obtain rapid and reproducible patterned gels for 3D cell cultures. When a liquid drop is placed on the device, spontaneous patterning is achieved in a reproducible manner. Compared to injection molding, the soft lithography based PDMS chip has a remarkable low production efficiency. There are additional manual steps such as curing, cutting and mixing, which is labor-intensive. However, in the case of injection molding, a large quantity of devices can be produced quickly, so the experiment can be carried out with ready-to-use devices (Figure 3.6). And, for the angiogenesis assay, the interface of this patterned gel forms a concave meniscus, which provides a beneficial advantage for placing cells on the gel. In previous studies, the angiogenesis assay had to be supplemented with a tilting of the device at an angle of 90 degrees for more than 30 min.38 We used a fluid meniscus to simplify this step. It is important to devise a method to place endothelial cells close to the matrix using a single gel patterning step. We patterned LFs with fibrin gel as a growth factor supplier, to induce angiogenesis underneath the structure. After the gel was cross-linked, HUVECs were exposed in suspension around the gel surface. Of the exposed HUVECs, the cells placed on the gel sprouted into the matrix over time (Figure 3.7A and B). Based on this outcome, we decided to study angiogenesis in terms of the amount of hydrogel, while taking into account the co-culture conditions of

the tumor spheroids. Angiogenesis modeling was performed under four patterning volume conditions, with identical concentrations of fibrin gel and LFs (Figure 3.7C and D). The morphologically quantified results showed that the sprouts were vigorous and uniform under 6.0 μl volume conditions. In the case of 2.0 μl, the HUVEC was not evenly placed due to the lack of volume of fibrin gel under the structure, resulting in uneven vascular sprouting. On the other hand, when filling up 8.0 μl of fibrin gel, the gel covered the edge of the fluid guide structure due to overfilling. As a result, the gel interface became so steep that placement of HUVECs was difficult. We introduced fluorescence microparticles in the media reservoirs of cultured samples at 6.0 μl volume conditions to demonstrate the perfusable characteristics of the blood vessels (Figure 3.7E). The center hole in the fluid guide structure can be filled up additionally as the volume of the LF embedded fibrin gel increases. This appearance can result in a larger amount of VEGF concentration than in the surrounding environment. Furthermore, it can induce vigorous growth of surrounding blood vessel cells. We focused on a preceding study that angiogenesis can occur actively near the central hole area and tried to show the effect in a different way by inserting the LF spheroid into the hole. We observed vasculogenesis by forming GFP-expressing HUVEC around the spheroids. The model cultured for 4 days showed that vasculogenesis was more active around the hole through F-actin staining (Figure 3.7F).

	Production Volume					
Production Volume (ea)	**Mold Fabrication**	**100**	**1k**	**10k**	**100k**	**1m**
Soft Lithography (day)	1	7	70	700	7k	70k
Injection Molding (day)	10	1	1	10	100	1k

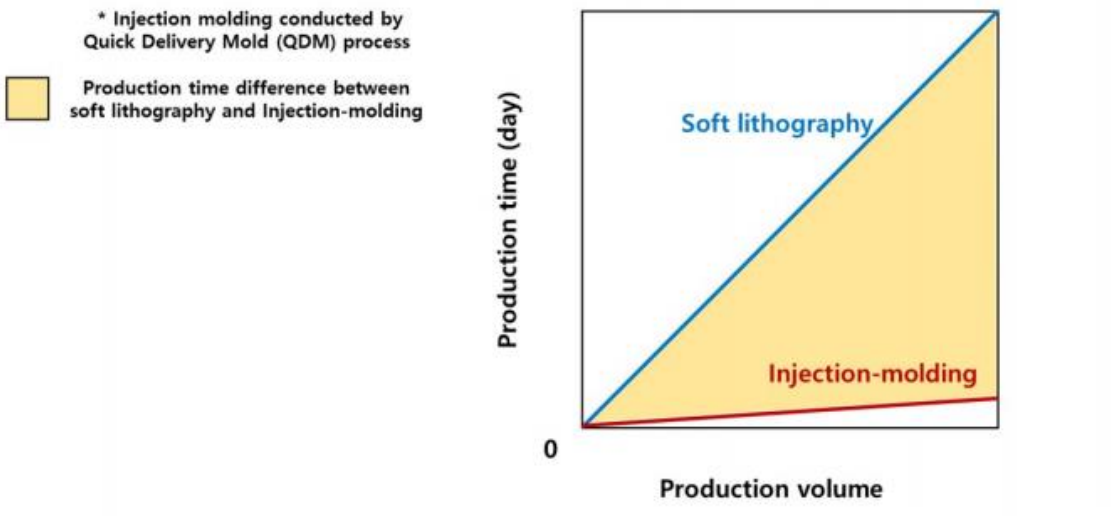

Figure 3.6 A diagram comparing the time required for production of the device between soft lithography and injection molding process.

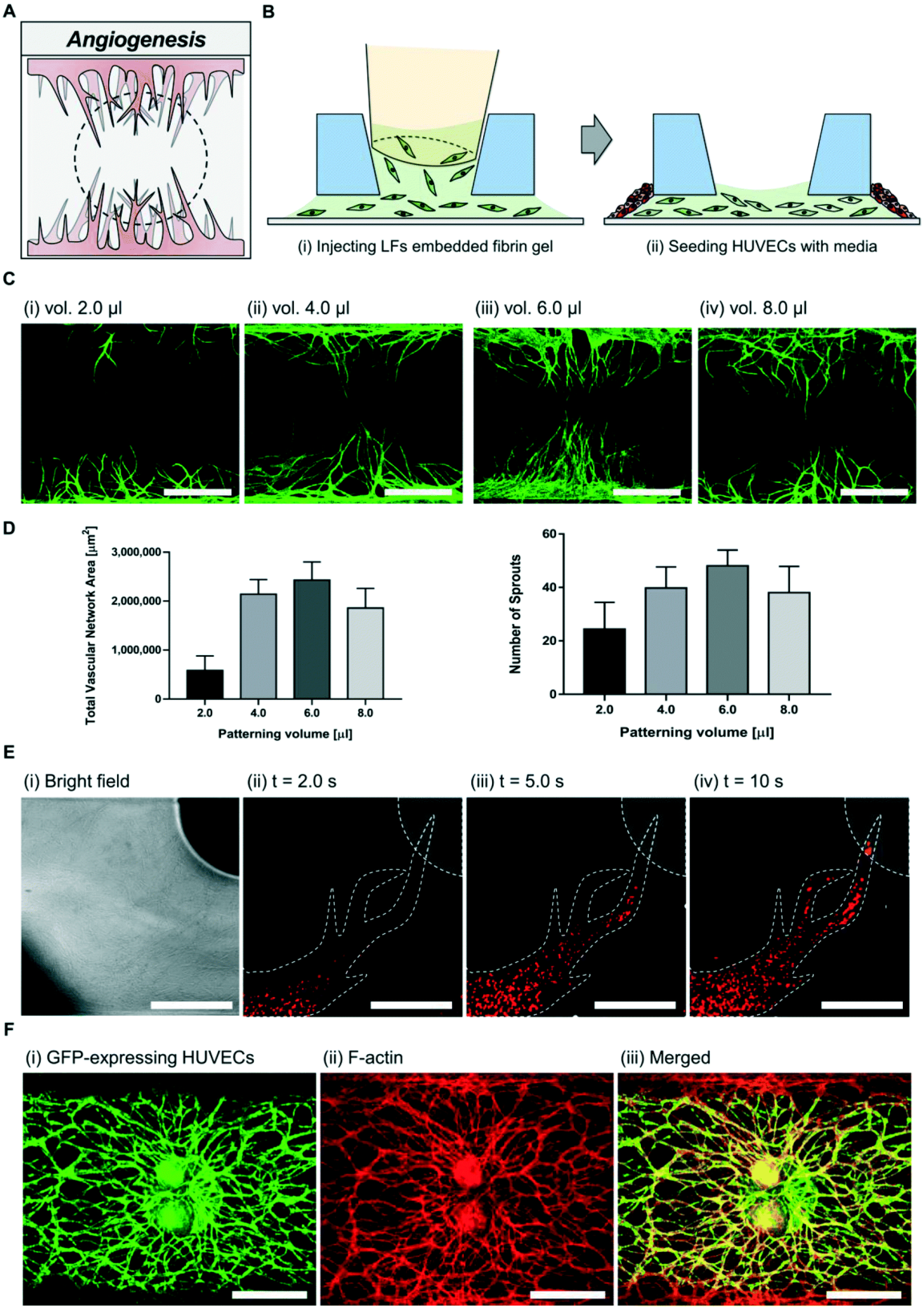
A
Angiogenesis
B
(i) Injecting LFs embedded fibrin gel
(ii) Seeding HUVECs with media
C
(i) vol. 2.0 µl
(ii) vol. 4.0 µl
(iii) vol. 6.0 µl
(iv) vol. 8.0 µl
D
Total Vascular Network Area [µm²]
3,000,000
2,000,000
1,000,000
0
2.0
4.0
6.0
8.0
Patterning volume [µl]
Number of Sprouts
60
40
20
0
2.0
4.0
6.0
8.0
Patterning volume [µl]
E
(i) Bright field
(ii) t = 2.0 s
(iii) t = 5.0 s
(iv) t = 10 s
F
(i) GFP-expressing HUVECs
(ii) F-actin
(iii) Merged

Figure 3.7 Engineered 3D perfusable blood vessel networks in Sphero-IMPACT. (A) An illustration of angiogenesis model configuration in Sphero-IMPACT. (B) A cell culture approach to construct angiogenesis model. (C) Investigating an optimal patterned volume for inducing effective angiogenic sprouts. Every sample was cultured for 5 days and stained with lectins (green) as markers of endothelial cells. Scale bar = 1000 μm. (D) The total vascular network area and the number of vessel sprouts were quantitatively evaluated to determine appropriate conditions for angiogenesis depending on the patterning volume. (E) Experimental Study on the transport of microbeads with the lapse of time through perfusable blood vessel developed under 6.0 μl patterning volume condition. Scale bar = 500 μm. (F) Confocal images exhibiting vasculogenesis formed from GFP-expressing HUVECs reflecting the effect of LFs spheroids. Observation of cytoskeleton through F-actin (red) antibody staining. Scale bar = 1000 μm.

Developmental studies and pathological studies on angiogenesis are very important studies. Various researchers are presenting a well-developed platform for angiogenesis in diverse styles. Nevertheless, the existing angiogenesis experimental model is not easy to use as a screening platform due to complicated device preparation and incompatibility with screening systems [109]. Our platform is feasible for use in various fields because it is convenient for the experimenter, from the preparation stage to the subsequent analysis. We obtained image results for all units in the device by performing one-time sample imaging with a microscope array setup for quantitative analysis. We considered the major factors and configurations of the cell conditions within a device. The modeling of the microvascular system through a fluid guide structure not only makes it easier to place cells, but also acts as a barrier to control the external and internal physicochemical stimulation. The main structural feature shows the hole provides a wider vertical space than the periphery, and this space can arrange the slope of the VEGF by additional sources. In other words, this space is effective in promoting angiogenesis once a tumor spheroid is captured.

These key findings are expected to reveal that the tumor spheroid-induced angiogenesis model can be implemented in an appropriate condition.

3.3.4 Tumor migration and invasion

Aggressive cancer cells are distinguished by increased cell migration and invasion. To investigate the role of TGF-β1 and TNF-α in cancer metastasis, the effects of TGF-β1 (20 ng mL^{-1}) and TNF-α (20 ng mL^{-1}) were evaluated using Sphero-IMPACT. The U87MG tumor spheroid was located in the center of Sphero-IMPACT and embedded into 3D fibrin ECM, enabling reproducible and quantitative analysis of tumor spheroid migration and invasion. As shown in Figure 3.8, the invasion area after 48 h. was significantly increased in both the TGF-β1 and TNF-α treated group compared to the control group. These results demonstrate that both TGF-β1 and TNF-α significantly enhance the migratory and invasive potential of U87MG cancer cells. Furthermore, there was a statistically significant difference between the U87MG migration distance of the TGF-β1-treated group and that of the control group, but not between the TNF-α-treated group and the control. This suggests that TGF-β1 may promote morphological changes in U87MG. Increased malignancy is frequently related to an epithelial–mesenchymal transition, resulting in enhanced motility and the generation of cancer stem-like cells. Tumor cell migration normally occurs in response to hypoxia and soluble mediators (e.g., cytokines) [110]. Previous studies demonstrated that, in glioma, TGF-β1 is secreted from glioma cells via autocrine signaling, or is released from microglial cells. TGF-β1 expression has been reported to promote tumor cell survival, migration and invasion[111]. TNF-α can activate the mitogen activated protein kinase (MAPK)/extracellular signal-regulated kinase (ERK) signaling pathway, upregulate matrix metalloproteinase (MMP)-9, and enhance tumor cell

invasion and metastasis [111]. Our findings are consistent with cancer cells becoming more aggressive when treated with TGF-β1 and TNF-α in the Sphero-IMPACT. Methods to investigate cell migration and invasion are important in cancer biology, immunology and cell biology. Conventional migration and invasion evaluation methods include cell culture wound closure assays, where a scratch is produced on a confluent cell monolayer, and Transwell cell migration and invasion assays, which are used to evaluate cell motility and invasiveness towards a chemo-attractant gradient [112]. However, these assays inherently lack 3D microenvironments with ECM and the ability to achieve reproducible, quantitative results. To address this issue, we developed a simple, reproducible single step tumor spheroid monitoring chip. We mixed tumor spheroids with ECM and loaded the tumor spheroid – gel suspension into the central channel. Our method can significantly accelerate and simplify the assay with a physiologically relevant 3D microenvironment, but at the same time produces highly reproducible results with 96-well plate format standardization. The assay can easily be modified with different types of matrices (e.g., collagen and Matrigel). Taken together, the Sphero-IMPACT can be applied to fully automated imaging and analysis of tumor cell migration with HTS and bridge the gap between 2D migration assays and in vivo studies.

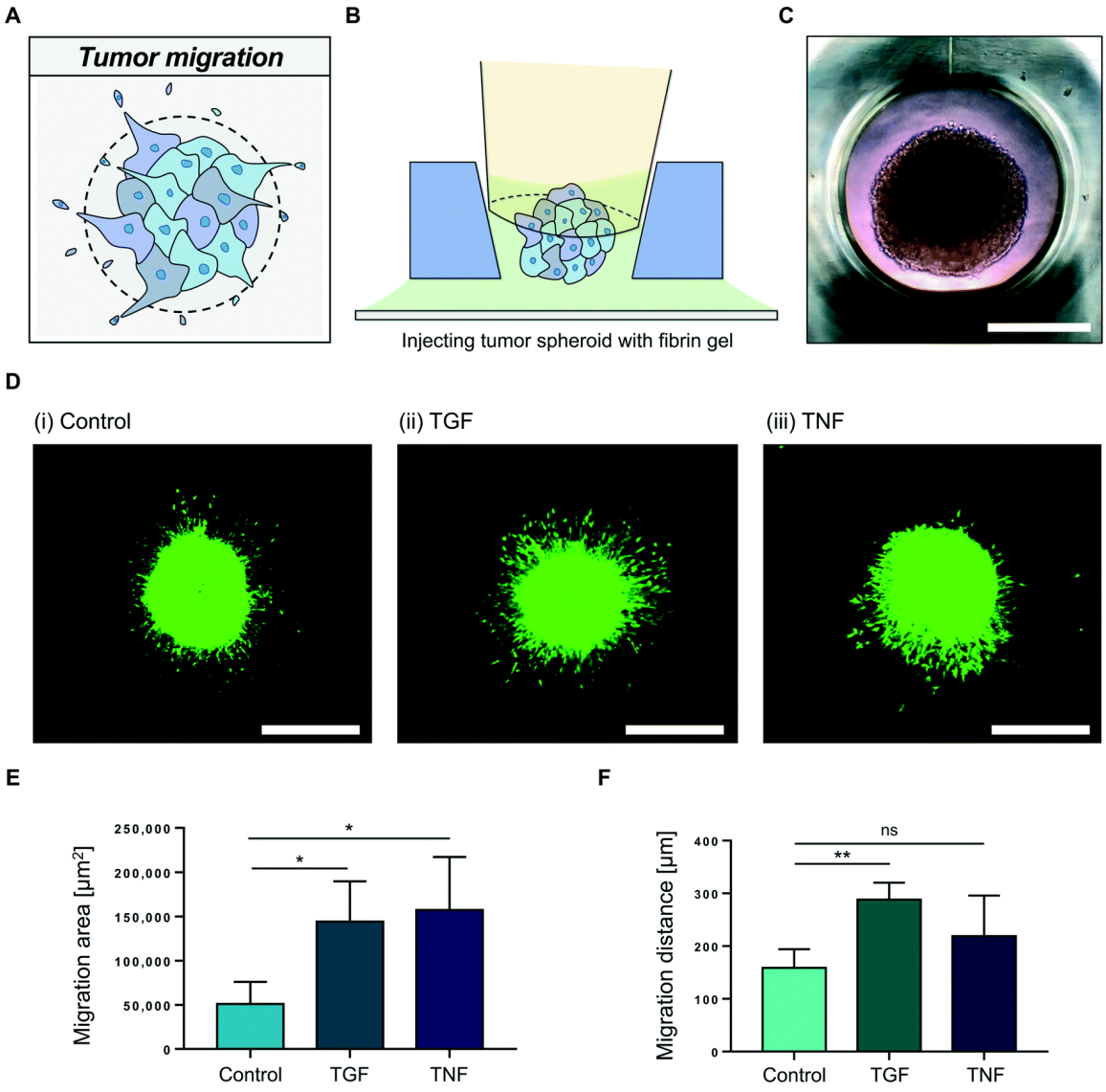

Figure 3.8 Tumor invasion assay using a spheroid model. (A) Schematic depiction of tumor migration and invasion. (B) Configuration of the microfluidic device for modeling tumor spheroid migration and invasion into 3D ECM. (C) The optical microscope image showing the U87MG tumor spheroid in the spheroid region. Scale bar = 400 μm. (D) Representative confocal images of tumor migration and invasion under three different conditions. Scale bar = 600 μm. (E and F) Quantitative analysis of tumor cell migration area and migration distance. Bars indicate mean ± SEM from at least 4 devices per condition. *$p < 0.1$ and **$p < 0.01$ in the unpaired two-tailed Student's t-test.

3.3.5 Tumor angiogenesis and drug screening

Angiogenesis is a key feature of tumor progression. The formation of new blood vessels from existing vessels can be induced by a number of tumor-derived soluble factors, such as the VEGF family[113]. Therefore, targeting these growth factors and their receptors has been used to treat several human cancers, including non-small cell lung cancer, glioblastoma, and renal cancers. We therefore investigated the effect of representative anti-angiogenic cancer drugs, bevacizumab and sunitinib, in the Sphero-IMPACT. Before we investigated the effect of these anti-angiogenic drugs in the Sphero-IMPACT, we observed that within 4 days of co-culture, HUVECs invaded the fibrin matrix, apparently in response to U87MG-derived factors (Figure 3.9). Compared to the LF mediated vascular sprouting experiment, U87MG tumor spheroid mediated sprouting exhibited aberrant morphology (Figure 3.10). The addition of 1 mg mL^{-1} of bevacizumab and 1.0 μM of sunitinib significantly decreased the vascular network area, number of sprouts, and sprouting length, demonstrating their anti-angiogenic effects. We also tested the effect of cetuximab, which is an epidermal growth factor receptor (EGFR) inhibitor. In our model, there were no statistical differences between the cetuximab (1.0 mg mL^{-1})-treated group and the control group, in terms of vascular network area, number of sprouts, and sprouting length (Figure 3.9D-F).

As new cancer drugs are introduced for cancer treatment, and an increasing number of candidates progress through preclinical and clinical development, it is important to improve our understanding of the effects of cancer drugs on tumor blood vessels and tissues. Traditional well plate-based drug assays are still widely used in industry, thanks to their standardized format that enables automated handling. The Sphero-IMPACT not only provides a patho-physiologically relevant 3D TME compared to traditional well plate

assays, but also has a standardized 96-well plate format with robust and reproducible patterning capabilities. Indeed, PDMS has been widely accepted for fabricating microfluidics devices in prototyping experiments. However, due to several material limitations, PDMS is somewhat inaccessible, and it is difficult to scale up production of microfluidic cell cultures using this method. Therefore, we suggested using an injection-molded device to replace existing PDMS microfluidics devices. The Sphero-IMPACT has the potential to provide a robust and reproducible high-throughput tumor spheroid experimental platform for vascularized TMEs.

3.4 Conclusion

Here, we presented an in vitro cell culture array platform "Sphero-IMPACT" that can be applied to large quantities drug screening for tumor angiogenesis. Our platform has several advantages, including compatibility with a range of laboratory equipment, ease of experimentation, and ready-to-use devices. We demonstrated the potential for this platform can be used as diverse assays in various fields such as biological laboratories and pharmaceutical companies. Through 3D printed prototypes, we performed optimized structural designs for 3D fluid patterning techniques and cell culture microenvironment. The final prototyped model was mass produced by injection molding. This process improves major problems with preexisting PDMS-based devices; low productivity, technical hurdles, and the validity of the results of experiments due to small molecule absorption. We developed Sphero-IMPACT that allows simultaneous patterning of a spheroid and cell-embedded hydrogels through a single-step patterning by open microfluidics. We established a variety of models on Sphero-IMPACT; (1) 3D perfusable blood vessel network, (2) tumor spheroid-based migration and invasion assay, and (3)

tumor spheroid-mediated angiogenesis model for drug screening. These in vitro models were reconstructed and validated under optimized conditions. Our previous research has included PDMS-based studies, these approaches have many limitations with respect to meeting the ultimate goals of cancer research. We aimed to develop a practical platform by focusing on improving the material properties of the device and experimental methods. Furthermore, we expect Sphero-IMPACT to be an experimental tool that end-user can easily apply to their target experimental purposes.

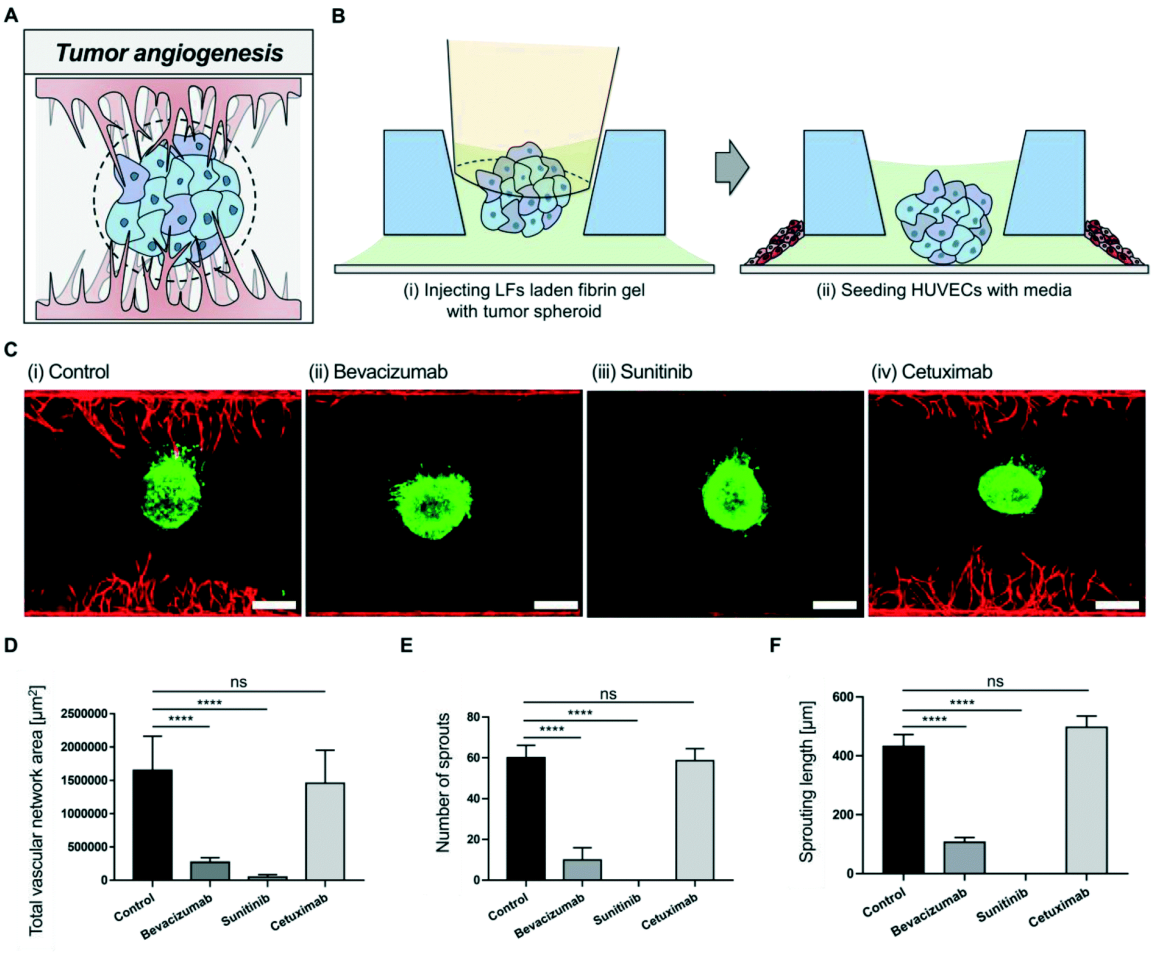

Figure 3.9 Tumor spheroid-induced angiogenesis and drug screening validation (A) Schematic depiction of angiogenic sprouts toward tumor spheroid positioned in the center hole. (B) Configuration of the microfluidic platform for modeling tumor angiogenesis. The tumor spheroid collected and mixed with fibrin gel is injected into the hole, and HUVECs are seeded on around the fibrin gel surface. (C) Maximum projection images of the tumor angiogenesis cultured for 4 days in Sphero-IMPACT. Tumor spheroid formed from GFP-expressing U87MG, and blood vessels assembled from RFP-expressing HUVECs. Under the same culture conditions, the types of target drugs were treated with medium every two days. Scale bar = 500 μm. (D–F) Quantitative analysis of the total vascular network area, number of sprouts and sprouting length depending on each drug condition. Bars represent mean ± SEM from at least 8 devices per condition. ****$p < 0.0001$ in the unpaired two-tailed Student's t-test.

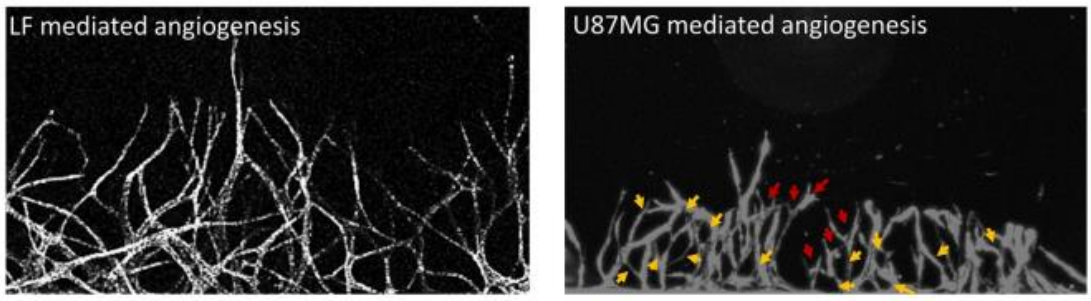

Figure 3.10 Comparison of angiogenic sprouts under different conditions. Under co-culture with U87MG cancer cells, angiogenic sprouts are characterized by the sprouts with branching tip cells (red arrow) and convoluted and aberrantly converged blood vessels (yellow arrow).

CHAPTER 4. GENERAL DISCUSSION AND FUTURE PERSPECTIVES

To reconstitute a physiologically relevant tumor microenvironment on a chip, several key parameters need to be taken into account. In this section, we will discuss unique characteristics of an in vivo TME to consider improvements to in vitro TME microfluidic models for drug delivery studies.

4.1 EPR Effect

The preferential accumulation of nanoparticles in a tumor is generally attributed to defective and leaky tumor vasculature [114] and dysfunctional lymphatic vessels in the tissue that cause poor drainage [115]. All of these factors are mainly known to contribute to the EPR effect, facilitating nanoparticle delivery to a solid tumor site [116]. Conventional in vitro 2D models however were unable to evaluate the full extent of the EPR effect.

4.2 Solid Tumor Stress

It has long been known that tissue stiffness is higher than normal in fibrotic solid tumors [117]. Tumors containing abnormally high amounts of collagen and other scaffolding proteins have been linked to several hallmark characteristics of cancer, including tumor growth, invasiveness, and metastasis [118]. Accumulation of mechanical stresses within the TME may lead to the constriction of intratumoral blood vessels, drastically reducing oxygen supply and increasing the risk of hypoxia and necrosis [119]. Moreover, vessel compression decreases blood flow, which also reduces the delivery efficacy of drugs to

ultimately compromise therapeutic outcomes [120]. Apart from compression of intratumoral vessels, the solid stress directly affects cancer cells by increasing their apoptotic rate and reducing proliferation [121]. With the widely-known contribution of mechanical stress to tumor progression, biomechanical models of tumor growth have been developed to consider the generation and accumulation of mechanical stresses in tumors [122]. However, few microfluidic model-based studies focused on the incorporation of solid tumor stress, which is key to the design of physiologically relevant in vitro tumor models.

4.3 Normalization of Tumor Blood Vessels

The physiological consequences of tumor vascular abnormalities include temporal and spatial heterogeneity in tumor blood flow and increased fluid pressure [123]. These abnormalities promote tumor progression and lead to reduction in the distribution of an anti-cancer drug. Therefore, one of the main purposes to include vascular normalization into microfluidic platforms is to examine the phenotypic transformation of abnormal vasculature into a phenotype that closely resembles functionally normal blood vessels by increasing coverage of pericytes and the basement membrane, eventually decreasing vessel permeability [124]. Tumor vascular normalization repairs not only abnormal morphology but also the function of tumor vasculature, by correcting angiogenic signaling pathways [125]. However, normalized vessels with reduced fenestration may also hinder EPR-effect based delivery of large nanoparticles to the tumor site. Therefore, exploring the appropriate tumor vessel normalization may be needed to improve and balance nanomedicine delivery to a tumor site [126]. Previous models to investigate dynamic changes during tumor vasculature normalization heavily rely on computational models and mouse models [127].

Microfluidic platforms may provide a better understanding of the molecular, cellular, and functional changes during dynamic tumor vessel normalization with physiological relevance.

4.4 Future Microfluidic Platforms

Many of the microfluidic platforms are based on soft lithographic PDMS designs that were developed and fabricated in-house or procured from limited fabrication runs from an associated institution. Initially developed as a means of rapid prototyping, soft lithography is ideal for microfabrication at the pilot scale, with low per-design initial investment for producing a limited run. Although soft lithography enables the production of a novel functional microfluidic design in PDMS within 24 h of drafting, the method utilizes fragile silicon wafer molds and heavily bottlenecked PDMS casting steps which limits the scalability of higher throughput fabrication. To address the larger scale production inefficiencies inherent to soft lithographic microfabrication, many commercial and academic ventures such as Emulate, MIMETAS, and Curiochips have looked to comparatively more upscalable manufacturing techniques such as injection molding and 3D printing for microfluidic device production. Incorporating large scale manufacturing practices into microfluidic chip production is a significant step towards ensuring that industrial scale demands can be supplied.

Development efforts to scale up production capabilities have also enabled a greater degree of quality control and form factor standardization for high throughput compatibility. Many conventionally produced PDMS microfluidic devices are punched manually or punched in a device-specific configuration, producing distinct form factors and input/output ports

which may vary significantly even within devices of the same design. The implementation of standardized, mass production friendly templates produced in large, uniform batches enables the possibility of automated handling through existing microtiter plate HTS infrastructure.

While the forefront of academic microfluidic tissue platform research continues to specialize towards increasingly sophisticated designs for higher fidelity in vivo like reconstitution, development for industrial applications have focused on simplifying designs in favor of flexible platforms that are simultaneously easier to use and are capable of applying to a wider range of tissues. Although the strategy of simplification sacrifices aspects of realistic tissue generation, a balance between lesser but still meaningful levels of realism and greater accessibility for a wider user base may prove instrumental for industrial scale adoption. Although organ-on-a-chip technology is still in its infancy, it will surely continue to expand to provide physiologically/pathologically relevant tumor microenvironments to evaluate multifunctional drug delivery particles in the near future.

CHAPTER 5. CONCLUSION

This thesis described two different approaches to reconstitute 3D vascularized tumor microenvironment using PDMS and injection-molded -based microengineered fabrication technology. We designed geometrically defined vascularized tumor spheroid model and investigated hallmarks of tumor vasculatures and highlighted significance of tumor vascularization and revealing the importance of treatment timing. Based on the model, we further developed injection-molded plastic array 3D spheroid culture platform, which made of polystyrene (PS) in a standardized 96-well plate format with user-friendly interface. The platform that mediate open microfluidics allows implement spontaneous fluid patterning with high repeatability from the end user. To demonstrate versatile use of the platform, we developed 3D perfusable blood vessel network and tumor spheroid assays. In addition, we established a tumor spheroid induced angiogenesis model that can be applicable for drug screening.

To build these in vitro TME model systems is essential to acquire a deeper understanding of the cellular and molecular mechanisms by which the TME contributes to tumor growth and metastasis. Traditional 2D in vitro systems, Transwell culture, and spheroid formation models that are used to mimic TME have shown limited effectiveness in predicting the efficacy of many candidate drug compounds. Vascularized tumor spheroid model that introduced in this thesis may enable us to study tumor microenvironment in real-time in a precisely controlled manner. Our vascularized model can address the key challenges of conventional platforms and enable more complex yet critical studies with multi-parametric interactions including cell-to-cell and cell-to-matrix interactions within the TME.

In this thesis, we incorporated tumor-like spheroids into a microfluidic chip showed the penetration of nanoparticles into a tumor tissue with physiological flow conditions, validating the EPR effect in vitro. Likewise, the next generation of microfluidic devices would possibly use patient derived cells and extracted non-cellular ECMs with the use of multiple biochemical, biophysical and biomechanical cues that are characterized in cancer (EPR effect, solid tumor stress, and blood vessel normalization). This approach will also be integrated with high detection efficiency and high throughput technologies to enhance the clinical relevance of microfluidic technologies for cancer biology.

REFERENCES

[1] Birgersdotter A, Sandberg R, Ernberg I. Gene expression perturbation in vitro—a growing case for three-dimensional (3D) culture systems. Seminars in cancer biology: Elsevier; 2005. p. 405-12.

[2] Swartz MA, Iida N, Roberts EW, Sangaletti S, Wong MH, Yull FE, et al. Tumor microenvironment complexity: emerging roles in cancer therapy. AACR; 2012.

[3] Huh D, Torisawa Y-s, Hamilton GA, Kim HJ, Ingber DE. Microengineered physiological biomimicry: organs-on-chips. Lab on a Chip 2012;12:2156-64.

[4] Wikswo JP. The relevance and potential roles of microphysiological systems in biology and medicine. Experimental biology and medicine 2014;239:1061-72.

[5] Trédan O, Galmarini CM, Patel K, Tannock IF. Drug resistance and the solid tumor microenvironment. Journal of the National Cancer Institute 2007;99:1441-54.

[6] Whiteside T. The tumor microenvironment and its role in promoting tumor growth. Oncogene 2008;27:5904.

[7] Kellermann MG, Sobral LM, da Silva SD, Zecchin KG, Graner E, Lopes MA, et al. Mutual paracrine effects of oral squamous cell carcinoma cells and normal oral fibroblasts: induction of fibroblast to myofibroblast transdifferentiation and modulation of tumor cell proliferation. Oral oncology 2008;44:509-17.

[8] Hanahan D, Weinberg RA. The hallmarks of cancer. cell 2000;100:57-70.

[9] Eklund L, Bry M, Alitalo K. Mouse models for studying angiogenesis and lymphangiogenesis in cancer. Molecular oncology 2013;7:259-82.

[10] Orimo A, Weinberg RA. Stromal fibroblasts in cancer: a novel tumor-promoting cell type. Cell cycle 2006;5:1597-601.

[11] Domenech M, Yu H, Warrick J, Badders NM, Meyvantsson I, Alexander CM, et al. Cellular observations enabled by microculture: paracrine signaling and population demographics. Integrative biology 2009;1:267-74.

[12] Liu T, Lin B, Qin J. Carcinoma-associated fibroblasts promoted tumor spheroid invasion on a microfluidic 3D co-culture device. Lab on a Chip 2010;10:1671-7.

[13] Xu Z, Gao Y, Hao Y, Li E, Wang Y, Zhang J, et al. Application of a microfluidic chip-based 3D co-culture to test drug sensitivity for individualized treatment of lung cancer. Biomaterials 2013;34:4109-17.

[14] Jeong S-Y, Lee J-H, Shin Y, Chung S, Kuh H-J. Co-culture of tumor spheroids and fibroblasts in a collagen matrix-incorporated microfluidic chip mimics reciprocal activation in solid tumor microenvironment. PloS one 2016;11:e0159013.

[15] Ghajar CM, Chen X, Harris JW, Suresh V, Hughes CC, Jeon NL, et al. The effect of matrix density on the regulation of 3-D capillary morphogenesis. Biophysical journal 2008;94:1930-41.

[16] Huang CP, Lu J, Seon H, Lee AP, Flanagan LA, Kim H-Y, et al. Engineering microscale cellular niches for three-dimensional multicellular co-cultures. Lab on a Chip 2009;9:1740-8.

[17] Carmeliet P, Jain RK. Angiogenesis in cancer and other diseases. nature 2000;407:249.

[18] Munn LL. Aberrant vascular architecture in tumors and its importance in drug-based therapies. Drug discovery today 2003;8:396-403.

[19] Kim S, Lee H, Chung M, Jeon NL. Engineering of functional, perfusable 3D microvascular networks on a chip. Lab on a Chip 2013;13:1489-500.

[20] Zheng Y, Sun Y, Yu X, Shao Y, Zhang P, Dai G, et al. Angiogenesis in Liquid Tumors: An In Vitro Assay for Leukemic-Cell-Induced Bone Marrow Angiogenesis. Advanced healthcare materials 2016;5:1014-24.

[21] Ehsan SM, Welch-Reardon KM, Waterman ML, Hughes CC, George SC. A three-dimensional in vitro model of tumor cell intravasation. Integrative Biology 2014;6:603-10.

[22] Fidler IJ. The pathogenesis of cancer metastasis: the'seed and soil'hypothesis revisited. Nature reviews cancer 2003;3:453.

[23] Friedl P, Wolf K. Tumour-cell invasion and migration: diversity and escape mechanisms. Nature reviews cancer 2003;3:362.

[24] Reymond N, d'Agua BB, Ridley AJ. Crossing the endothelial barrier during metastasis. Nature Reviews Cancer 2013;13:858.

[25] Zervantonakis IK, Hughes-Alford SK, Charest JL, Condeelis JS, Gertler FB, Kamm RD. Three-dimensional microfluidic model for tumor cell intravasation and endothelial barrier function. Proceedings of the National Academy of Sciences 2012;109:13515-20.

[26] Bersini S, Jeon JS, Dubini G, Arrigoni C, Chung S, Charest JL, et al. A microfluidic 3D in vitro model for specificity of breast cancer metastasis to bone. Biomaterials 2014;35:2454-61.

[27] Jeon JS, Bersini S, Gilardi M, Dubini G, Charest JL, Moretti M, et al. Human 3D vascularized organotypic microfluidic assays to study breast cancer cell extravasation. Proceedings of the National Academy of Sciences 2015;112:214-9.

[28] Chen MB, Whisler JA, Fröse J, Yu C, Shin Y, Kamm RD. On-chip human microvasculature assay for visualization and quantification of tumor cell extravasation dynamics. Nature protocols 2017;12:865.

[29] Xu Z, Li E, Guo Z, Yu R, Hao H, Xu Y, et al. Design and construction of a multi-organ microfluidic chip mimicking the in vivo microenvironment of lung cancer metastasis. ACS applied materials & interfaces 2016;8:25840-7.

[30] Pattabiraman DR, Weinberg RA. Tackling the cancer stem cells—what challenges do they pose? Nature reviews Drug discovery 2014;13:497.

[31] Kumar S, Weaver VM. Mechanics, malignancy, and metastasis: the force journey of a tumor cell. Cancer and Metastasis Reviews 2009;28:113-27.

[32] Young EW. Cells, tissues, and organs on chips: challenges and opportunities for the cancer tumor microenvironment. Integrative Biology 2013;5:1096-109.

[33] Song JW, Munn LL. Fluid forces control endothelial sprouting. Proceedings of the National Academy of Sciences 2011;108:15342-7.

[34] Huang S, Ingber DE. Cell tension, matrix mechanics, and cancer development. Cancer cell 2005;8:175-6.

[35] Paszek MJ, Zahir N, Johnson KR, Lakins JN, Rozenberg GI, Gefen A, et al. Tensional homeostasis and the malignant phenotype. Cancer cell 2005;8:241-54.

[36] Roovers K, Assoian RK. Effects of Rho kinase and actin stress fibers on sustained extracellular signal-regulated kinase activity and activation of G1 phase cyclin-dependent kinases. Molecular and cellular biology 2003;23:4283-94.

[37] Pathak A, Kumar S. Biophysical regulation of tumor cell invasion: moving beyond matrix stiffness. Integrative Biology 2011;3:267-78.

[38] Bellail AC, Hunter SB, Brat DJ, Tan C, Van Meir EG. Microregional extracellular matrix heterogeneity in brain modulates glioma cell invasion. The international journal of biochemistry & cell biology 2004;36:1046-69.

[39] Bignami A, Hosley M, Dahl D. Hyaluronic acid and hyaluronic acid-binding proteins in brain extracellular matrix. Anatomy and embryology 1993;188:419-33.

[40] Pampaloni F, Reynaud EG, Stelzer EH. The third dimension bridges the gap between cell culture and live tissue. Nature reviews Molecular cell biology 2007;8:839.

[41] Wootton RC, Demello AJ. Microfluidics: Analog-to-digital drug screening. Nature 2012;483:43.

[42] Wlodkowic D, Faley S, Zagnoni M, Wikswo JP, Cooper JM. Microfluidic single-cell array cytometry for the analysis of tumor apoptosis. Analytical chemistry 2009;81:5517-23.

[43] Yu L, Chen MC, Cheung KC. Droplet-based microfluidic system for multicellular tumor spheroid formation and anticancer drug testing. Lab on a Chip 2010;10:2424-32.

[44] Weiswald L-B, Bellet D, Dangles-Marie V. Spherical cancer models in tumor biology. Neoplasia 2015;17:1-15.

[45] Weltin A, Slotwinski K, Kieninger J, Moser I, Jobst G, Wego M, et al. Cell culture monitoring for drug screening and cancer research: a transparent, microfluidic, multi-sensor microsystem. Lab on a Chip 2014;14:138-46.

[46] Kwak B, Ozcelikkale A, Shin CS, Park K, Han B. Simulation of complex transport of nanoparticles around a tumor using tumor-microenvironment-on-chip. Journal of controlled release 2014;194:157-67.

[47] Albanese A, Lam AK, Sykes EA, Rocheleau JV, Chan WC. Tumour-on-a-chip provides an optical window into nanoparticle tissue transport. Nature communications 2013;4:2718.

[48] Duffy DC, McDonald JC, Schueller OJ, Whitesides GM. Rapid prototyping of microfluidic systems in poly (dimethylsiloxane). Analytical chemistry 1998;70:4974-84.

[49] Lee H, Park W, Ryu H, Jeon NL. A microfluidic platform for quantitative analysis of cancer angiogenesis and intravasation. Biomicrofluidics 2014;8:054102.

[50] Junaid A, Mashaghi A, Hankemeier T, Vulto P. An end-user perspective on organ-on-a-chip: assays and usability aspects. Current Opinion in Biomedical Engineering 2017;1:15-22.

[51] Halldorsson S, Lucumi E, Gómez-Sjöberg R, Fleming RM. Advantages and challenges of microfluidic cell culture in polydimethylsiloxane devices. Biosensors and Bioelectronics 2015;63:218-31.

[52] Lee Y, Choi JW, Yu J, Park D, Ha J, Son K, et al. Microfluidics within a well: an injection-molded plastic array 3D culture platform. Lab on a Chip 2018;18:2433-40.

[53] Luo H, Tu G, Liu Z, Liu M. Cancer-associated fibroblasts: a multifaceted driver of breast cancer progression. Cancer letters 2015;361:155-63.

[54] Folkman J. Role of angiogenesis in tumor growth and metastasis. Seminars in oncology: Elsevier; 2002. p. 15-8.

[55] Ahn J, Sei YJ, Jeon NL, Kim Y. Tumor microenvironment on a chip: the progress and future perspective. Bioengineering 2017;4:64.

[56] Koontongkaew S. The tumor microenvironment contribution to development, growth, invasion and metastasis of head and neck squamous cell carcinomas. Journal of Cancer 2013;4:66.

[57] Hanahan D, Weinberg RA. Hallmarks of cancer: the next generation. cell 2011;144:646-74.

[58] Tsai H-F, Trubelja A, Shen AQ, Bao G. Tumour-on-a-chip: microfluidic models of tumour morphology, growth and microenvironment. Journal of the Royal Society Interface 2017;14:20170137.

[59] Chen MB, Kamm RD, Moeendarbary E. Engineered Models of Metastasis with Application to Study Cancer Biomechanics. Biomechanics in Oncology: Springer; 2018. p. 189-207.

[60] Chung M, Ahn J, Son K, Kim S, Jeon NL. Biomimetic model of tumor microenvironment on microfluidic platform. Advanced healthcare materials 2017;6:1700196.

[61] Nishiguchi A, Matsusaki M, Kano MR, Nishihara H, Okano D, Asano Y, et al. In vitro 3D blood/lymph-vascularized human stromal tissues for preclinical assays of cancer metastasis. Biomaterials 2018;179:144-55.

[62] Kim J, Chung M, Kim S, Jo DH, Kim JH, Jeon NL. Engineering of a biomimetic pericyte-covered 3D microvascular network. PloS one 2015;10:e0133880.

[63] Hirschhaeuser F, Menne H, Dittfeld C, West J, Mueller-Klieser W, Kunz-Schughart LA. Multicellular tumor spheroids: an underestimated tool is catching up again. Journal of biotechnology 2010;148:3-15.

[64] Carver K, Ming X, Juliano RL. Multicellular tumor spheroids as a model for assessing delivery of oligonucleotides in three dimensions. Molecular Therapy-Nucleic Acids 2014;3:e153.

[65] Moshksayan K, Kashaninejad N, Warkiani ME, Lock JG, Moghadas H, Firoozabadi B, et al. Spheroids-on-a-chip: Recent advances and design considerations in microfluidic platforms for spheroid formation and culture. Sensors and Actuators B: Chemical 2018;263:151-76.

[66] Huang B-W, Gao J-Q. Application of 3D cultured multicellular spheroid tumor models in tumor-targeted drug delivery system research. Journal of Controlled Release 2018;270:246-59.

[67] Shoval H, Karsch-Bluman A, Brill-Karniely Y, Stern T, Zamir G, Hubert A, et al. Tumor cells and their crosstalk with endothelial cells in 3D spheroids. Scientific reports 2017;7:10428.

[68] Sobrino A, Phan DT, Datta R, Wang X, Hachey SJ, Romero-López M, et al. 3D microtumors in vitro supported by perfused vascular networks. Scientific reports 2016;6:31589.

[69] Song J, Miermont A, Lim CT, Kamm RD. A 3D microvascular network model to study the impact of hypoxia on the extravasation potential of breast cell lines. Scientific reports 2018;8:17949.

[70] Grimes DR, Kelly C, Bloch K, Partridge M. A method for estimating the oxygen consumption rate in multicellular tumour spheroids. Journal of The Royal Society Interface 2014;11:20131124.

[71] Lee SW, Kwak HS, Kang M-H, Park Y-Y, Jeong GS. Fibroblast-associated tumour microenvironment induces vascular structure-networked tumouroid. Scientific reports 2018;8:2365.

[72] Lee H, Kim S, Chung M, Kim JH, Jeon NL. A bioengineered array of 3D microvessels for vascular permeability assay. Microvascular research 2014;91:90-8.

[73] Wang M, Zhao J, Zhang L, Wei F, Lian Y, Wu Y, et al. Role of tumor microenvironment in tumorigenesis. Journal of Cancer 2017;8:761.

[74] Li H, Fan X, Houghton J. Tumor microenvironment: the role of the tumor stroma in cancer. Journal of cellular biochemistry 2007;101:805-15.

[75] Upreti M, Jamshidi-Parsian A, Koonce NA, Webber JS, Sharma SK, Asea AA, et al. Tumor-endothelial cell three-dimensional spheroids: new aspects to enhance radiation and drug therapeutics. Translational oncology 2011;4:365-IN3.

[76] Cheng H-W, Chen Y-F, Wong J-M, Weng C-W, Chen H-Y, Yu S-L, et al. Cancer cells increase endothelial cell tube formation and survival by activating the PI3K/Akt signalling pathway. Journal of Experimental & Clinical Cancer Research 2017;36:27.

[77] Dudley AC. Tumor endothelial cells. Cold Spring Harbor perspectives in medicine 2012;2:a006536.

[78] Susaki EA, Tainaka K, Perrin D, Yukinaga H, Kuno A, Ueda HR. Advanced CUBIC protocols for whole-brain and whole-body clearing and imaging. Nature protocols 2015;10:1709.

[79] Seo J, Choe M, Kim S-Y. Clearing and labeling techniques for large-scale biological tissues. Molecules and cells 2016;39:439.

[80] McDonald DM, Baluk P. Significance of blood vessel leakiness in cancer. AACR; 2002.

[81] Mashreghi M, Azarpara H, Bazaz MR, Jafari A, Masoudifar A, Mirzaei H, et al. Angiogenesis biomarkers and their targeting ligands as potential targets for tumor angiogenesis. Journal of cellular physiology 2018;233:2949-65.

[82] Millard M, Yakavets I, Zorin V, Kulmukhamedova A, Marchal S, Bezdetnaya L. Drug delivery to solid tumors: the predictive value of the multicellular tumor spheroid model for nanomedicine screening. International journal of nanomedicine 2017;12:7993.

[83] Hobbs SK, Monsky WL, Yuan F, Roberts WG, Griffith L, Torchilin VP, et al. Regulation of transport pathways in tumor vessels: role of tumor type and microenvironment. Proceedings of the National Academy of Sciences 1998;95:4607-12.

[84] Hashizume H, Baluk P, Morikawa S, McLean JW, Thurston G, Roberge S, et al. Openings between defective endothelial cells explain tumor vessel leakiness. The American journal of pathology 2000;156:1363-80.

[85] Paech F, Bouitbir J, Krähenbühl S. Hepatocellular toxicity associated with tyrosine kinase inhibitors: mitochondrial damage and inhibition of glycolysis. Frontiers in pharmacology 2017;8:367.

[86] Choueiri TK. Axitinib, a novel anti-angiogenic drug with promising activity in various solid tumors. Current opinion in investigational drugs (London, England: 2000) 2008;9:658-71.

[87] Bellesoeur A, Carton E, Alexandre J, Goldwasser F, Huillard O. Axitinib in the treatment of renal cell carcinoma: Design, development, and place in therapy. Drug design, development and therapy 2017;11:2801.

[88] Zhang XH, Qiao EQ, Gao Z, Yuan HQ, Cai PF, Li XM, et al. Efficacy of combined axitinib with dacarbazine in a B16F1 melanoma xenograft model. Oncology letters 2013;6:69-74.

[89] Hu-Lowe DD, Zou HY, Grazzini ML, Hallin ME, Wickman GR, Amundson K, et al. Nonclinical antiangiogenesis and antitumor activities of axitinib (AG-013736), an oral, potent, and selective inhibitor of vascular endothelial growth factor receptor tyrosine kinases 1, 2, 3. Clinical Cancer Research 2008;14:7272-83.

[90] Folberg R, Hendrix MJ, Maniotis AJ. Vasculogenic mimicry and tumor angiogenesis. The American journal of pathology 2000;156:361-81.

[91] Williamson SC, Metcalf RL, Trapani F, Mohan S, Antonello J, Abbott B, et al. Vasculogenic mimicry in small cell lung cancer. Nature communications 2016;7:13322.

[92] Huh D, Matthews BD, Mammoto A, Montoya-Zavala M, Hsin HY, Ingber DE. Reconstituting organ-level lung functions on a chip. Science 2010;328:1662-8.

[93] Friedrich J, Seidel C, Ebner R, Kunz-Schughart LA. Spheroid-based drug screen: considerations and practical approach. Nature protocols 2009;4:309.

[94] Sung KE, Beebe DJ. Microfluidic 3D models of cancer. Advanced drug delivery reviews 2014;79:68-78.

[95] Lee S, Ko J, Park D, Lee S-R, Chung M, Lee Y, et al. Microfluidic-based vascularized microphysiological systems. Lab on a Chip 2018;18:2686-709.

[96] Oh S, Ryu H, Tahk D, Ko J, Chung Y, Lee HK, et al. "Open-top" microfluidic device for in vitro three-dimensional capillary beds. Lab on a Chip 2017;17:3405-14.

[97] Truong D, Puleo J, Llave A, Mouneimne G, Kamm RD, Nikkhah M. Breast cancer cell invasion into a three dimensional tumor-stroma microenvironment. Scientific reports 2016;6:34094.

[98] Berry SB, Zhang T, Day JH, Su X, Wilson IZ, Berthier E, et al. Upgrading well plates using open microfluidic patterning. Lab on a Chip 2017;17:4253-64.

[99] Bhattacharjee N, Urrios A, Kang S, Folch A. The upcoming 3D-printing revolution in microfluidics. Lab on a Chip 2016;16:1720-42.

[100] Vladisavljević GT, Khalid N, Neves MA, Kuroiwa T, Nakajima M, Uemura K, et al. Industrial lab-on-a-chip: Design, applications and scale-up for drug discovery and delivery. Advanced drug delivery reviews 2013;65:1626-63.

[101] Berthier E, Young EW, Beebe D. Engineers are from PDMS-land, Biologists are from Polystyrenia. Lab on a Chip 2012;12:1224-37.

[102] Berthier J, Brakke K, Furlani E, Karampelas I, Poher V, Gosselin D, et al. Whole blood spontaneous capillary flow in narrow V-groove microchannels. Sensors and Actuators B: Chemical 2015;206:258-67.

[103] Lee JJ, Berthier J, Brakke KA, Dostie AM, Theberge AB, Berthier E. Droplet behavior in open biphasic microfluidics. Langmuir 2018;34:5358-66.

[104] van Duinen V, Zhu D, Ramakers C, van Zonneveld A, Vulto P, Hankemeier T. Perfused 3D angiogenic sprouting in a high-throughput in vitro platform. Angiogenesis 2019;22:157-65.

[105] Nashimoto Y, Hayashi T, Kunita I, Nakamasu A, Torisawa Y-s, Nakayama M, et al. Integrating perfusable vascular networks with a three-dimensional tissue in a microfluidic device. Integrative Biology 2017;9:506-18.

[106] Bischel LL, Young EW, Mader BR, Beebe DJ. Tubeless microfluidic angiogenesis assay with three-dimensional endothelial-lined microvessels. Biomaterials 2013;34:1471-7.

[107] Kim C, Kasuya J, Jeon J, Chung S, Kamm RD. A quantitative microfluidic angiogenesis screen for studying anti-angiogenic therapeutic drugs. Lab on a chip 2015;15:301-10.

[108] Semenza GL. The hypoxic tumor microenvironment: A driving force for breast cancer progression. Biochimica et Biophysica Acta (BBA)-Molecular Cell Research 2016;1863:382-91.

[109] Waheed S, Cabot JM, Macdonald NP, Lewis T, Guijt RM, Paull B, et al. 3D printed microfluidic devices: enablers and barriers. Lab on a Chip 2016;16:1993-2013.

[110] Seoane J. Escaping from the TGFβ anti-proliferative control. Carcinogenesis 2006;27:2148-56.

[111] Ferrantini M, Belardelli F. Gene therapy of cancer with interferon: lessons from tumor models and perspectives for clinical applications. Seminars in cancer biology: Elsevier; 2000. p. 145-57.

[112] Ferrara N. VEGF and the quest for tumour angiogenesis factors. Nature Reviews Cancer 2002;2:795.

[113] Dunn DA, Feygin I. Challenges and solutions to ultra-high-throughput screening assay miniaturization: submicroliter fluid handling. Drug discovery today 2000;5:S84-S91.

[114] Nagy JA, Dvorak AM, Dvorak HF. VEGF-A and the induction of pathological angiogenesis. Annu Rev Pathol Mech Dis 2007;2:251-75.

[115] Peer D, Karp JM, Hong S, Farokhzad OC, Margalit R, Langer R. Nanocarriers as an emerging platform for cancer therapy. Nature nanotechnology 2007;2:751.

[116] Maeda H. Toward a full understanding of the EPR effect in primary and metastatic tumors as well as issues related to its heterogeneity. Advanced drug delivery reviews 2015;91:3-6.

[117] Masuzaki R, Tateishi R, Yoshida H, Sato T, Ohki T, Goto T, et al. Assessing liver tumor stiffness by transient elastography. Hepatology international 2007;1:394-7.

[118] Levental KR, Yu H, Kass L, Lakins JN, Egeblad M, Erler JT, et al. Matrix crosslinking forces tumor progression by enhancing integrin signaling. Cell 2009;139:891-906.

[119] Stylianopoulos T, Martin JD, Chauhan VP, Jain SR, Diop-Frimpong B, Bardeesy N, et al. Causes, consequences, and remedies for growth-induced solid stress in murine and human tumors. Proceedings of the National Academy of Sciences 2012;109:15101-8.

[120] Chauhan VP, Martin JD, Liu H, Lacorre DA, Jain SR, Kozin SV, et al. Angiotensin inhibition enhances drug delivery and potentiates chemotherapy by decompressing tumour blood vessels. Nature communications 2013;4:2516.

[121] Desmaison A, Frongia C, Grenier K, Ducommun B, Lobjois V. Mechanical stress impairs mitosis progression in multi-cellular tumor spheroids. PloS one 2013;8:e80447.

[122] Ciarletta P, Ambrosi D, Maugin G, Preziosi L. Mechano-transduction in tumour growth modelling. The European Physical Journal E 2013;36:23.

[123] Goel S, Duda DG, Xu L, Munn LL, Boucher Y, Fukumura D, et al. Normalization of the vasculature for treatment of cancer and other diseases. Physiological reviews 2011;91:1071-121.

[124] Jain RK, Martin JD, Stylianopoulos T. The role of mechanical forces in tumor growth and therapy. Annual review of biomedical engineering 2014;16:321-46.

[125] Goel S, Wong AH-K, Jain RK. Vascular normalization as a therapeutic strategy for malignant and nonmalignant disease. Cold Spring Harbor perspectives in medicine 2012;2:a006486.

[126] Chauhan VP, Stylianopoulos T, Martin JD, Popović Z, Chen O, Kamoun WS, et al. Normalization of tumour blood vessels improves the delivery of nanomedicines in a size-dependent manner. Nature nanotechnology 2012;7:383.

[127] Rohner NA, Thomas SN. Melanoma growth effects on molecular clearance from tumors and biodistribution into systemic tissues versus draining lymph nodes. Journal of Controlled Release 2016;223:99-108.